IDENTIFICATION OF THE MODE OF REGULATION OF SINE SENSE AND ANTISENSE RNAS DURING CELLULAR RESPONSE TO THE STRESS

ALYONA GERASIMOVA
B.Sc Applied Mathematics and Physics, MIPT, 2022

A thesis submitted
in partial fulfilment of the requirements for the degree of

MASTER OF SCIENCE

in

BIOCHEMISTRY

Department of Chemistry and Biochemistry
University of Lethbridge,
Lethbridge, Alberta, Canada

IDENTIFICATION OF THE MODE OF REGULATION OF SINE SENSE AND ANTISENSE RNAS DURING CELLULAR RESPONSE TO THE STRESS

ALYONA GERASIMOVA

Date of defense: August 29, 2024

Dr. Athanasios Zovoilis	Associate Professor	M.D. Ph.D.
Dr. Igor Kovalchuk	Professor	Ph.D.
Thesis Co-supervisors		
Dr. Olga Kovalchuk	Professor	Ph.D.
Thesis Examination Committee Member		
Dr. Artur Luczak	Professor	Ph.D.
Thesis Examination Committee Member		
Dr. Robbin Gibb	Professor	Ph.D.
Chair, Thesis Examination Committee		

Abstract

A large portion of the mammalian genome comprises non-coding sequences, such as B2 SINEs, which play a role in gene regulation during stress. Despite their significance, the regulatory mechanisms governing SINEs remain unclear. This study explores the relationship between sense and antisense B2 SINE transcripts in a mouse cell line model exposed to heat shock and other stress conditions, including transfection with locked nucleic acids and in vitro transcribed B2. The results of qPCR and sequencing data analysis demonstrate an inverse relationship between the expression levels of sense and antisense B2 SINEs, with these effects being transient and diminishing over time. This indicates a complex, dynamic regulatory network that likely involves additional factors or feedback loops.

Acknowledgements

I would like to express my deepest gratitude to my supervisor, Dr. Zovoilis, whose constant support, constructive feedback, and encouragement have been essential to my project.

I would also like to extend my thanks to my co-supervisor, Dr. Kovalchuk, and the members of my thesis committee for their time and valuable suggestions, which have contributed greatly to the development of this thesis.

A special thanks to Syed Beenish Rufai for her help and guidance in performing and designing the qPCR experiments. Her expertise was crucial to the success of this project.

I am also immensely grateful to Alex Sizykh for his training and guidance with bioinformatic analysis. His knowledge was invaluable to my research.

I am deeply appreciative of Luke Saville for providing me with the gBlock and LNA sequences and protocols for some procedures.

Finally, I would like to thank my colleagues, whose collaboration and support have made this journey more manageable and enjoyable. Special thanks to Riya Roy for her assistance and for teaching me all the necessary wet lab techniques.

Table of Contents

Abbreviations:

SINEs: short interspersed nuclear elements
ncRNA: non-coding RNA
rRNA: ribosomal RNA
tRNA: transfer RNA
lncRNA: long non-coding RNA
siRNA: small interfering RNA
miRNA: microRNA
snoRNA: small nucleolar RNA
mRNA: messenger RNA
LTR: long terminal repeats
LINEs: long interspersed nuclear elements
Pol II: RNA polymerase II
Pol III: RNA polymerase III
A-to-I editing: adenosine to inosine conversions
ADAR: adenosine deaminase acting on RNA
cDNA: complementary DNA
SE - sense
AS - antisense
ASO - antisense oligonucleotide
LNA - locked nucleic acid

Chapter 1. Introduction

1.1 Non-coding RNAs

The human genome comprises both protein-coding genes and non-protein-coding DNA sequences, the latter of which do not encode proteins. Notably, up to 80% of the human genome is transcribed into RNA molecules, although only approximately 2% of the genome directly encodes proteins (de Koning et al., 2011). The RNA transcripts that are not translated into proteins are termed non-coding RNAs (ncRNAs). Historically, ncRNAs were perceived as non-functional byproducts of a non-coding genome, devoid of significant biological function. Nevertheless, recent research on the biological roles of ncRNAs has expanded rapidly, revealing that these RNAs are associated with various crucial biological processes, such as chromatin modification and transcription regulation. Moreover, they can act as epigenetic regulators of gene expression, influencing which genes are turned on or off (Palazzo et al., 2014); (Fernandes et al., 2019). Furthermore, studies of various classes of ncRNAs have demonstrated their potential as therapeutic agents and biomarkers for diagnosing diseases, offering new ways for medical treatment and diagnosis (Winkle et al., 2021).

ncRNAs are classified into two principal categories: structural ncRNAs and regulatory ncRNAs. The structural ncRNAs include ribosomal RNA (rRNA) and transfer RNA (tRNA). rRNA forms the main structural component of ribosomes, which are essential for protein biosynthesis, making it one of the most abundant molecules in cells (Kobayashi et al., 2014); (Hori et al., 2023). In addition, recent studies indicate that rRNA plays a vital role in maintaining genome stability, which is crucial for preventing mutations and ensuring proper cell function (Li and Yu, 2024); (Fleurier et al., 2022). The role of tRNA in cellular processes has also been extensively studied. tRNA serves as a crucial link between messenger RNA (mRNA) and the growing polypeptide chain during protein synthesis, facilitating the translation of genetic information into functional proteins (Fernandez-Millan et al., 2016). Additionally, the relationship of the presence of rRNA modifications with the development of diseases such as diabetes or cancer is known (Cui et al., 2023); (Wang et al., 2023); (Zhou et al., 2019).

The second category of ncRNAs includes a diverse group of molecules such as long non-coding RNAs (lncRNA), small interfering RNAs (siRNA), microRNAs (miRNA), and small-interspersed nuclear elements RNAs (SINE RNA), among many others (Quinn et al., 2015). This group is classified as regulatory RNAs due to their role in

regulating numerous cellular pathways. Regulatory RNAs are involved in a wide range of cellular processes, including gene silencing, post-transcriptional regulation, and chromatin remodeling (Zong et al., 2023). For example, by attracting chromatin-reconstructing complexes to specific genomic loci, long ncRNAs are able to mediate epigenetic changes (Mercer et al., 2009).

Small regulatory RNAs are further divided into two main classes: 1) small nucleolar RNAs (snoRNAs), which are primarily responsible for the chemical modification and processing of rRNA, ensuring the proper assembly and function of ribosomes (Bratkovic et al., 2019); (Filipowicz et al., 1999) as well as for guiding the spliceosome machinery; and 2) miRNA and siRNA, which play crucial roles in gene regulation by targeting messenger RNA (mRNA) for degradation or translational repression, thereby controlling the levels of proteins produced within the cell (Fabian et al., 2010); (Wang et al., 2021); (Zovoilis et al., 2010); (Liao et al., 2011). Additionally, small RNAs can be used as predictive biomarkers to determine the status of cancer (Zovoilis et al., 2014), and studies show they can be considered potential targets in the treatment of dementia (Zovoilis et al., 2011).

1.2 Transposable elements

Some non-coding RNAs (ncRNAs) are derived from transposable elements, which are sequences of non-protein-coding DNA capable of inserting themselves into various locations within the genome. Based on their transposition mechanisms, transposable elements can be classified into two major classes (Wells and Feschotte, 2020). Class 1 elements, also known as retrotransposons, utilize a "copy and paste" mechanism. This process involves transcription from DNA to RNA, followed by reverse transcription of the RNA intermediate into complementary DNA (cDNA), which is then reinserted into the genome. It is known that retrotransposons are one of the main sources of genome instability, which can cause and contribute to the development of cancer, as well as many other serious diseases (Wu et al., 2021); (Payer and Burns, 2019); (Sargurupremraj and Wjst, 2013).

Retrotransposons are further categorized into two subgroups based on the presence of long terminal repeats (LTRs) at their ends: LTR retrotransposons and non-LTR retrotransposons (Hayward et al., 2022). Class 2 elements, also referred to as DNA transposons, transpose using a "cut and paste" mechanism that directly involves a DNA intermediate (Pace and Feschotte, 2007).

Non-LTR transposons are composed of long interspersed nuclear elements (LINEs) and short interspersed nuclear elements (SINEs). Both LINEs and SINEs have

significantly impacted the evolution of the mammalian genome due to their inherent retrotransposon activity (Richardson et al., 2015). LINEs are autonomous retrotransposons capable of moving within the genome and encoding the reverse transcriptase enzyme necessary for their own transposition. Conversely, SINEs are non-autonomous retrotransposons that rely on the enzymatic machinery provided by LINEs. SINEs mimic the 3'-ends of LINEs to ensure their propagation (Szafranski et al., 2004).

Recent research has highlighted the involvement of non-LTR transposons in various disease processes and immune responses (Terry and Devine, 2022). For example, the increase in the LINE copy amount leads to genome instability and is associated with the development of severe diseases such as cancer (Scarfò et al., 2016). Beyond this, LINEs are known to be involved in the development of systemic autoimmune diseases (Crow, 2010) and severe health conditions like ataraxia (Takahashi et al., 2022). Although at the same time, they have been proven to play an important role in brain development by regulating the rate of differentiation of neurons in both humans and mice (Toda et al., 2024).

1.3 SINEs

Although SINE elements have a reduced capacity for retrotransposition and are generally less autonomous compared to other transposable elements, they constitute a significant portion of the genome. In both human and murine genomes, SINEs occur in millions of copies (Zhang et al., 2021). The retrotransposon activity of L1 LINEs has facilitated the increased representation of SINEs over time (Stenz et al., 2021). Additionally, SINEs contribute to exonization within the genome through the insertion of internal exons (Schmitz et al., 2011). Unlike other transposable elements that are transcribed by RNA polymerase II (Pol II), SINEs rely on RNA polymerase III (Pol III), with transcription initiated at an internal promoter. This transcription mechanism enables the generation of short non-coding RNAs known as SINE RNAs (Dunker et al., 2017). SINE-encoded ncRNAs typically range in length from 100 to 500 base pairs (bp). A typical SINE is composed of three distinct parts: the 5′-terminal 'head', the 'body', and the 3′-terminal 'tail' (Sharma et al., 2023). The heads of all SINEs exhibit a clear similarity to one of the three types of cellular RNAs synthesized by Pol III: tRNA, 7SL RNA, or 5S rRNA (Pe'llissier et al., 2004).

A major family of SINE elements is derived from the 7SL RNA, which evolved independently in certain eukaryotes and gave rise to a branch in mammals. In rodents, this evolution resulted in the B1 SINE elements (Nikaido et al., 2022). Rodent genomes also contain transfer RNA-derived SINE elements known as B2

elements (Karijolich et al., 2017). In primates, including humans, the 7SL RNA-derived SINE elements evolved into the Alu family of SINE elements (Kriegs et al., 2007). The B2 and Alu retrotransposons represent two of the most prevalent subclasses of SINEs, with millions of copies present in mice and humans, respectively.

Moreover, SINE RNAs in different ways control gene expression by participating in processes such as mRNA transcriptional control, adenosine to inosine conversions (A-to-I editing) by deamination, alternative splicing and nuclear retention (Walters et al., 2009); (Maquat et al., 2020).

1.4 B2 elements

B2 elements are classified into several subfamilies based on their evolutionary history and sequence variations (Figure 1.1). For example, B2Mm2 is the oldest subfamily, B2Mm1o is intermediate, while B2Mm1a and B2Mm1t are the youngest subfamilies (Ichiyanagi et al., 2021). Among these, the Mm1a subfamily is the most widely distributed in mice and rats (Vassetzky et al., 2021).

B2 RNAs have been known for years to be up-regulated in response to various types of cellular stress (Tatosyan and Kramerov, 2016). However, the underlying mechanisms remained unclear until a series of studies revealed that SINE B2 RNA levels increase under stress conditions, suppressing mRNA transcription by binding to RNA polymerase II (Figure 1.2, Ichiyanagi et al., 2021); (Espinoza et al., 2007). This genome-wide transcriptional repression during cellular stress results in the suppression of housekeeping genes, potentially allowing the redistribution of cellular energy resources to support survival (Allen et al., 2004). Housekeeping genes - genes that are necessary for the existence of cells, regardless of their specific function. Which are also expressed relatively stably regardless of the external signal (Joshi et al., 2022).

Besides transcriptional repression, B2 as well as Alu RNAs have been shown to form intermolecular RNA-RNA interactions with complementary mRNAs, which leads to retention of the target mRNA in the nucleus (Karijolich et al., 2017); (Khan et al., 2023).

Further research from my lab demonstrated that SINE RNAs can also mediate cellular stress responses through another mechanism. Specifically, it was shown that SINE B2 RNAs in mice exhibit protein-accelerated self-cleavage activity (Zovoilis et

al., 2016), leading to their fragmentation and subsequent inability to bind to and suppress RNA polymerase II (Hernandez et al., 2020).

In general, during stress responses, SINE RNAs in mice function as transcriptional switches. They bind to RNA polymerase II at several stress response genes, thereby suppressing their transcription. Such binding to Pol II is possible due to the features of the structure of B2 RNA, which is why Pol II is released during the fragmentation of B2 (Ponicsan et al., 2015).

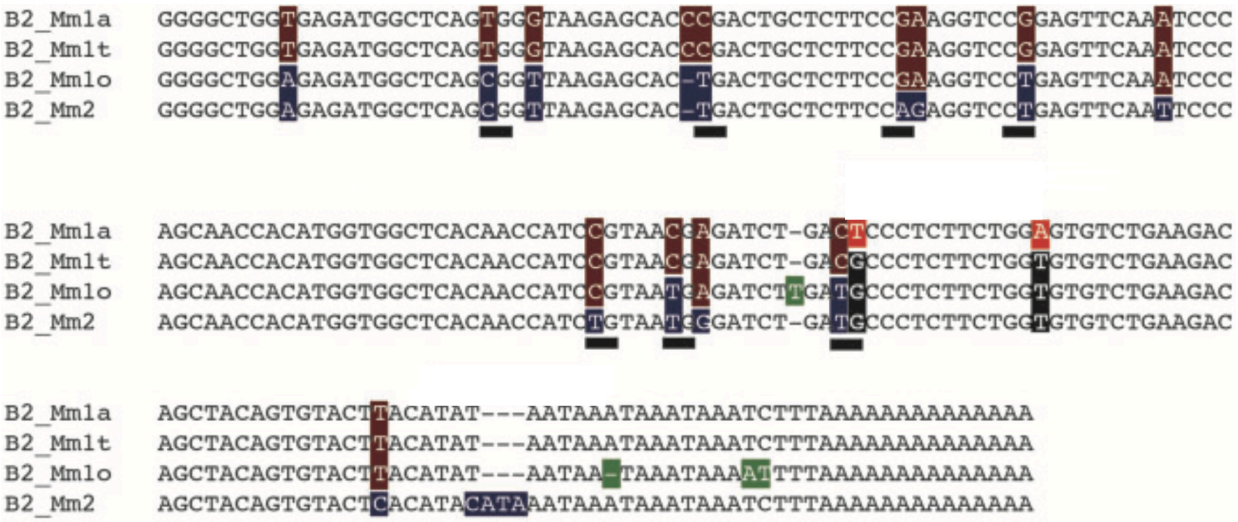

Figure 1.1: The alignment of the consensus sequences of B2 subfamilies.
Nucleotides that are different between the subfamilies are highlighted.
(Figure adapted from Tomoko Ichiyanagi et al., 2021).

Upon exposure to stress, B2 RNAs are processed, which results in the release of the delayed or stalled RNA polymerase at these stress response genes, allowing their transcription to proceed (Zovoilis et al., 2016). Recent studies have indicated that increased levels of B2 RNA processing enhance the expression of B2 RNA-targeted genes during the cellular stress response. For example, this pathway has been identified as being deregulated in amyloid-beta pathology in the mouse hippocampus (Cheng et al., 2020).

1.5 Alu elements

Full-length human Alu elements are typically about 300 base pairs (bp) in length and exhibit a dimeric structure. Individual Alu elements exert diverse influences on gene expression, including effects on polyadenylation, splicing, and adenosine deaminase editing (Deininger, 2011). Similar to B2 elements, Alu elements are categorized into specific subfamilies based on sequence variations. Several Alu subfamilies are currently active within human populations (Konkel et al., 2015); (Hadjiargyrou and Delihas, 2013).

Recent studies have demonstrated that, much like B2 RNAs, Alu RNAs are self-cleaving and can become destabilized in vitro (Hernandez et al., 2020). Additionally, Alu RNAs are up-regulated in response to stress stimuli, with a mechanism of action similar to that of B2 RNAs: they inhibit mRNA transcription by binding to Pol II (Shankar et al., 2004) (Mariner et al., 2008); (Yakovchuk et al., 2009).

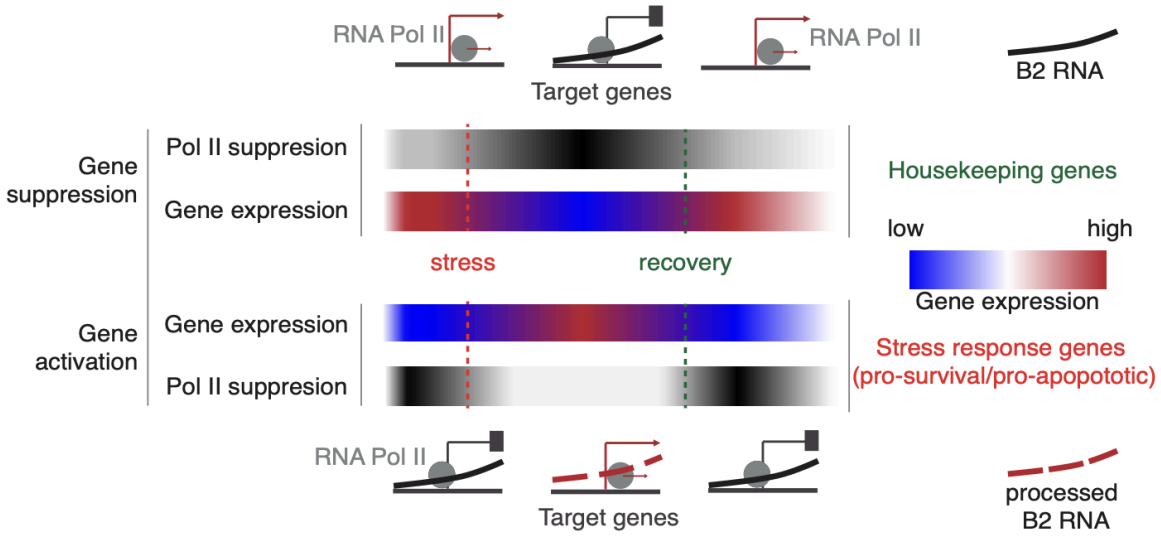

Figure 1.2: The mode of action of SINE RNAs in response to cellular stress.
(*Figure adapted from Cheng et al., 2021).*

Alu RNAs have been known to help selectively inhibit translation by binding the 40S subunit of the ribosome with the SRP9/14 protein, which prevents 48S complex formation. In addition, Alu RNAs are able to inhibit the translation of mRNAs, resuming it after stress (Ivanova et al., 2015).

1.6 Biological significance of SINE RNA

The epitranscriptome (all the biochemical modifications of ribonucleotides within a cell) response is a modulating force of SINE RNA function. One of the most widely spread modifications is A-to-I editing facilitated by ADAR (Adenosine Deaminase Acting on RNA) family proteins (Nossent, 2023). They act post-transcriptionally, changing the nucleotide content of RNA (Witman et al., 2013). In more detail, Alu elements can form double-stranded RNAs because of their repetitive structure. The formation of duplex structures leads to A-to-I editing by the ADAR enzymes (Chen et al., 2008). Another type of modification within RNA is N6-methylation of adenosine (Rottman et al., 1994) facilitated by the Mettl3/14 complex (Liu et al., 2014), along with pseudouridylation, facilitated by pseudouridine synthases (Schwartz et al., 2014); (Ketele et al., 2016). All this is only a small part of all the modifications that can possibly occur with RNA.

The modifications of RNA affect gene expression and regulate a lot of different pathways within a cell. Many studies have shown that the loss of Alu RNA A-to-I editing is associated with diverse human diseases including viral and autoimmune diseases. For example, reduced A-to-I editing correlates with the increased severity of COVID-19 (Crooke et al., 2021) and the incidence of systemic diseases such as multiple sclerosis (Tossberg et al., 2020), rheumatoid arthritis (Vlachogiannis et al., 2020). Additionally, recent research revealed that the loss of A-to-I editing is also associated with inflammatory bowel diseases (Aune et al., 2022). Because of such a close association of A-to-I editing with many serious diseases, it can be a good therapeutic target or biomarker, as has been shown in many studies (Datta et al., 2023); (Liao et al., 2020); (Rodriguez Morales et al., 2023).

SINE in both humans and mice plays a critical role in various diseases. For instance, a significant relationship has been established between SINE recombination, mutation, or amplification events and human cancers (Hancks et al., 2012); (Jiang et al., 2019). SINEs were found to contribute the majority of transposable element-generated alternative splice sites in cancer genes. A number of cancer-associated genes, including CANT1, MYH11, and WHSC1, were shown to have overexpressed transposable element-derived isoforms across a range of

cancer types (Clayton et al., 2020). Plenty of different insertions of Alu elements have been associated with diseases. The predominant mechanisms through which this occurs are alterations to normal splicing patterns, exonic insertions causing loss-of-function mutations, and large genomic deletions (Pfaff et al., 2022). Additionally, Alu RNA accumulation induces epithelial-to-mesenchymal transition. Moreover, this process is associated with the progression of cancer (Ruocco et al., 2018). In addition, an increase in the level of Alu insertions leads to impaired functioning of blood cells (Roos et al., 2018).

Experiments on mouse models have shown that an increased number of B2 insertions leads to disruption of molecular processes in cells (Leong et al., 2012). Another striking example, is studies of rat models have shown, that in the juvenile brain of maternal immune activation exposed rat offspring the dysregulation of B2 SINE expression in the prefrontal cortex as a response to stress (Richter et al., 2023). Also, the processing of B2 is considered dysfunctional during amyloid beta toxicity and pathology in the mouse hippocampus due to increased levels of B2 RNA processing, leading to constitutively elevated B2 RNA target gene expression, as shown in the mouse model of Alzheimer’s disease. In amyloid beta pathology, this could be a potential pathway contributing to the deregulation of many processes within the cell (Cheng et al., 2020).

In addition, an increased presence of SINE RNA was found in neurons obtained from patients with Parkinson's disease. This finding may shed light on new disease mechanisms and provide insight into the epigenetic landscape of sporadic Parkinson's disease, which is particularly regulated by small RNAs (Schulze et al., 2018); (Zhang et al., 2023); (Tshilenge et al., 2024). Generally, transposable elements are involved in the progression of Alzheimer's disease, and SINEs are known to participate in disease pathogenesis (Mustafin and Khusnutdinova, 2024). Furthermore, a recent study revealed that in Alzheimer's disease, the rate of Alu RNA processing is elevated. While increased levels of intact Alu RNA correlate with downregulated gene expression in Alzheimer's disease patients, enhanced Alu RNA processing correlates with the activation of upregulated genes in these patients (Cheng et al., 2021).

Also, many studies have shown that Alu elements are modulating the progression of macular degeneration of retinal pigmented epithelium (Kaneko et al., 2011). In more detail, the accumulation of Alu RNAs due to DICER1 deficiency leads to cytotoxicity by activating the NLRP3 inflammasome and triggering toll-like receptor-independent MyD88 signaling in the cell (Tarallo et al., 2012). DICER is a large multi-domain protein, which not only is involved in the cleavage of pre-miRNAs but also has many other different functions (Vergani-Junior et al., 2021). Moreover, the same pattern

was revealed in the mouse model, where B2 accumulation leads to cytotoxicity (Sundermeier et al., 2017). In addition, the activation of the NLRP3 inflammasome facilitated by Alu elements is also one of the mechanisms of colorectal cancer progression (Magliacane Trotta et al., 2024).

1.7 Role of antisense SINEs in the cell

An intriguing but relatively unexplored feature of SINE RNAs is the activity of their often-transcribed antisense analogs, which can potentially support cellular homeostasis. For example, a recent study demonstrated that Alu repeats harbor heat shock factor (HSF) binding sites in heat shock-responsive transcripts. Also, it was shown that more ofter HSF binding sites are located in antisense Alu transcripts. This finding underlies an antisense-mediated mechanism, representing a novel component of Alu and HSF involvement in the heat shock response (Pandey et al., 2011); (Vourc'h et al., 2022).

Additionally, antisense-containing sequences can play a role in mediating various diseases. For instance, a natural long non-coding RNA antisense to the Parkinson's disease-associated gene Ubiquitin carboxyl-terminal esterase L1 (Uchl1) has been shown to enhance UchL1 protein synthesis at the post-transcriptional level in mouse (Zucchelli et al., 2015). This lncRNA requires an embedded inverted SINE B2 sequence to increase translation and the overlapping region to target its sense mRNA (Zucchelli et al., 2015). A similar mechanism was shown to occur with Tspo (translocator protein), whose transcription is regulated via a SINE B2- natural antisense transcript (Fan and Papadopoulos, 2012).

Another example is the gene Brca1 (BReast CAncer gene 1), which is a potent inhibitor of Pol III transcription during stress. However, upon inactivation of Brca1, SINE RNA activation occurs (De Brakeleer et al., 2013); (Wang et al., 2019). Given the high intronic representation of Alu sequences in Brca1 pre-mRNA, Brca1 can be post-transcriptionally repressed by activated Pol II antisense Alu transcripts, thereby returning cells to the transcriptional homeostasis of Pol III.

Investigation of these examples gave rise to a new breakthrough therapeutic strategy based on antisense long noncoding RNAs as an activator of translation of target genes (Arnoldi et al., 2022). These molecules were named SINEUPs, as they require an embedded inverted SINE B2 element for their UP-regulation of translation (Podbevšek et al., 2018). They have been shown to increase the translation of

different target genes both in mice and humans (Espinoza et al., 2021); (Schein et al., 2016); (Takahashi et al., 2018).

Moreover, many other cellular processes are regulated by antisense SINEs. For example, Staufen1 (encoded by the STAU1 gene) mediates mRNA decay, an RNA-guided protein mechanism for post-transcriptional nonsense-mediated decay (Park and Maquat, 2013). Staufen1-mediated decay is often directed by antisense SINE RNAs to the intronic and 3’ UTR regions of pre-mRNAs (LeGendre et al., 2013); (Heber et al., 2019).

Investigating how SINE RNAs and their antisense analogs self-regulate to balance the cell's response to stress and return to homeostasis will uncover a novel negative feedback loop with broad implications for transcriptome and cellular regulation.

1.8 Rationale

1.8.1 Hypothesis

Despite extensive research efforts, our understanding of SINE RNAs remains limited beyond their established roles in regulating cellular responses to stress stimuli and their associations with various diseases. SINE RNAs have been implicated in a range of cellular functions, yet the full scope of their regulatory capabilities and mechanisms is not entirely understood. Specifically, while it is known that antisense SINE RNAs are also produced within cells and may participate in critical biological processes (Kaneko et al., 2011), the potential interactions between sense and antisense SINE RNAs have not been thoroughly investigated. This aspect of SINE RNA biology represents a significant knowledge gap in the field.

Addressing this gap is crucial as it could substantially enhance our understanding of the regulatory networks involving SINE RNAs. Our working hypothesis suggests a model in which sense SINE RNAs might inhibit the transcriptional activity of RNA polymerase II on antisense SINE RNAs. Conversely, it is posited that antisense SINE RNAs might regulate the expression of sense SINE RNAs. These bidirectional regulatory interactions between sense and antisense SINE RNAs could constitute a novel layer of gene regulation, with implications for understanding cellular homeostasis and responses to environmental changes.

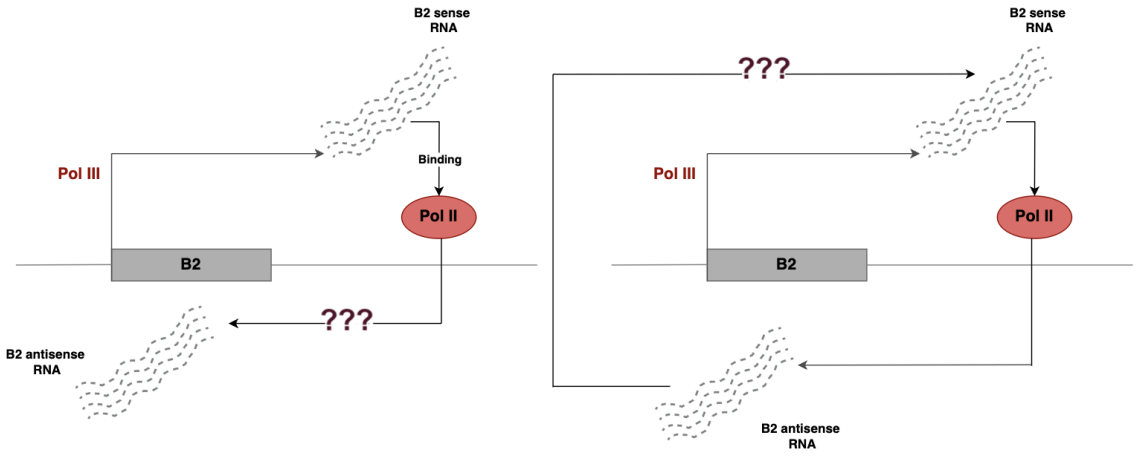

Figure 1.3: Hypothesis of sense/antisense SINE RNA regulation.

Therefore, the overarching goal of this project is to identify and characterize the reciprocal effects of sense and antisense SINE RNA expression (see aims section below). By clarifying these regulatory functions, I hope to gain a deeper understanding of SINE RNAs' role in cellular physiology and their potential contribution to disease development. Such insights could pave the way for novel therapeutic strategies targeting SINE RNA pathways, offering new avenues for treating diseases associated with their dysregulation.

1.8.2 Aims

• **Aim 1:** To identify if changes in the expression of the antisense B2 RNA can affect the expression of sense B2 RNA.

• **Aim 2:** To identify if changes in the expression of the sense B2 RNA can affect the expression of antisense B2 RNA.

Chapter 2. Methods

2.1 Cell culture

For cell culture, I utilized NIH-3T3 cells, a well-established fibroblast cell line originally derived from the tissue of an NIH Swiss mouse embryo. These cells are widely used in research due to their robust growth characteristics. The NIH-3T3 cells were cultured in a high-glucose Dulbecco's Modified Eagle Medium (DMEM, Sigma), which was carefully formulated to support optimal cell growth and metabolism. The medium was supplemented with 1% penicillin-streptomycin (5,000 U/mL, Gibco) to provide broad-spectrum antibiotic protection, minimizing the risk of bacterial contamination. Additionally, 10% fetal calf serum (FCS, Sigma) was added to supply essential growth factors, hormones, and nutrients necessary for cell proliferation. To further support cell growth, 1% L-glutamine (200 mM; Gibco) was included as a vital source of amino acids and as an energy substrate.

The cells were maintained in T75 flasks, each containing 10 ml of the complete medium, and incubated at 37°C in a humidified atmosphere with 5% CO2. This controlled environment ensured the cells remained healthy and proliferative.

Cell passaging, a procedure to prevent over-confluency and maintain cell health, was carried out at approximately 70-80% confluency. To detach the adherent cells, 5 ml of Trypsin-EDTA (0.25%, Gibco) was added to the flask, followed by incubation at 37°C for 5 minutes. The trypsin enzymatically cleaved the proteins anchoring the cells to the flask surface. To neutralize the trypsin and prevent over-digestion, an equal volume of fresh medium was added immediately. The cells were then collected by centrifugation at 1000 rpm for 5 minutes. The resulting cell pellet was gently resuspended in fresh medium and transferred to new T75 flasks for continued culture. Before conducting any experimental assays, total RNA was extracted from the cells using the Trizol reagent (Thermo Fisher), following the supplier's protocol. This method is well-known for its efficiency in isolating high-quality RNA.

For this study's cell culture experiments, four biological replicates were used, consistent with previous studies (Zovoilis et al., 2016); (Cheng et al., 2020). However, in cases with big standard deviations, the use of four biological replicates may not always satisfy the normal distribution assumption of the t-test.

2.2 Heat shock experiment

In preparation for the heat shock experiments, the concentration of fetal calf serum in the medium was reduced from 10% to 5% during the final cell split. This reduction was implemented to ensure a more uniform stress response. Following this adjustment, the cells were collected from the T75 flasks, pelleted by centrifugation at 1000 rpm for 5 minutes, and the resulting pellet was resuspended in fresh medium, ready for the subsequent heat shock treatment.

To induce heat shock stress, the cell cultures were exposed to a high temperature of 45°C for a precise duration of 15 minutes. This temperature is known to induce a robust cellular stress response, including the activation of heat shock proteins and other protective mechanisms. Following the heat shock induction, the samples were promptly transferred back to the standard incubator conditions (37°C with 5% CO2) to allow the cells to recover. The recovery process was carefully monitored at specific time points: immediately (0 minutes), 5 minutes, 15 minutes, 30 minutes, 45 minutes, 1 hour, and 3 hours post-heat shock. For each time point, four biological replicates were prepared, ensuring the collection of statistically reliable data.

At each designated recovery time point, the cells were harvested by centrifugation at 1600 rpm for 5 minutes. The cell pellets were then immediately resuspended in 1 ml of Trizol reagent per sample to facilitate RNA extraction. The samples were subsequently stored at -80°C, ensuring the preservation of RNA integrity until further analysis.

2.3 Transfection of locked nucleic acids (LNAs)

To allow the NIH-3T3 cells to recover from cryopreservation, they were carefully thawed and cultured in appropriate conditions for a minimum of three days before proceeding with the transfection experiments. Cryopreservation is a method whereby cells are frozen to maintain their viability, allowing them to be stored for months or even years and then defrosted for future use. This technique is crucial for minimizing genetic changes and preventing loss through contamination. During this critical recovery period, the cells were maintained in a medium containing 5% fetal calf serum. This lower serum concentration was selected to reduce the potential variability in gene expression and ensure consistent conditions across experiments.

After the recovery phase, the cells were gently pelleted by centrifugation at 1600 rpm for 5 minutes. The pelleted cells were then resuspended in a fresh medium, following the previously described protocol. This process ensured that the cells were

adequately nourished and ready for subsequent experimental manipulations. The cells were subsequently transferred to a 6-well plate, with 1 ml of cell suspension added to each well, in preparation for the transfection procedures. This setup allowed for efficient handling and ensured uniform exposure to transfection reagents.

2.3.1 Transfection of anti-B2 sense LNAs

For the knockdown of sense B2 RNA, a specific pool of two anti-B2 sense locked nucleic acids (LNAs) was utilized. The sequences of these LNAs were carefully designed to target the B2 sense transcripts effectively. The sequences were as follows:

1. +G*+T*+T*+ACGGATGGT+T+G*+T*+G
2. +T*+A*+TAGCTGTCTT+C+A*+G*

In these sequences, the asterisk (*) denotes a phosphorothioate bond, which provides increased stability and resistance to nucleases, while + indicates an LNA modification, enhancing the binding affinity to the target RNA. These modifications were crucial for achieving efficient and specific knockdown of the target transcripts. LNAs allow for the silencing of short targets with high specificity. They are complementary to the target sequence and contain modified ribose residues, enabling them to bind to the target region. This binding leads to the degradation of the target RNA via cleavage by RNase H, an enzyme that recognizes RNA-DNA hybrids and catalyzes the cleavage of the RNA strand (Beane et al., 2007).

To serve as a negative control for the knockdown experiments, a scrambled LNA sequence was employed. This sequence, referred to as "Scramble," was designed as follows: +C*+C*+T*+CAATTTTA+T+C*+A*+C*. The scrambled LNA was chosen because it does not specifically interfere with gene expression, thereby serving as a control to differentiate the specific effects of the anti-B2 sense LNAs from non-specific effects.

The transfection procedure involved mixing the two anti-B2 sense LNAs with the HiPerfect transfection reagent (Qiagen) and water to a final volume of 20 µl per sample. This mixture was carefully prepared to achieve a final concentration of 500 nM for each LNA. Similarly, the scrambled LNA was combined with water and the HiPerfect transfection agent to the same final volume and concentration. The mixtures were then incubated at room temperature for 20 minutes, allowing for proper complex formation between the LNAs and the transfection reagent. This step was crucial to ensure efficient delivery of the LNAs into the cells.

Following the incubation, the LNA-reagent complexes were added drop-wise to the cells in the 6-well plates. The cells were then incubated under standard conditions (37°C with 5% CO2) to facilitate LNA uptake. Samples were collected at specific time points - 0 minutes (no transfection), 30 minutes, 1 hour, 3 hours, 12 hours, and 24 hours post-transfection. At each time point, four biological replicates were performed to ensure the reliability and reproducibility of the data. After the designated incubation periods, the cells were harvested by centrifugation, and the cell pellets were stored in Trizol reagent, as previously described.

2.3.2 Transfection of anti-B2 antisense LNAs

For the knockdown of antisense B2 RNA, a different pool of three anti-B2 antisense LNAs was used. These LNAs were specifically designed to target the antisense B2 transcripts, with sequences as follows:

1. +A*+G*+T*+TCAAATCCC+A+G*+C*+A*
2. +A*+G*+T*+TCAATTCC+C+A*+G*+C*
3. +A*+G*+T*+TCAAATCC+C+A*+G*+C*

Here, the asterisk (*) represents a phosphorothioate bond, and the plus sign (+) indicates an LNA modification. These modifications were essential for the specificity and stability of the LNAs, enabling effective targeting of the antisense transcripts.

A scrambled LNA sequence, identical to the one used for the sense B2 knockdown experiments (+C*+C*+T*+CAATTTTA+T+C*+A*+C*), was also employed as a negative control. This control was vital to confirm that any observed effects were specific to the targeted antisense B2 RNA and not due to off-target interactions.

The transfection process for the anti-B2 antisense LNAs followed a similar protocol to that of the sense LNAs. The HiPerfect reagent was mixed with the three anti-B2 antisense LNAs and water, achieving a final concentration of 500 nM for each LNA and a total volume of 30 µl per sample. The preparation, incubation, and addition of the complexes to the cells were carried out as described previously, ensuring consistency across all transfection experiments.

The cells were incubated under standard conditions post-transfection, and samples were collected at the specified time points to monitor the effects of the knockdown. This included careful harvesting, RNA extraction, and storage, all following standardized protocols to maintain data integrity.

This comprehensive approach allowed for the detailed investigation of the roles of sense and antisense B2 RNAs in the cellular context, providing valuable insights into their regulatory mechanisms. The use of LNAs, with their high specificity and stability, ensured the accuracy and reliability of the knockdown experiments, while the inclusion of scrambled controls validated the specificity of the observed effects.

2.4 B2 RNA synthesis and transfection

2.4.1. RNA in vitro trascription

A Mm1a B2 g-block was ordered from IDT for the purpose of in vitro transcription. The g-block had the following sequence:
5'-
taatacgactcactataGGGGCTGGTGAGATGGCTCAGTGGGTAAGAGCACCCGACTG
CTCTTCCGAAGGTCCGGAGTTCAAATCCCAGCAACCACATGGTGGCTCACAACC
ATCCGTAACGAGATCTGACTCCCTCTTCTGGAGTGTCTGAAGACAGCTACAGTG
TACTTACATATAATAAATAAATAAA TCTTTAAAAAAAAA -3'.

In this sequence, the lowercase letters represent the T7 promoter sequence, which is a crucial component for initiating transcription. The T7 promoter sequence serves as a binding site for the T7 RNA polymerase, enabling the transcription of the downstream DNA sequence into RNA. This promoter is commonly used in molecular biology for the high-yield production of RNA in vitro. The design of the g-block ensured that the promoter was positioned at the 5' end, facilitating efficient transcription initiation.

The template was subsequently amplified by polymerase chain reaction (PCR), a standard technique for amplifying specific DNA sequences. The amplification utilized the T7 promoter as the forward primer and a B2-specific reverse primer, as detailed in Table 2.1. The primers were designed to flank the region of interest, ensuring the accurate amplification of the target sequence. For this process, the Q5 High-Fidelity DNA polymerase kit (NEB) was used, chosen for its high accuracy and fidelity, which are essential for minimizing errors during amplification.

The reaction mixture for the PCR included primers diluted to a final concentration of 20 mM, 5x Q5 Buffer, 10 mM dNTPs, and Q5 DNA polymerase, along with the B2-template. The PCR conditions were optimized to achieve efficient amplification: an initial denaturation step at 98°C for 30 seconds to separate the DNA strands, followed by 35 cycles of denaturation at 98°C for 5 seconds, annealing at 58°C for

10 seconds, and extension at 72°C for 10 seconds. A final extension step at 72°C for 10 minutes ensured the complete synthesis of the PCR products. These conditions were carefully selected to maximize yield and specificity while minimizing non-specific amplification.

The resulting PCR product was verified using agarose gel electrophoresis, a technique that separates DNA fragments based on size. The samples were loaded onto an agarose gel and subjected to an electric field, causing the DNA fragments to migrate through the gel matrix. The bands corresponding to the expected length of the amplified product were excised from the gel. The DNA was then purified using the BioBasic EZ-10 gel extraction kit, which efficiently removes impurities and concentrates the DNA. This purified DNA served as the template for subsequent PCR amplifications, ensuring a high-quality starting material for further experiments.

To further purify and concentrate the PCR products, the Oligo Clean and Concentrator kit (Zymo Research) was employed. This step was crucial for removing any remaining contaminants and concentrating the DNA to a suitable level for in vitro transcription. The purified DNA was quantified and verified for quality before proceeding to the transcription step.

For the in vitro transcription, the Hiscribe T7 High Yield RNA Synthesis Kit (NEB) was utilized. This kit is designed for the efficient synthesis of RNA using the T7 RNA polymerase. The reaction setup included 1 µg of template DNA, 10x Reaction Buffer, 10 mM DTT (a reducing agent that helps maintain the stability of the enzyme), 1.5 µl of each NTP (ATP, CTP, GTP, and UTP), and T7 RNA Polymerase Mix. The reaction mixture was brought to a final volume of 20 µl with water. The samples were incubated at 37°C for 2 hours, allowing for the transcription of the DNA template into RNA. This incubation period was optimized to ensure maximum yield of RNA.

Following transcription, the synthesized RNA was purified using the 'Zymo Research RNA Clean and Concentrator - 25' kit. This purification step is essential for removing any residual DNA, proteins, or other impurities that may interfere with downstream applications. The purified RNA was then subjected to quality control analyses to assess its integrity and concentration.

To evaluate the quality of the synthesized RNA, the samples were analyzed by polyacrylamide gel electrophoresis (PAGE) using a 10-15% gel. PAGE allows for the resolution of RNA molecules based on their size, providing a detailed analysis of the RNA products. The gel was stained with SYBR II (Invitrogen), a nucleic acid stain that binds to RNA and fluoresces under UV light. The stained gel was examined under UV light to visualize the RNA bands. The appearance of distinct, sharp bands indicated the successful synthesis of high-quality RNA.

Table 2.1 Primers for in-vitro transcription

Primer name	*Sequence*
T7 promoter	*5’- TAATACGACTCACTATAG -3’*
B2 reverse	*5’- TTTTTTTTTAAAGATTTATTTATTTATTATATGTAAGTACA -3’*

3.4.2 Transfection of full-length B2 RNA

For the transfection experiments involving full-length B2 RNA, a precisely measured amount of 16 pmol of B2 RNA was utilized per sample. This RNA amount was carefully chosen to ensure adequate delivery into the cells while minimizing potential toxicity. The RNA was initially combined with 2 µl of enhancer (QIAGEN) and EC Buffer (QIAGEN), with the final volume adjusted to 100 µl. The purpose of the enhancer and buffer combination is to facilitate the efficient formation of transfection complexes. The mixture was incubated for 5 minutes at room temperature to allow proper complex formation, which is a crucial step in ensuring the RNA is adequately packaged and protected for cellular delivery.

Following this initial incubation, 8 µl of TransMessenger Transfection Reagent (QIAGEN) was added to the mixture. This reagent is specifically designed to mediate the delivery of RNA into mammalian cells. Another 10-minute incubation at room temperature was performed to further facilitate the formation of transfection complexes. This step ensures that the RNA is efficiently bound to the transfection reagent, forming stable complexes capable of being taken up by the cells.

The NIH-3T3 cells were prepared for transfection. These cells had been cultured in a medium containing 5% serum for at least two days prior to the experiment. The reduced serum concentration helps to prime the cells for transfection, as serum components can sometimes interfere with transfection efficiency. The cells were harvested by pelleting, a process that involves centrifugation to collect the cells at the bottom of the tube. They were then resuspended in a serum-free (0%) medium to remove any residual serum that could affect the transfection process.

The cells were subsequently seeded into 6-well plates, with 500 µl of the cell suspension carefully added to each well. This seeding was done immediately before the transfection process to ensure that the cells were evenly distributed and in optimal condition for uptake of the RNA complexes. The use of serum-free medium

at this stage is critical, as serum can inhibit the transfection efficiency of certain reagents, including TransMessenger reagent.

Each time point in the experiment was conducted with three biological replicates, ensuring the reliability and reproducibility of the results. Biological replicates are essential in experimental biology as they account for biological variability and help to validate the findings. The prepared transfection mixture was added drop-wise to the cells, a method that facilitates uniform distribution of the transfection complexes across the cell culture. The cells were then incubated at 37°C in a 5% CO2 atmosphere for 30 minutes. This controlled environment is standard for maintaining mammalian cell cultures and provides the necessary conditions for cellular uptake of the transfection complexes.

After this initial incubation period, which allowed for sufficient uptake of the RNA, 500 µl of medium containing 10% fetal calf serum was added to each well. The addition of serum serves to terminate the transfection process, stabilizing the cellular environment and providing essential nutrients for cell recovery and growth. This step is crucial as it helps to minimize any potential cytotoxic effects from the transfection reagents and ensures the cells can continue to proliferate and function normally.

The cells were then further incubated under the same conditions (37°C in a 5% CO2 atmosphere) for subsequent time points: 0 minutes, 6 hours, and 24 hours post-transfection. These specific time points were chosen to monitor the immediate and longer-term effects of the RNA transfection, providing a comprehensive overview of the cellular response over time.

As a negative control for the transfection experiments, Tet150 RNA was utilized. The use of a negative control is essential in experiments to establish a baseline and to ensure that any observed effects are due to the transfection of the target RNA (in this case, full-length B2 RNA) rather than non-specific effects. Tet150 RNA does not interfere with gene expression, thus serving as a baseline for comparison.

The sequence of the Tet150 RNA is as follows: 5’-
TAATACGACTCACTATAGGGTTACCGTACGTACCTCAACAGGTGATGACACAATG
TGATTTCTGCCCAGTGCTCTGAATGTCAAAGTGACGCAATTCAACCAAGCGCGG
GTAAACGGCGGGGAGTAACTATGACTCTCTAAATAGCA -3’.

The Tet150 RNA sequence is specifically chosen to not target or interfere with any known cellular processes, ensuring that any experimental effects observed with the full-length B2 RNA are not due to off-target interactions or other non-specific factors. The integrity and efficacy of the transfection process were confirmed by careful monitoring and analysis of the transfected cells at each designated time point.

2.5 Reverse transcription and quantitative PCR

Before reverse transcription, RNA quality was assessed using a Bioanalyzer, and RNAs with an RIN score of less than two were excluded.

To accurately quantify the levels of B2 RNA, extracted RNA samples underwent reverse transcription, utilizing the Superscript IV reverse transcriptase (Invitrogen). The reverse transcription process is crucial for converting RNA into complementary DNA, enabling subsequent quantitative PCR (qPCR) analysis.

For each reverse transcription reaction, 50 ng of total RNA was used. This RNA was initially combined with 1 µl of 10 mM random primers (New England Biolabs) and 1 µl of 10 mM dNTPs. Random primers are short sequences that anneal at random locations along the RNA, providing a starting point for cDNA synthesis. The mixture was then heated to 65°C for 5 minutes. This denaturation step is critical as it breaks the hydrogen bonds between RNA strands, ensuring the RNA is single-stranded and accessible for primer binding. Immediately after heating, the mixture was placed on ice to quickly cool the reaction, preventing the RNA from re-annealing.

Following this denaturation step, several components were added to the reaction mixture to initiate the reverse transcription. These included 4 µl of 5x First Strand Buffer (Invitrogen), which provides the necessary ionic strength and optimal conditions for the enzyme, 1 µl of 0.1 M DTT (Invitrogen), a reducing agent that helps maintain the stability and activity of the reverse transcriptase, and 1 µl of Superscript IV reverse transcriptase. The inclusion of DTT is particularly important as it prevents oxidation of the enzyme's sulfhydryl groups, preserving its catalytic function.

The reaction mixture was then incubated at 23°C for 10 minutes. This temperature is optimal for the annealing of random primers to the RNA template, allowing for efficient priming of the reverse transcription process. Following primer annealing, the reaction was incubated at 55°C for 10 minutes. This step facilitates the synthesis of cDNA by the reverse transcriptase, as the enzyme synthesizes a complementary DNA strand by extending from the annealed primer. The reaction was then terminated by heating at 80°C for 10 minutes, a step that inactivates the reverse transcriptase and ensures the reaction does not continue indefinitely.

To specifically quantify the sense and antisense B2 RNAs, gene-specific primers were employed instead of random primers. Gene-specific primers bind to specific

sequences within the target RNA, allowing for precise quantification of particular RNA species. The sequences and details of these primers are outlined in Table 2.2.

Following the reverse transcription, the resulting cDNA was subjected to qPCR using the Luna Universal qPCR mix (NEB). qPCR is a highly sensitive technique that quantifies nucleic acids in real-time, providing accurate measurements of gene expression levels. The cDNA generated was diluted 1:10 in water, ensuring that the concentration was within the optimal range for accurate quantification. Each qPCR reaction contained 5 µl of Luna master mix, which includes DNA polymerase, dNTPs, and other components necessary for the amplification reaction. Additionally, 0.5 µl of 10 mM gene-specific primers (each) was included in the reaction, along with the diluted cDNA. The reaction volume was adjusted to a final volume of 10 µl with water.

To facilitate the accurate quantification of target gene expression, standard dilution pools for qPCR were generated. These pools consist of serially diluted cDNA samples, creating a series of known concentrations that are used to generate a standard curve. The standard curves enable the precise determination of unknown sample concentrations by comparing their qPCR signals to the signals from the standards. The qPCR reactions were performed and analyzed using the Bio-Rad CFX384 Real-Time Detection System, a robust platform for high-throughput gene expression analysis.

The thermocycler conditions for the qPCR were as follows: an initial denaturation step at 95°C for 3 minutes, which activates the DNA polymerase and denatures the cDNA, followed by 40 cycles of amplification. Each cycle consisted of denaturation at 95°C for 15 seconds, annealing at 54°C for 30 seconds, and extension at 66°C for 30 seconds. These specific temperatures and times were optimized for the primers used, ensuring efficient and specific amplification of the target sequences.

To determine relative gene expression levels, standard curve analysis was performed. Standard curves were prepared by serially diluting a mixture of cDNA samples into a series of dilutions (SD1:1:2, SD2:1:4, SD3:1:8, SD4:1:16, SD5:1:32). This dilution series allows for the creation of a standard curve that relates the cycle threshold (Ct) values obtained during qPCR to the concentration of the target gene, enabling precise quantification.

To ensure the accuracy and reliability of the qPCR results, housekeeping genes GAPDH and HPRT, along with the Pol-III transcribed gene 7SK, were used as normalization controls. These genes are commonly used as internal controls because their expression levels remain relatively constant across different experimental conditions. The use of these controls allows for the normalization of

gene expression data, accounting for any variations in RNA quantity and quality. For each qPCR assay, three technical replicates were performed per sample, ensuring the reproducibility and robustness of the data.

Table 2.2 Primers for reverse transcription of B2 and qPCR

Primer name	*Sequence*
B2 forward	*5'- GGGGCTGGTGAGATG -3'*
B2 reverse	*5'- AGCTGTCTTCAGACACTCC -3'*
GAPDH (mouse) forward	*5'- ACCACAGTCCATGCCATCAC -3'*
GAPDH (mouse) reverse	*5'- TCCACCACCCTGTTGCTGTA -3'*
HPRT (mouse) forward	*5'- TCCTCCTCAGACCGCTTTT -3'*
HPRT (mouse) reverse	*5'- CCTGGTTCATCATCGCTAATC -3'*
7SK (mouse) forward	*5'- GTTGTGGTATTTGGCACCCC -3'*
7SK (mouse) reverse	*5'- GAGCTACTCGGACAGCCTTG -3'*

2.6 Bioinformatics analysis of short RNA-seq and long RNA-seq data

All data for the analysis of short-RNA-seq and long-RNA-seq utilized in this study were obtained from a public functional genomics data repository. Specifically, the data were sourced from the GSE82255 series of SRA files. These files were initially in the Sequence Read Archive (SRA) format and were converted to the fastq format using SRA Tools version 3.1.1 (https://github.com/ncbi/sra-tools) (Li et al., 2009). The conversion process was executed for each file using the command: $fasterq-dump /filename. Once the data were in fastq format, they were aligned to the mouse genome (UCSC mm39) using the BWA-0.7.18 (r1243) aligner (https://github.com/lh3/bwa) in single-end mode, employing default alignment parameters (Li and Durbin, 2009); (Li and Durbin, 2010).

To focus specifically on B2 elements, the sequences of all B2 subfamilies, including B2_Mm1a, B2_Mm1t, and B2_Mm2, were retrieved from the UCSC Table Browser.

To ensure high data quality and prevent potentially spurious alignments, sequences shorter than 100 bp were excluded from the analysis.

The aligned SAM files, along with the filtered list of B2 sequences, were subsequently imported into SeqMonk 1.48.1, a program designed for the visualization and analysis of mapped sequence data.(https://www.bioinformatics.babraham.ac.uk/projects/seqmonk/)

This software was instrumental in creating a model of the distribution of read fragments within the B2 loci, with a specific focus on the B2_Mm1a, B2_Mm1t, and B2_Mm2 subfamilies.

To further investigate the occurrences of B2 elements in the genome, specialized probes were created from the list of B2 subfamilies. These probes allowed for the identification and display of B2 elements' occurrences within the genome. The analysis distinguished between B2 sense and B2 antisense RNAs, with each being analyzed separately. For the analysis of B2 sense, the "same strand as probe" mode was selected. This was because all sequences in the original list of B2 subfamilies were oriented in the sense direction, enabling the identification of all occurrences of B2 sense in the genome. To visualize the expression changes of B2 sense under various conditions, such as heat shock stress, a graph was plotted using the "Relative Distribution Plot" setting. Specific parameters were chosen: -50 base pairs and 210 base pairs, with +1 representing the first nucleotide in the B2 sense sequence. Given that the average length of B2 elements is approximately 200 nucleotides, these settings ensured the inclusion of the entire B2 sequence in the analysis.

For the analysis of B2 antisense, the "opposite to a probe" mode was selected to identify all occurrences of antisense B2 in the genome. The subsequent analysis followed the same procedure as described for B2 sense, including the creation of a "Relative Distribution Plot" graph. The parameters used mirrored those for the B2 sense analysis, ensuring consistency in the examination of both sense and antisense RNA expression.

2.7 Library preparation for direct RNA-sequencing and bioinformatics analysis

To accurately synthesize complementary DNA (cDNA) from RNA for sequencing purposes, a total of 750 ng of total RNA was subjected to reverse transcription using the Superscript III reverse transcriptase (Invitrogen). This process was carried out in

conjunction with a reverse transcription adapter ligation, as outlined in the Direct RNA Sequencing Kit SQK-RNA004 (Oxford Nanopore Technologies). The integration of adapter ligation enhances the efficiency and specificity of the subsequent sequencing steps.

The procedure began with the preparation of a ligation mixture, essential for attaching the reverse transcription adapter to the RNA. Specifically, 3 µl of Quick Ligation Reaction Buffer (New England Biolabs, NEB) was mixed with 1 µl of the reverse transcription adapter and 1.5 µl of T4 DNA Ligase (NEB). The Quick Ligation Reaction Buffer provides the necessary ionic environment to facilitate the ligation process, while the T4 DNA Ligase catalyzes the formation of a covalent bond between the adapter and the RNA. This prepared ligation mixture was added to the RNA sample and incubated at room temperature for 15 minutes. This incubation period is critical for ensuring the efficient ligation of the adapter, which is a key step in the preparation of the RNA for reverse transcription.

For the reverse transcription step, another mixture was prepared. This mixture contained 2 µl of 10 mM dNTPs (NEB), which provide the building blocks for DNA synthesis, 8 µl of 5x First Strand Buffer, which maintains the optimal conditions for the enzyme's activity, 4 µl of 0.1 M DTT, a reducing agent that preserves the enzyme's activity by maintaining a reducing environment, and 2 µl of Superscript III reverse transcriptase. The addition of Superscript III reverse transcriptase is crucial as it synthesizes the complementary DNA strand from the RNA template, thus converting RNA into cDNA. This reaction mixture was then added to the RNA sample, and the entire mixture was incubated under controlled conditions: 50 minutes at 50°C to enable the synthesis of the cDNA strand, followed by 10 minutes at 70°C to inactivate the enzyme, ensuring that the reaction does not continue indefinitely and preventing any potential degradation of the synthesized cDNA.

Post-reverse transcription, the resulting RNA-DNA duplexes were purified using 1.8x Omega NGS Total Pure Mag Beads. These magnetic beads facilitate the separation of the RNA-DNA duplexes from unincorporated components, such as free nucleotides and enzymes, ensuring the purity of the cDNA for downstream applications. The purification step is vital for removing any impurities that could interfere with subsequent sequencing steps.

To ensure the proper orientation of RNA during sequencing, an RNA adaptor ligation step was conducted. This step is crucial for aligning the RNA correctly in the sequencing apparatus, allowing for accurate data collection. For this purpose, 8 µl of Quick Ligation Reaction Buffer was mixed with 6 µl of RMX and 3 µl of T4 DNA Ligase. RMX is a component that aids in the orientation and alignment of RNA for sequencing. The mixture was incubated at room temperature for 15 minutes,

allowing the ligation of the RNA adaptor. Following this, a cleanup was performed using 1x Omega NGS Total Pure Mag Beads. This cleanup step was essential to remove any excess reagents and adapters, thereby ensuring that only the properly ligated RNA was retained. This purification is critical for achieving high-quality sequencing results, as any excess reagents could potentially interfere with the sequencing process.

Next, all samples were meticulously processed following the detailed instructions provided by the SQK-RNA004 kit supplier. This final processing step is essential for preparing the samples for sequencing, ensuring that they meet the necessary quality and concentration requirements for accurate and reliable data collection.

After sequencing, the obtained fastq files were aligned to the mouse genome (UCSC mm39) using Minimap2-2.28 (r1209) (https://github.com/lh3/minimap2), a highly efficient tool for sequence mapping (Li, 2018). Minimap2-2.28 produces output files that include coordinates of read matches to genome parts. These files rank the matches from the highest to the lowest alignment quality, as exact matches are not always guaranteed. To ensure the accuracy of subsequent analyses, it was crucial to retain only those reads with the best matches. Therefore, a Python script was employed to filter out and retain only the highest-quality primary reads.

The aligned SAM files, which now included only the high-quality primary reads, were then processed further using SeqMonk 1.48.1 (https://www.bioinformatics.babraham.ac.uk/projects/seqmonk/).

This software was used to visualize and analyze the mapped sequence data, following the methodology outlined in the previous steps (2.7 Library preparation for direct RNA-sequencing and bioinformatics analysis). By adhering to this consistent approach, both accuracy and reliability in the identification and analysis of B2 elements were ensured.

For comparison of the plots, the Kolmogorov-Smirnov test (KS test) was used.

Chapter 3. Results

3.1 Changes in B2 SINE RNA levels in response to heat shock stress

Heat shock is one of the canonical ways of putting stress on a cell and is therefore often used in research. One immediate response during stress is to suppress the transcription of certain cellular genes - an adaptation to suppress the expression of unnecessary genes. An equally important immediate response is the activation of transcription of so-called “early genes” - genes activated within the first 15 minutes to protect against cell damage and promote the re-folding or removal of damaged cell structures (Murray et al., 2004). It is known that in response to heat shock, the B2 level increases (Allen et al., 2004); (Zovoilis et al., 2016).

Additionally, during the response to this kind of stress, B2 RNA binds to POL-II, blocks its activity and thereby changes the level of gene expression, reducing the rate of mRNA transcription (Espinoza et al., 2007). At the same time, it is interesting that during heat shock B2 interacts with various proteins, such as EZH2 and HSF1, which leads to accelerated self-cleavage of B2 (Zovoilis et al., 2016); (Cheng et al., 2020).

However, the interplay between these processes and the temporal dynamics of B2 RNA levels post-stress remains unclear. Specifically, how the levels of SE and AS B2 RNAs change after heat shock, and whether these changes affect each other, is not well understood. Therefore, here we wanted to investigate how SE and AS B2 RNA levels vary over time following heat shock. To do so, we designed an experiment (Figure 3.1.1) in which we subjected mouse fibroblasts NIH-3T3 to heating to 45°C for 15 minutes and after that stress gave the cells different recovery times, from 0 minutes to 3 hours. 0 minutes correspond to the 15 minutes of heat shock (start of recovery time). After that, RNA was extracted from the cells and used for subsequent analyses, including quantitative PCR and RNA sequencing (more detailed in Chapter 2.). This cell line and heating conditions were selected based on their previous use in studies on B2 RNA (Zovoilis et al., 2016); (Allen et al., 2004).

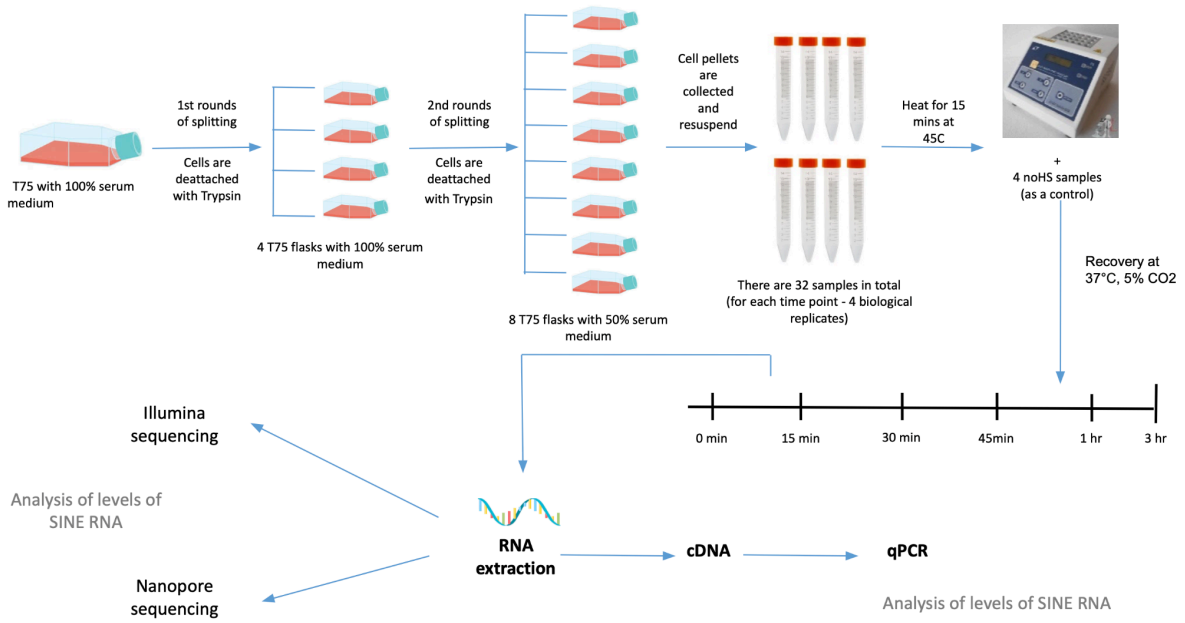

Figure 3.1.1: The workflow of the heat shock experiment.

3.1.1 Total B2 SINE RNA expression level

Initially, I aimed to investigate how the levels of B2 RNA change over time following recovery from heat shock. To achieve this, I prepared complementary DNA from the extracted RNA using random primers and conducted qPCR to measure the levels of total B2 RNA. In this context, "total B2" refers to both SE and AS B2 RNAs.

Results indicate that the level of total B2 RNA increases during the first 15 minutes of recovery, followed by a slight decrease at the 45-minute mark. This decrease is then followed by a rise in B2 levels by the 60th minute, with a subsequent decline observed by the 3-hour time point (Figure 3.1.2). Statistical analysis reveals that all post-heat shock expression levels differ significantly from pre-heat shock values (Table 3.1, two-tailed t-test). The pattern of B2 expression over time does not follow a linear trend but instead shows fluctuations, with peak values at 15 minutes and 60 minutes of recovery following the stress.

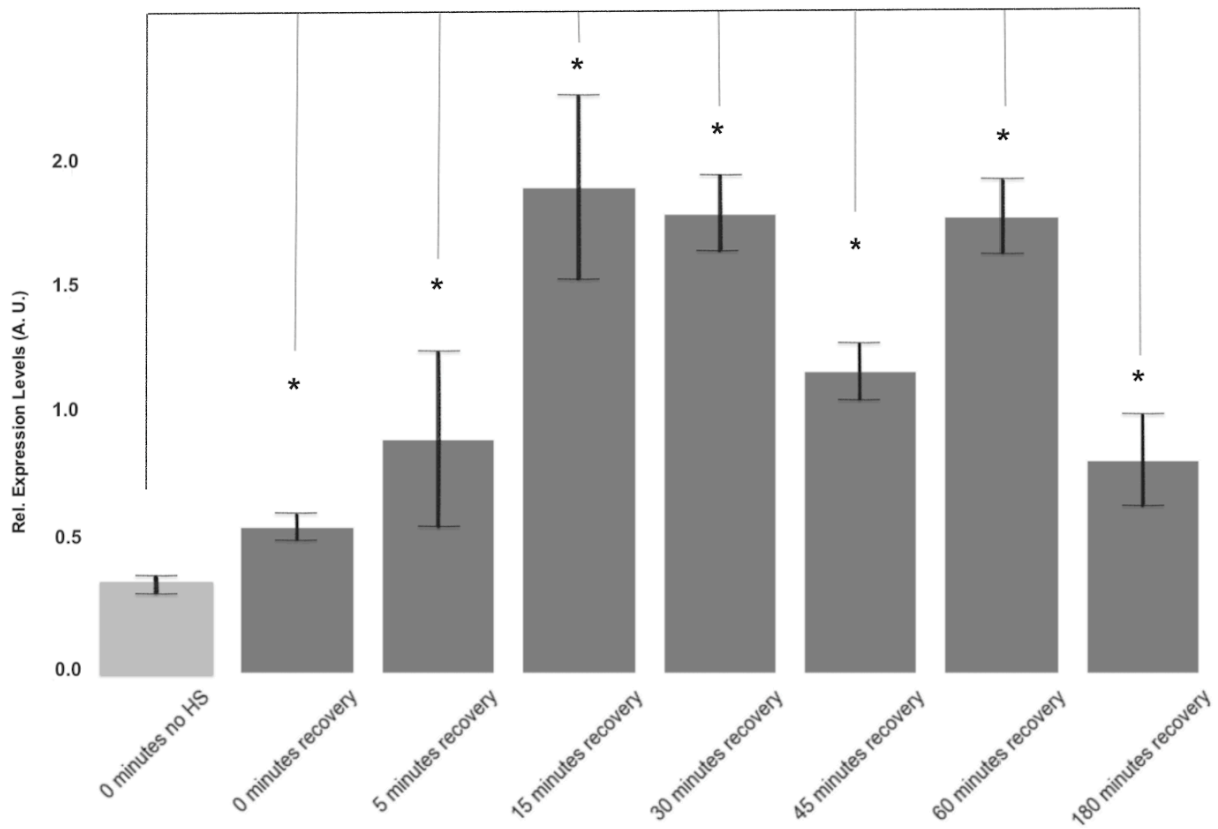

Figure 3.1.2: qPCR results. Total B2 levels normalized with GAPDH level.
Light grey represents the level of total B2 in pre-HS cells, dark grey represents the post-HS level of total B2. $p < 0.05$ is depicted as an asterisk, t-test two-tailed. Error bars denote standard deviation (n=4). All statistics for this graph are in Table 3.1. Standard curves for qPCR quality assessment are in Figure A1.

These findings align with previous studies that reported an increase in B2 expression immediately after heat shock (Allen et al., 2004; Zovoilis et al., 2016). However, the cause of the subsequent decrease in expression levels and the observed fluctuations remains unclear.

It is important to note that the qPCR data does not distinguish between full-length B2 RNA and its fragmented forms. The qPCR results reflect the combined expression of both intact B2 RNA and its fragments. Previous studies have shown that B2 RNAs are subject to active fragmentation by various proteins (Zovoilis et al., 2016); (Cheng et al., 2020).

To verify these results and gain further insights, it will be essential to analyze sequencing data, which will be addressed in subsequent sections. Additionally, to

understand how SE and AS B2 RNAs might regulate each other following stress, it is necessary to examine their expression levels separately, as the expression data presented in Figure 3.1.2 includes both SE and AS RNAs.

Table 3.1 Statistics for qPCR results for heat shock experiment for total B2

Condition 1	*Condition 2*	*p-value*	*Significance*
T0 NoHS	*T0 HS*	*0.0031*	*Significant*
T0 NoHS	*T5 HS*	*0.0474*	*Significant*
T0 NoHS	*T15 HS*	*0.0018*	*Significant*
T0 NoHS	*T30 HS*	*0.00008*	*Significant*
T0 NoHS	*T45 HS*	*0.0002*	*Significant*
T0 NoHS	*T60 HS*	*0.00007*	*Significant*
T0 NoHS	*T180 HS*	*0.0111*	*Significant*
T0 HS	*T5 HS*	*0.1584*	*Not Significant*
T0 HS	*T15 HS*	*0.0032*	*Significant*
T0 HS	*T30 HS*	*0.00018*	*Significant*
T0 HS	*T45 HS*	*0.0009*	*Significant*
T0 HS	*T60 HS*	*0.00017*	*Significant*
T0 HS	*T180 HS*	*0.075*	*Significant*

3.1.2 Sense B2 SINE RNA

To investigate how sense B2 expression responds to stress, we prepared complementary DNA from RNA extracted from cells using SE B2-specific primers and conducted qPCR analysis.

The results, as shown in Figure 3.1.3, reveal that SE B2 expression initially increases during the first 5 minutes of recovery. This increase is followed by a decline at the 15-minute mark. SE B2 levels then rise again, peaking at the 30-minute time point. Following this peak, SE B2 expression drops to a minimum at

45 minutes, before rising again at the 1-hour and 3-hour time points. Statistical analysis of these results is provided in Table 3.2, using a two-tailed t-test.

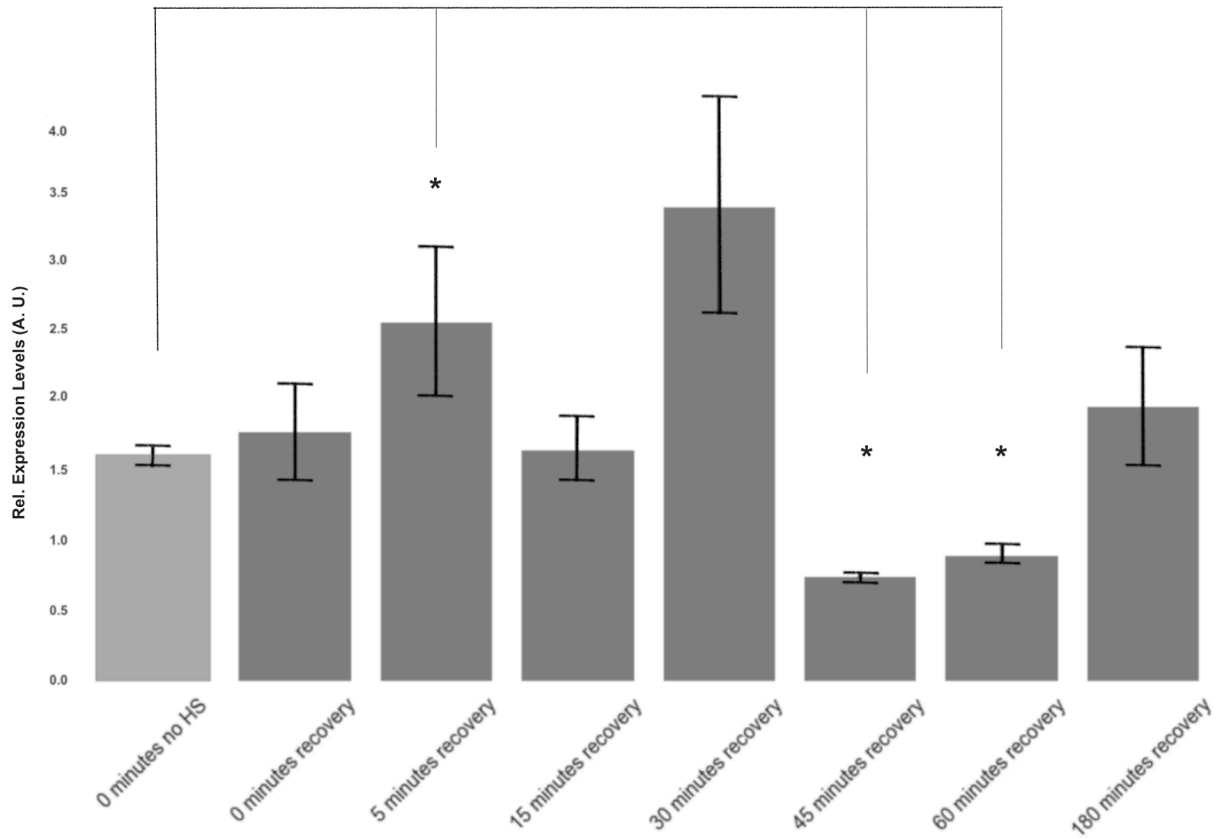

Figure 3.1.3: qPCR results. Sense B2 levels normalized with GAPDH level.
Light grey represents the level of sense B2 in pre-HS cells, dark grey represents the post-HS level of sense B2. $p < 0.05$ is depicted as an asterisk, t-test two-tailed. Error bars denote standard deviation (n=4). All statistics for this graph are in Table 3.2. Standard curves for qPCR quality assessment are in Figure A2.

The observed changes in SE B2 expression over time do not follow a linear pattern. While the trend initially resembles that of total B2 expression, the reasons behind the fluctuations in SE B2 levels remain unclear. Further analysis of sequencing data, which will be detailed in subsequent sections, may provide insights into these variations and help elucidate the underlying mechanisms.

Table 3.2 Statistics for qPCR results for heat shock experiment for sense B2

Condition 1	*Condition 2*	*p-value*	*Significance*

T0 NoHS	*T0 HS*	*0.4784*	*Not Significant*
T0 NoHS	*T5 HS*	*0.0381*	*Significant*
T0 NoHS	*T15 HS*	*0.8317*	*Not Significant*
T0 NoHS	*T30 HS*	*0.0661*	*Not Significant*
T0 NoHS	*T45 HS*	*0.0027*	*Significant*
T0 NoHS	*T60 HS*	*0.0008*	*Significant*
T0 NoHS	*T180 HS*	*0.1319*	*Not Significant*

3.1.3 Antisense B2 SINE RNA

To evaluate how the expression level of antisense B2 RNA changes in response to heat shock stress, we prepared complementary DNA from RNA extracted from cells using AS B2-specific primers and performed quantitative PCR (qPCR).

As shown in Figure 3.1.4, the expression level of AS B2 RNA before heat shock is notably higher compared to immediately after the heat treatment. Within the first 5 minutes post-heat shock, AS B2 expression decreases sharply to a global minimum. This is followed by a significant increase by the 15-minute mark, with AS B2 levels continuing to rise until reaching a peak at 30 minutes. After 45 minutes of recovery, the expression drops to another minimum, but increases again at the 1-hour and 3-hour time points. Statistical analysis reveals that all conditions differ significantly from the pre-heat shock state, except for the 45-minute recovery time, as indicated in Table 3.3 using a two-tailed t-test.

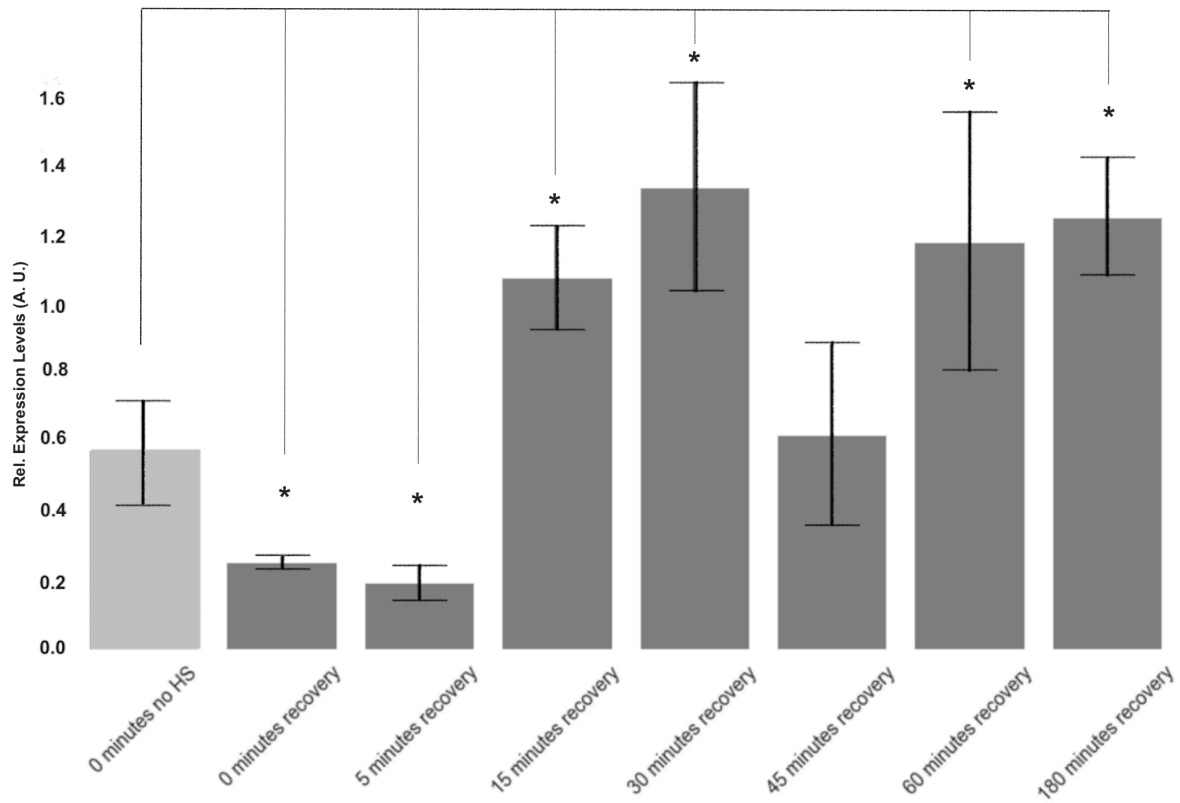

Figure 3.1.4: qPCR results. Antisense B2 levels normalized with GAPDH level. *Light grey represents the level of antisense B2 in pre-HS cells, dark grey represents the post-HS level of antisense B2. $p < 0.05$ is depicted as an asterisk, t-test two-tailed. Error bars denote standard deviation (n=4). All statistics for this graph are in Table 3.3. Standard curves for qPCR quality assessment are in Figure A3.*

The observation that AS B2 levels are higher before heat shock compared to immediately after might be explained by the presence of two distinct promoters within the B2 loci. The first promoter, associated with Pol III, drives the synthesis of sense B2 RNA, while the second promoter, linked to Pol II, regulates the synthesis of antisense B2 RNA (Ferrigno et al., 2001). It is known that in response to heat shock, B2 RNA can repress mRNA transcription by binding to Pol II (Espinoza et al., 2007); (Zovoilis et al., 2016). Therefore, the initial decrease in AS B2 levels could be attributed to this general repression of mRNA transcription by B2 RNA (Allen et al., 2004).

Table 3.3 Statistics for qPCR results for heat shock experiment for antisense B2

Condition 1	*Condition 2*	*p-value*	*Significance*
T0 NoHS	*T0 HS*	*0.016*	*Significant*
T0 NoHS	*T5 HS*	*0.007*	*Significant*
T0 NoHS	*T15 HS*	*0.005*	*Significant*
T0 NoHS	*T30 HS*	*0.0065*	*Significant*
T0 NoHS	*T45 HS*	*0.7956*	*Not Significant*
T0 NoHS	*T60 HS*	*0.0793*	*Significant*
T0 NoHS	*T180 HS*	*0.0022*	*Significant*
T0 HS	*T5 HS*	*0.1466*	*Not Significant*
T0 HS	*T15 HS*	*0.0003*	*Significant*
T0 HS	*T30 HS*	*0.0035*	*Significant*
T0 HS	*T45 HS*	*0.0759*	*Significant*
T0 HS	*T60 HS*	*0.02*	*Significant*
T0 HS	*T180 HS*	*0.00052*	*Significant*

The reasons behind the subsequent fluctuations in AS B2 expression levels remain unclear. Further analysis of sequencing data, which will be discussed in later sections, may provide insights into these variations and help clarify the underlying mechanisms.

3.2 The effect of artificial repression of sense and antisense B2 on each other's expression levels

Previous studies have demonstrated that in response to B2 knockdown, the expression of heat shock-responsive genes is upregulated (Zovoilis et al., 2016).

Many of these heat shock-responsive genes are also involved in other critical cellular processes, including responses to various forms of cellular stress, synaptic function, and learning in nerve cells (Cheng et al., 2020). However, the separate effects of repressing sense B2 versus antisense B2 RNA have not been thoroughly investigated. Consequently, we aimed to explore whether the expression of AS B2 would be altered following the artificial degradation of SE B2 RNA, and vice versa.

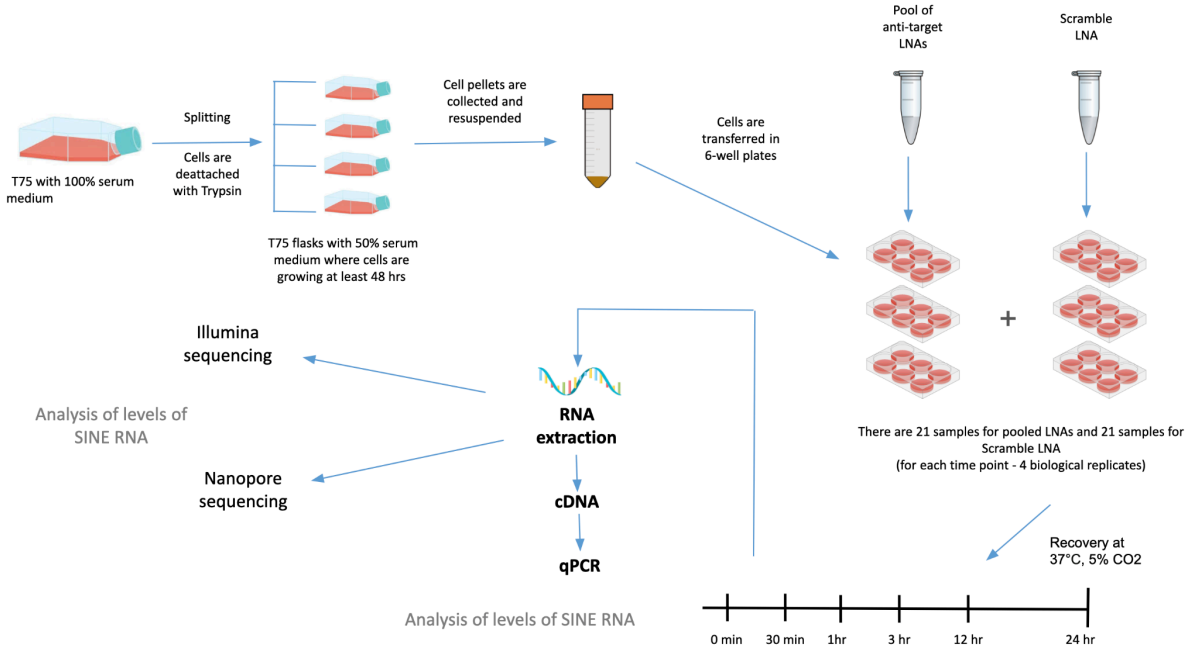

Figure 3.2.1: The workflow of the LNAs transfection experiment.

To achieve specific repression of B2 RNAs, we employed antisense oligonucleotides (ASOs) with locked nucleic acid (LNA) chemistry. LNA-ASOs are designed to target short RNA sequences with high specificity. These ASOs are complementary to the target sequence and feature modified ribose residues, allowing them to bind to the target RNA and facilitate its degradation through cleavage by RNase H (Beane et al., 2007); (Veedu and Wengel, 2010).

To investigate this, I conducted an experiment outlined in Figure 3.2.1, where NIH-3T3 mouse fibroblasts were transfected with LNAs targeting either SE B2, AS B2, or a scrambled LNA used as a negative control. Post-transfection, the cells were allowed to recover at 37°C for various time points, ranging from 0 minutes to 24 hours. Subsequently, RNA was extracted from the cells, and quantitative PCR along with RNA sequencing was performed to analyze the effects of the transfections. The

ASO LNAs targeting B2 and the scrambled LNA were chosen based on their established application in previous B2 RNA research (Cheng et al., 2020).

3.2.1 Sense B2 knockdown

Firstly, I conducted transfections with a set of LNAs designed to knock down B2 SE, as depicted in Figure 3.2.1. Following the transfections, I aimed to assess how the expression level of AS B2 would change over different recovery times.

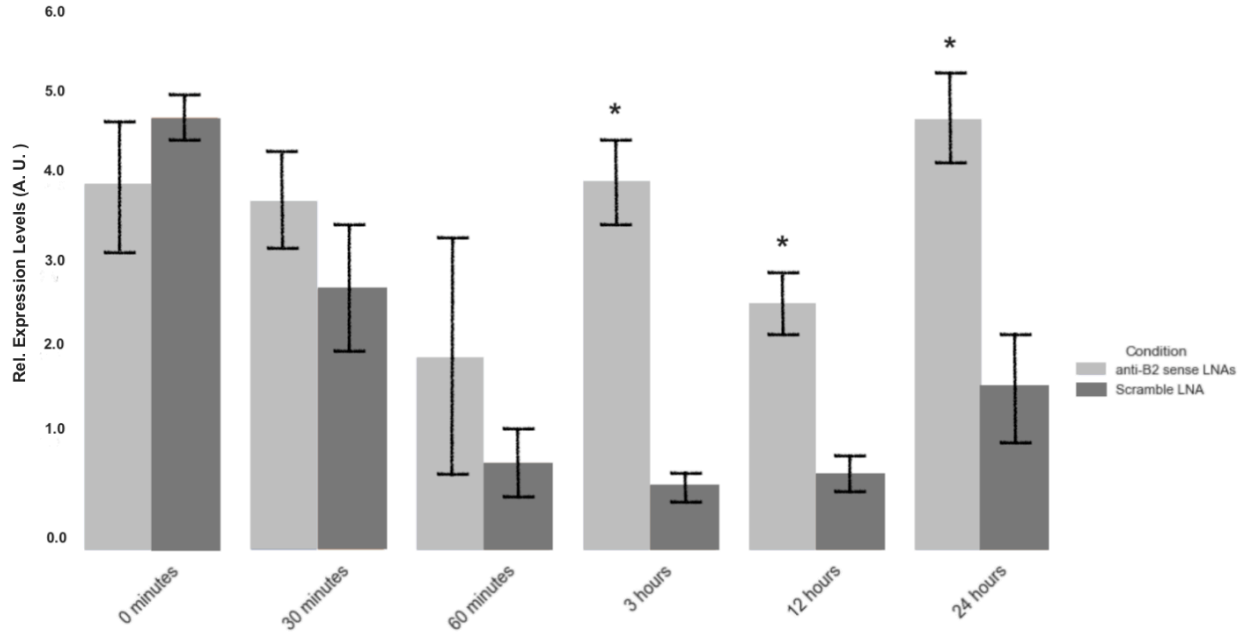

Figure 3.2.2: qPCR results. Antisense B2 levels normalized with GAPDH level after transfection of LNAs against B2 SE and Scrable LNA as a control.
Light grey represents the level of antisense B2 after anti-B2 SE LNAs transfection, dark grey represents the level of antisense B2 after Scramble LNA transfection. $p < 0.05$ is depicted as an asterisk, t-test two-tailed. Error bars denote standard deviation (n=4). All statistics for this graph are in Table 3.4. Standard curves for qPCR quality assessment are in Figure A4.

To achieve this, I prepared cDNA from RNA extracted from the treated cells using AS B2-specific primers and performed quantitative PCR (qPCR). The results of this experiment are illustrated in Figure 3.2.2.

Initially, at the 0-minute mark, the level of AS B2 in samples treated with anti-B2 SE LNAs remained comparable to the levels observed in samples treated with the Scramble LNA. Within the first 60 minutes after transfection, there was a general decrease in AS B2 expression in both the anti-B2 SE LNA and scrambled LNA groups. However, the differences between the two groups were not statistically significant during this period.

By 3 hours post-transfection, the AS B2 levels in samples treated with B2-specific LNAs began to rise. Conversely, in samples treated with the Scramble LNA, the AS B2 expression continued to decrease. After 12 hours, the AS B2 level in the B2 SE knockdown samples showed a reduction compared to the level observed at 3 hours. However, by 24 hours of recovery, AS B2 expression levels in these samples were higher than those observed initially. For samples treated with the Scramble LNA, AS B2 expression gradually increased over time. The differences in AS B2 expression between the B2 SE knockdown and 'Scramble' conditions were statistically significant at the 3-, 12-, and 24-hour time points (Table 3.4).

Table 3.4 Statistics for qPCR results for anti-B2 sense LNAs transfection

Anti-B2 sense LNAs	*Scramble LNA*	*p-value*	*Significance*
0 minutes	*0 minutes*	*0.208*	*Not Significant*
30 minutes	*30 minutes*	*0.158*	*Not Significant*
60 minutes	*60 minutes*	*0.271*	*Not Significant*
3 hours	*3hours*	*0.0003*	*Significant*
12 hours	*12 hours*	*0.0005*	*Signifiant*
24 hours	*24 hours*	*0.0003*	*Significant*

3.2.2 Antisense B2 knockdown

Similarly, I conducted transfections using a set of LNAs designed to repress B2 AS, as illustrated in Figure 3.2.1. The objective was to determine whether the expression level of B2 SE would change over time following B2 AS knockdown. To achieve this, I prepared cDNA from RNA extracted from the treated mouse cells using B2 SE-specific primers, and then performed qPCR.

As shown in Figure 3.2.3, 30 minutes after the transfection, B2 SE expression is higher compared to its level right before transfection (0 minutes). In samples treated with the B2 AS-specific set of LNAs, B2 SE expression levels increase faster, and the difference between these samples and those treated with the scrambled LNA is significant. Then, at 1 hour, 3 hours, and 12 hours, B2 SE expression remains approximately at the same level. During this time, the differences are not significant compared to Scramble-treated samples (Table 3.5). However, after 24 hours of recovery, a maximum in B2 SE expression can be observed, which is significantly different from its level in samples treated with the scrambled LNA.

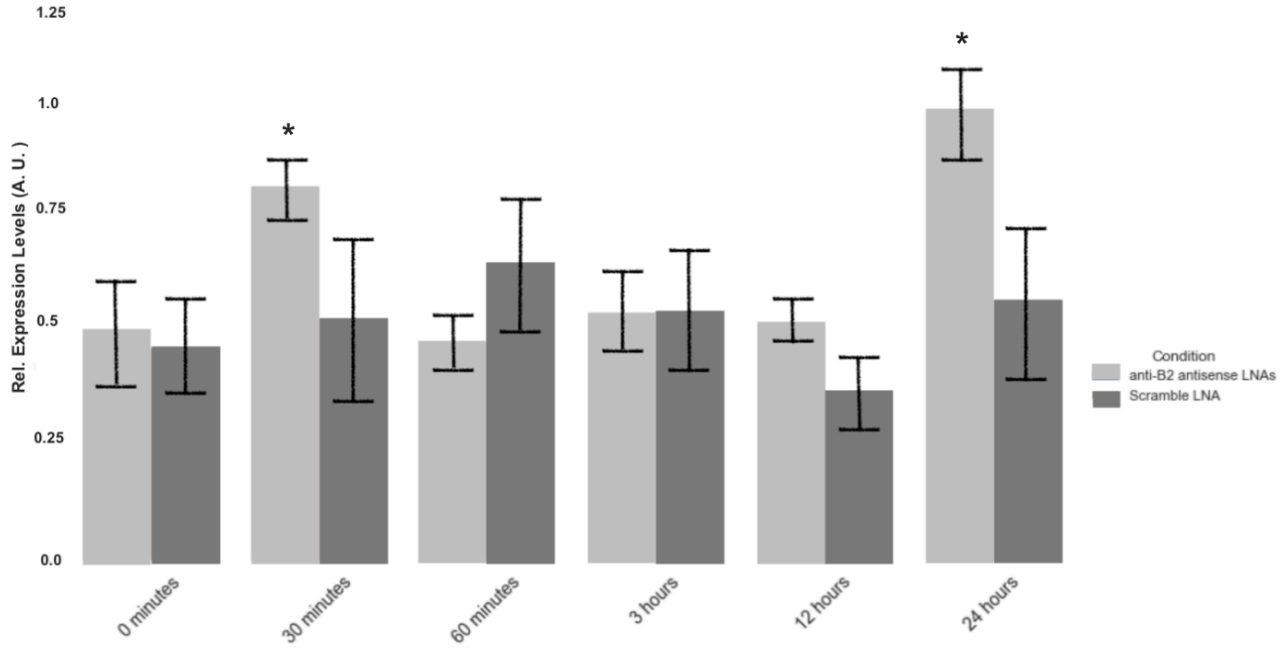

Figure 3.2.3: qPCR results. Sense B2 levels normalized with GAPDH level after transfection of LNAs against B2 AS and Scrable LNA as a control.
Light grey represents the level of sense B2 after anti-B2 AS LNAs transfection, dark grey represents the level of sense B2 after Scramble LNA transfection. $p < 0.05$ is depicted as an asterisk, t-test two-tailed. Error bars denote standard deviation (n=4). All statistics for this graph are in Table 3.5. Standard curves for qPCR quality assessment are in Figure A5.

Table 3.5 Statistics for qPCR results for anti-B2 antisense LNAs transfection

Anti-B2 antisense LNAs	*Scramble LNA*	*p-value*	*Significance*
0 minutes	*0 minutes*	*0.693*	*Not Significant*
30 minutes	*30 minutes*	*0.0717*	*Significant*
60 minutes	*60 minutes*	*0.1068*	*Not Significant*
3 hours	*3hours*	*0.9814*	*Not Significant*
12 hours	*12 hours*	*0.1309*	*Not Significant*
24 hours	*24 hours*	*0.071*	*Significant*

3.3 The effect of in vitro transcribed B2 transfection on the expression levels of B2 SE and B2 AS

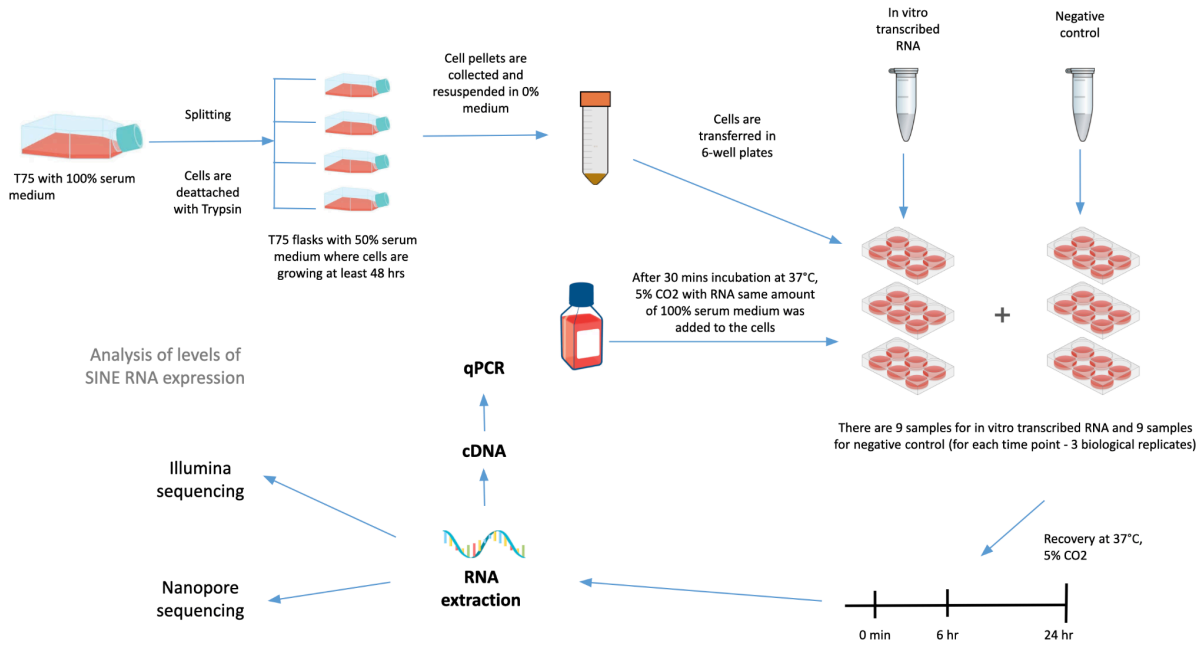

Figure 3.3.1: The workflow of in vitro transcribed B2 transfection.

Previously, I investigated how B2 expression levels are affected by stress or the artificial repression of one of its components. I next aimed to examine how the expression levels of B2 SE and B2 AS change in response to the transfection of in vitro transcribed (IVT) B2 RNA. To accomplish this, B2 RNA was synthesized in vitro using a g-block of B2 Mm1a as the template, which included a T7 promoter sequence at the beginning. This g-block sequence was sourced from a prior study (Cheng et al., 2020). Subsequently, the in vitro transcribed B2 RNA was transfected into mouse fibroblasts NIH-3T3, as depicted in Figure 3.3.1. Tet150 was used as a control for the transfection process.

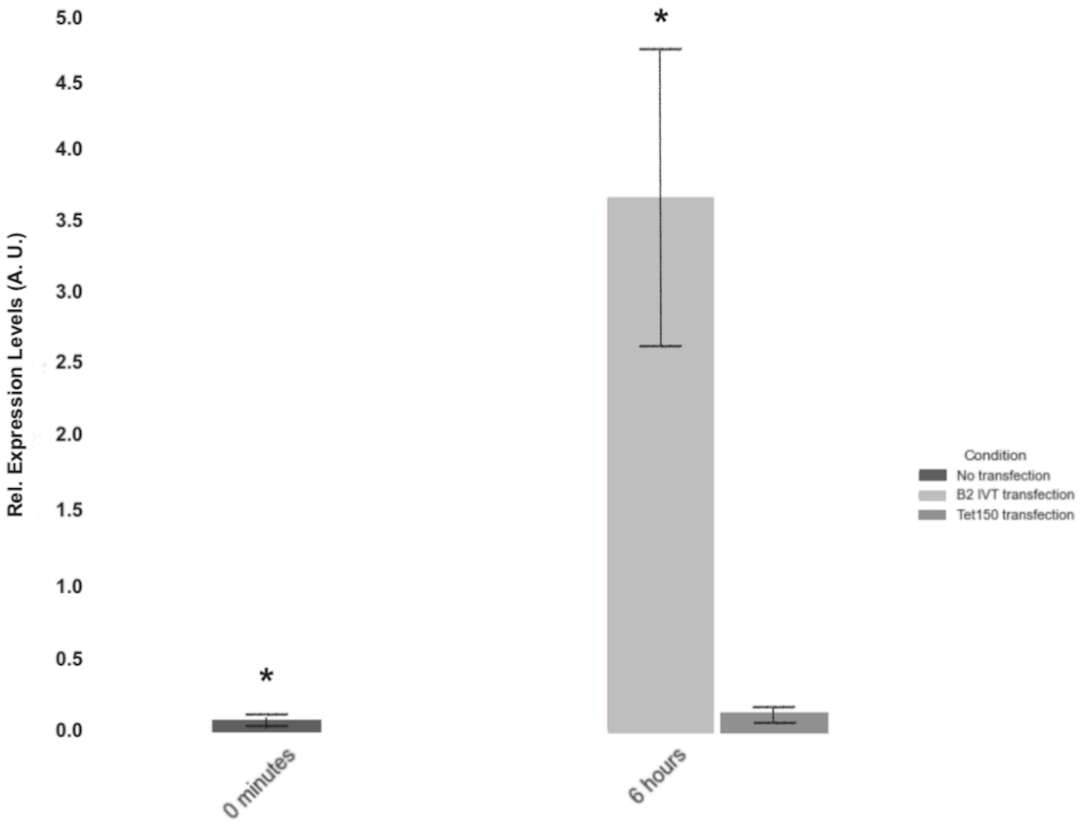

Figure 3.3.1: qPCR results. Sense B2 levels normalized with HPRT level after transfection of in vitro transcribed B2.

Light grey represents the level of sense B2 after IVT B2 transfection, dark grey represents the level of sense B2 after Tet150 transfection. $p < 0.05$ is depicted as an asterisk, t-test two-tailed. Error bars denote standard deviation (n=4).

All statistics for this graph are in Table 3.6. Standard curves for qPCR quality assessment are in Figure A6.

Following transfection, the cells were allowed to recover at 37°C for either 6 hours or 24 hours. To evaluate changes in B2 SE and B2 AS expression levels, cDNA was prepared from the extracted RNA using SE-specific and AS-specific B2 primers, respectively. The housekeeping gene HPRT was used for normalization during this process and for the subsequent quantitative PCR (qPCR).

The results regarding changes in B2 SE expression levels are illustrated in Figure 3.2. After 6 hours of recovery, B2 SE expression significantly increased compared to the "no transfection" condition (Table 3.6). Additionally, B2 levels in samples transfected with Tet150 were lower at this time point. All observed differences were statistically significant (Table 3.6).

Table 3.6 Statistics for qPCR results of B2 IVT transfection for B2 sense levels

Condition 1	*Condition 2*	*p-value*	*Significance*
0 minutes No transfection	*6 hours B2 transfection*	*0.00192*	*Significant*
0 minutes No transfection	*6 hours Tet150 transfection*	*0.00012*	*Significant*
6 hours B2 transfection	*6 hours Tet150 transfection*	*0.00193*	*Significant*

Regarding the changes in B2 AS expression following transfection (Figure 3.3), there is a notable increase at the 6-hour mark. This increase is significant when compared to the “no transfection” condition, as well as when compared to samples treated with Tet150 (Table 3.7).

Overall, the trend observed for B2 SE is as expected. Since B2 SE RNA was introduced into the cells, its level naturally rises. The subsequent decrease over time can also be anticipated as the cells work to maintain homeostasis, thereby diminishing the significance of the effects caused by the transfection. These results align with previous experiments involving heat shock and transfection.

Table 3.7 Statistics for qPCR results of B2 IVT transfection for B2 antisense levels

Condition 1	*Condition 2*	*p-value*	*Significance*
0 minutes No transfection	*6 hours B2 transfection*	*0.00034*	*Significant*
0 minutes No transfection	*6 hours Tet150 transfection*	*0.25371*	*Not Significant*
6 hours B2 transfection	*6 hours Tet150 transfection*	*0.00225*	*Significant*

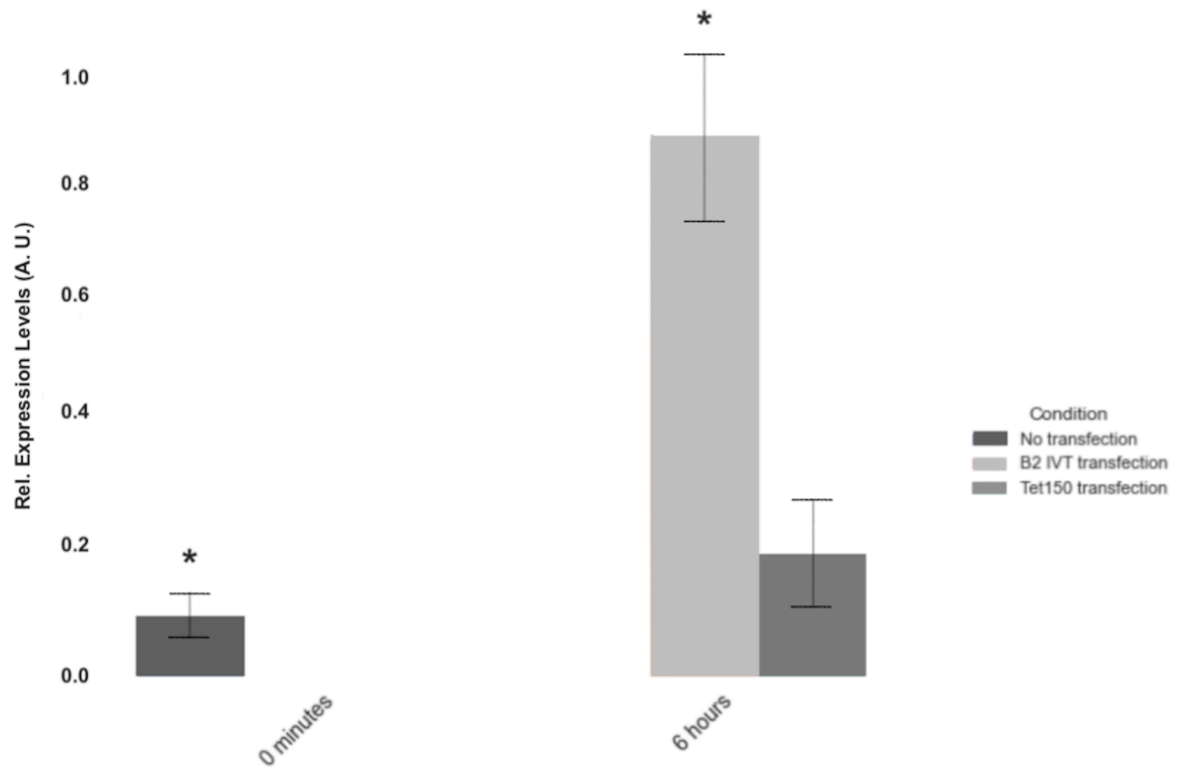

Figure 3.3.2: qPCR results. Antisense B2 levels normalized with HPRT level after transfection of in vitro transcribed B2.

Light grey represents the level of antisense B2 after IVT B2 transfection, dark grey represents the level of antisense B2 after Tet150 transfection. $p < 0.05$ is depicted as an asterisk, t-test two-tailed. Error bars denote standard deviation (n=4).

All statistics for this graph are in Table 3.7. Standard curves for qPCR quality assessment are in Figure A7.

However, the increase in AS B2 levels is particularly noteworthy. This increase could be attributed to changes in HPRT expression, which was used for normalization under the assumption of its constant expression during cellular stress. The introduction of an extremely high concentration of B2 RNA could act as a strong repressor of Pol II, potentially leading to the repression of HPRT expression as part of a broader mRNA transcription repression (Allen et al., 2004). Consequently, any alterations in HPRT expression would affect the qPCR results in this experimental setup.

To determine whether the observed behavior of AS B2 expression is influenced by the repression of HPRT, I conducted an additional qPCR analysis using 7SK - a Pol III transcribed gene - as the normalization control. The expression of 7SK is known to remain stable even when B2 levels increase (Allen et al., 2004).

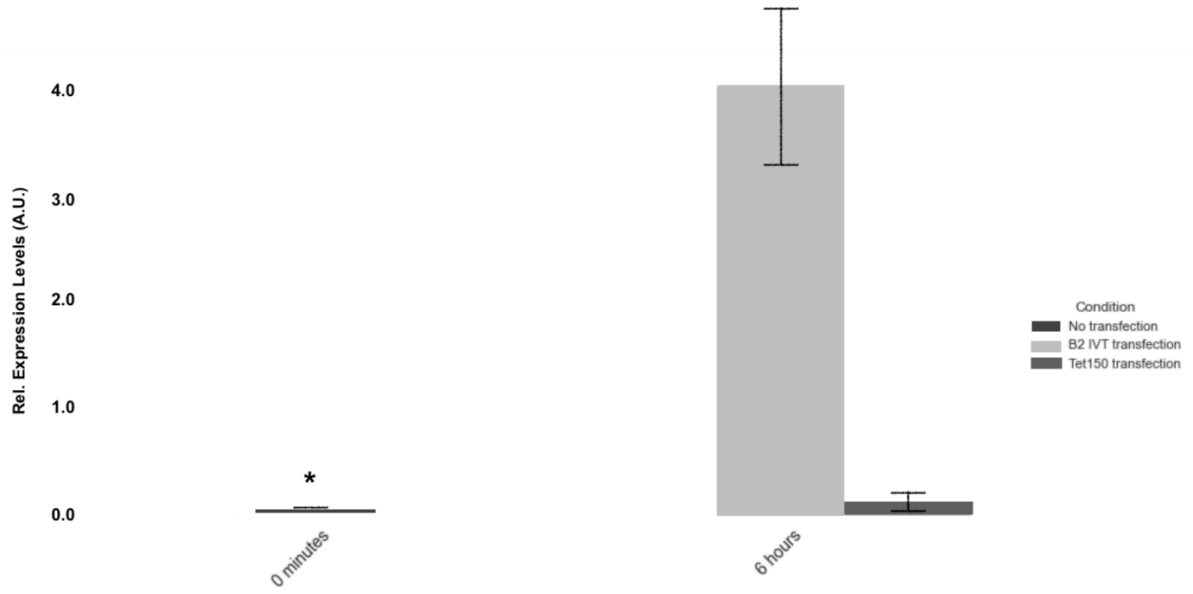

Figure 3.3.3: qPCR results. Sense B2 levels normalized with 7SK level after transfection of in vitro transcribed B2.
Light grey represents the level of sense B2 after IVT B2 transfection, dark grey represents the level of sense B2 after Tet150 transfection. $p < 0.05$ is depicted as an asterisk, t-test two-tailed. Error bars denote standard deviation (n=4).

All statistics for this graph are in Table 3.8. Standard curves for qPCR quality assessment are in Figure A8.

Table 3.8 Statistics for qPCR results of B2 IVT transfection for B2 sense levels

Condition 1	*Condition 2*	*p-value*	*Significance*
0 minutes No transfection	*6 hours B2 transfection*	*0.00014*	*Significant*
0 minutes No transfection	*6 hours Tet150 transfection*	*0.6294*	*Not Significant*
6 hours Tet150 transfection	*24 hours B2 transfection*	*0.00014*	*Significant*

As illustrated in Figure 3.3.3, the level of B2 SE continues to rise significantly following B2 SE IVT transfection, when compared to both the “no transfection” and “Tet150 transfection” conditions (Table 3.8).

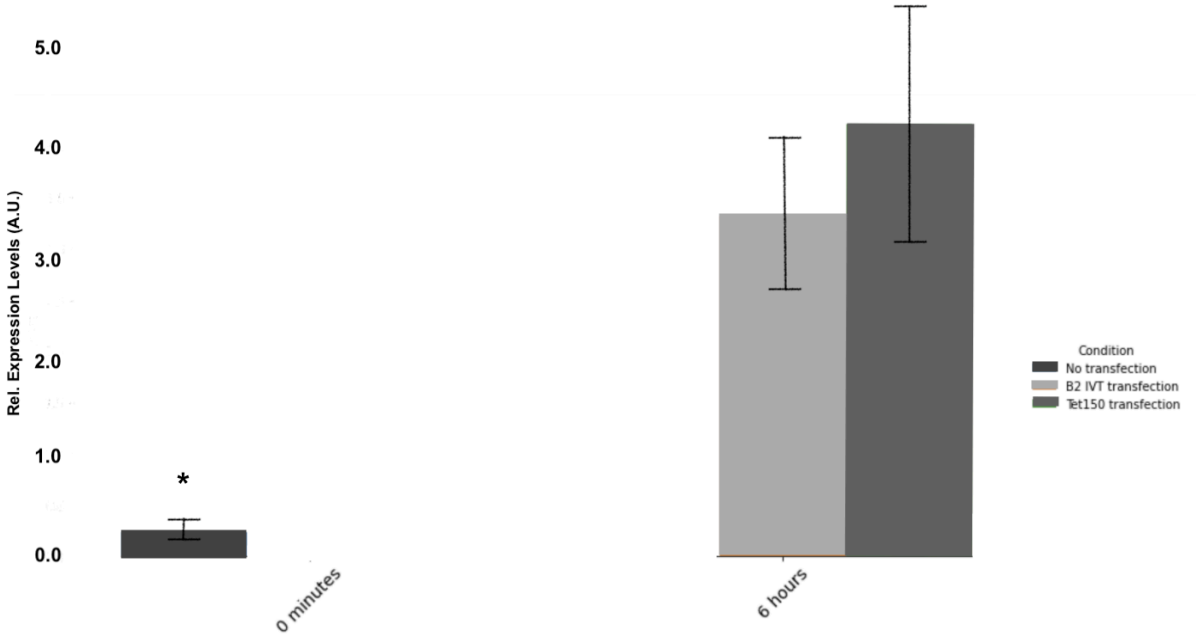

Figure 3.3.4: qPCR results. Antisense B2 levels normalized with 7Sk level after transfection of in vitro transcribed B2.
Light grey represents the level of antisense B2 after IVT B2 transfection,

dark grey represents the level of antisense B2 after Tet150 transfection. $p < 0.05$ is depicted as an asterisk, t-test two-tailed. Error bars denote standard deviation (n=4). All statistics for this graph are in Table 3.9. Standard curves for qPCR quality assessment are in Figure A9.

In contrast, the behavior of B2 AS expression shows a different pattern (Figure 3.3.4). After B2 SE IVT transfection, the B2 AS level remains relatively unchanged compared to the “Tet150 transfection” condition (Table 3.9).

Table 3.9 Statistics for qPCR results of B2 IVT transfection for B2 antisense levels

Condition 1	Condition 2	p-value	Significance
0 minutes No *transfection*	6 hours B2 transfection	0.00169	Significant
0 minutes No transfection	6 hours Tet150 transfection	0.3207	Not Significant
6 hours Tet150 transfection	24 hours B2 transfection	0.5445	Not Significant

3.4 Assessment of changes in B2 expression levels in response to stress based on sequencing data

To validate or question the results obtained from the PCR experiments, I performed RNA sequencing on samples collected from two distinct experimental treatments: heat shock and LNA transfection. Additionally, I reanalyzed sequencing data from a previous study (Zovoilis et al., 2016) to enrich our analysis. By comparing the sequencing results from these two experimental approaches, I aimed to determine whether the observed changes in the expression levels of sense B2 SINEs and antisense transcripts are genuine increases or if they could be attributed to the fragmentation of B2 SINEs, which is known to occur during cellular stress (Zovoilis et al., 2016); (Cheng et al., 2020).

This comprehensive analysis is intended to clarify whether the increases in B2 SE or AS levels are a direct consequence of the experimental treatments or if they are influenced by stress-induced fragmentation. Understanding these dynamics is crucial

for accurately interpreting the role of B2 SINEs in stress responses and ensuring the reliability of the experimental findings.

3.4.1 Short- and long-RNA-sequencing data

Short- and long-RNA sequencing was employed to detect both fragmented and full-length B2 RNAs. During the library preparation, short and long RNA fragments were separated and processed separately. Sequencing data were downloaded from GSE82255. The same cell line, NIH-3T3, was used for both heat shock and LNA transfection experiments (Zovoilis et al., 2016). For the heat shock experiment, samples were collected before and immediately after heating. For the LNA transfection experiment, samples were collected 24 hours post-transfection with either B2-specific LNAs or scrambled LNA.

3.4.1.1 Heat shock experiment

The analysis of sequencing data revealed that after 15 minutes of heating at 45°C, the expression level of full-length B2 SE remained similar to the pre-heat shock condition (Figure 3.4.1, B: long-RNA sequencing). However, following heat shock, the level of fragmented B2 SE increased compared to the pre-heat shock level. As shown in Figure 3.4.1 A (short-RNA sequencing), fragmentation was more pronounced after heat shock, as evidenced by more explicit peaks for this condition (orange).

According to this data, the total amount of B2 SE appears to increase after heat shock. This is accompanied by a rise in the level of fragmented B2, while the level of unprocessed B2 remains unchanged.

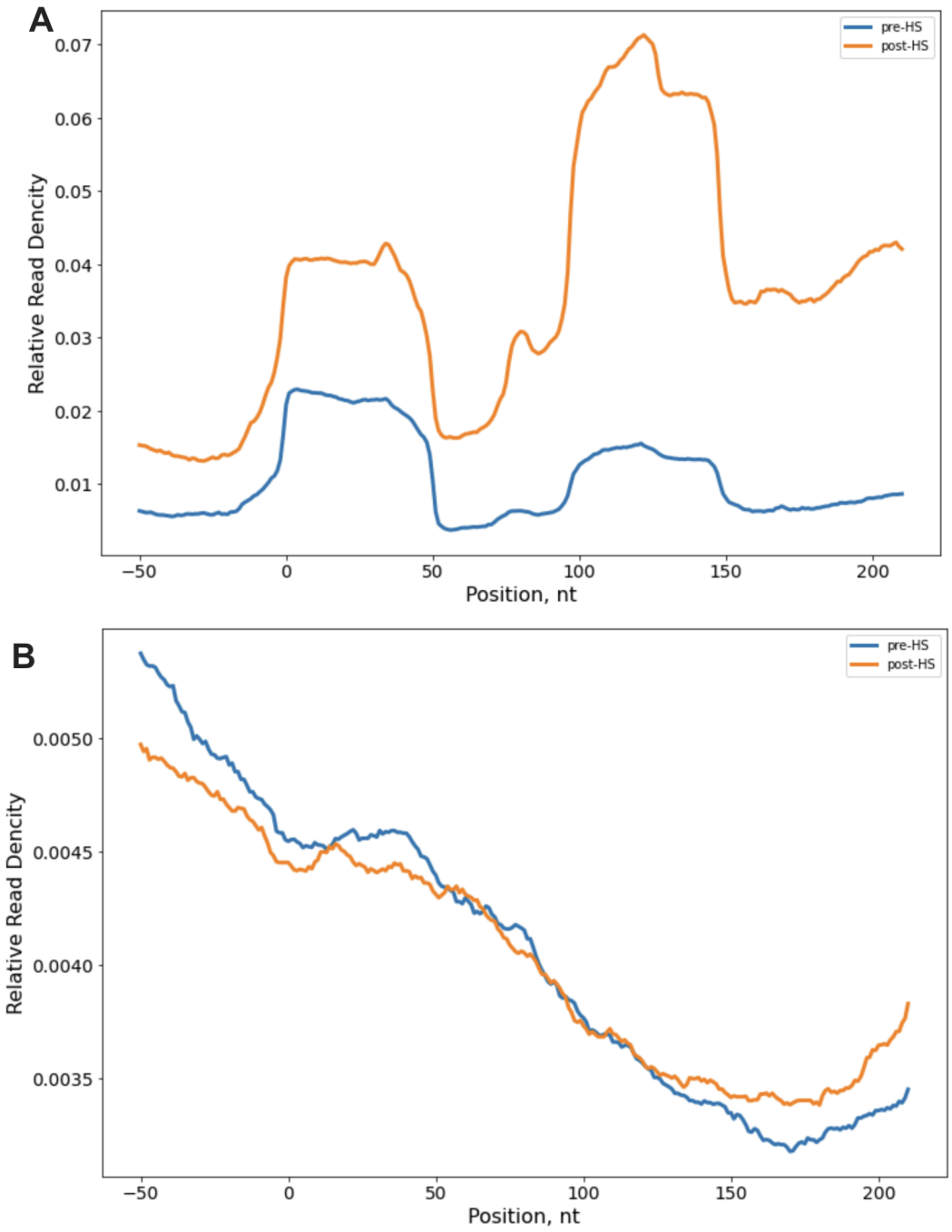

Figure 3.4.1: Short-RNA (A) and long-RNA (B) sequencing data for the heat shock experiment. Sense B2 relative read density.

The x-axis is a metagene that unites all B2 RNA loci aligned to the starting point of their consensus sequence (position +1). The y-axis shows the relative number of 5'-terminal B2 RNA fragments aligned at any position below +1. Conditions: before heat shock - blue, after heat shock - orange. $p < 0.05$ for both A and B, KS test.

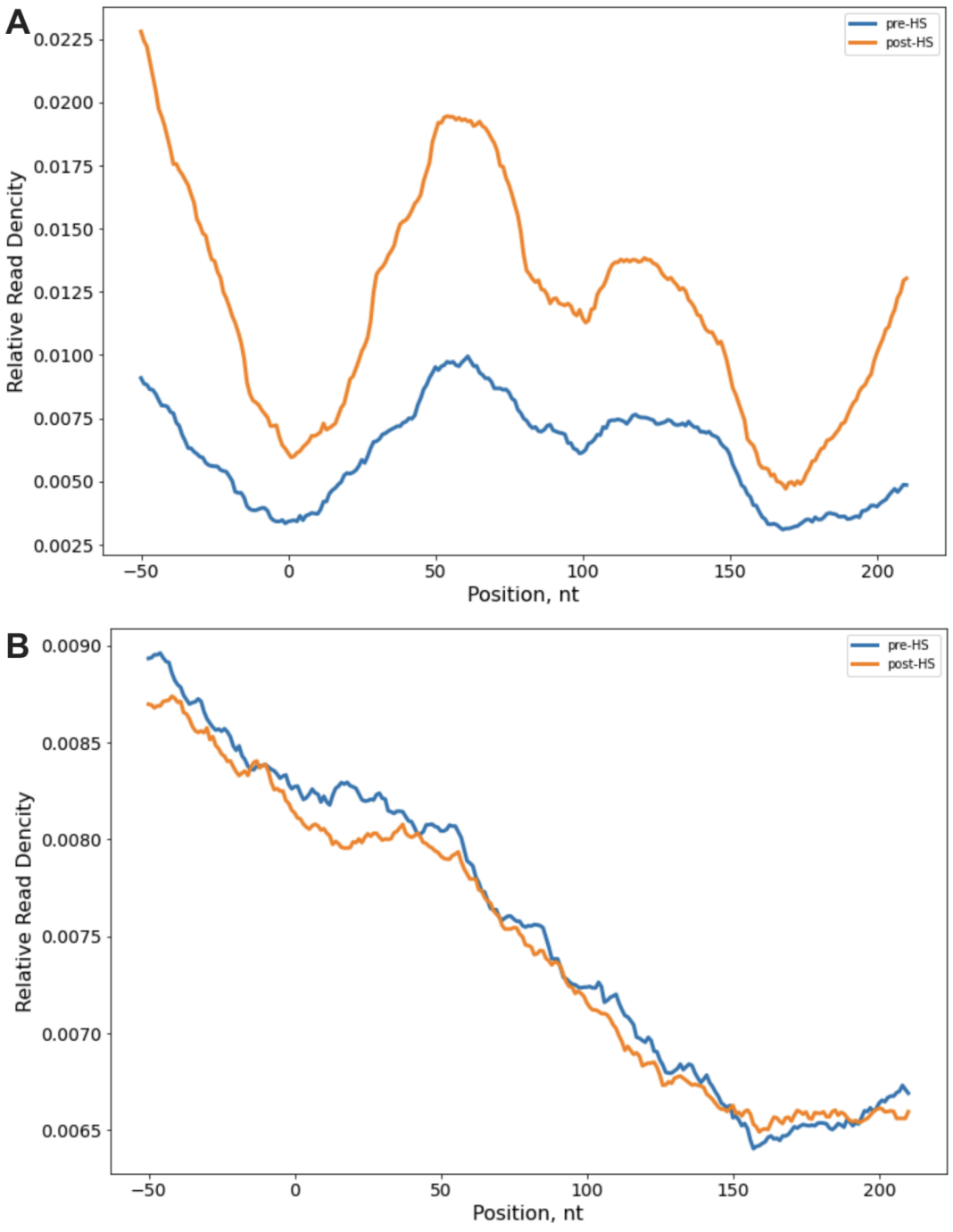

Figure 3.4.2: Short-RNA (A) and long-RNA (B) sequencing data for the heat shock experiment. Antisense B2 relative read density.

The x-axis is a metagene that unites all B2 RNA loci aligned to the starting point of their consensus sequence (position +1). The y-axis shows the relative number of 5'-terminal B2 RNA fragments aligned at any position below +1. Conditions: before heat shock - blue, after heat shock - orange. $p < 0.05$ for A, KS test.

Regarding AS B2 expression, the analysis revealed that after heat shock, the expression level of full-length B2 AS remained consistent with the pre-heat shock level (Figure 3.4.2, B: long-RNA sequencing). However, as shown in Figure 3.4.2 (A: short-RNA sequencing), the AS B2 level was higher post-heat shock, with clearer peaks, indicating that B2 AS may also undergo processing during stress.

3.4.1.2 LNAs transfection experiments

Following the transfection with anti-B2 SE LNAs, there was a notable enhancement in the processing of B2 SE compared to the control with Scramble (Figure 3.4.3, A: short-RNA sequencing). Concurrently, the level of full-length B2 SE decreased relative to the control (Figure 3.4.3, B: long-RNA sequencing). These results indirectly support the effective knockdown of B2 SE, as evidenced by the reduction in full-length RNA due to increased processing.

After the knockdown of B2 SE, the level of full-length B2 AS increased compared to the Scramble control (Figure 3.4.4, B: long-RNA sequencing). However, the amount of fragmented B2 AS remained unchanged compared to the Scramble-treated samples (Figure 3.4.4, A: short-RNA sequencing).

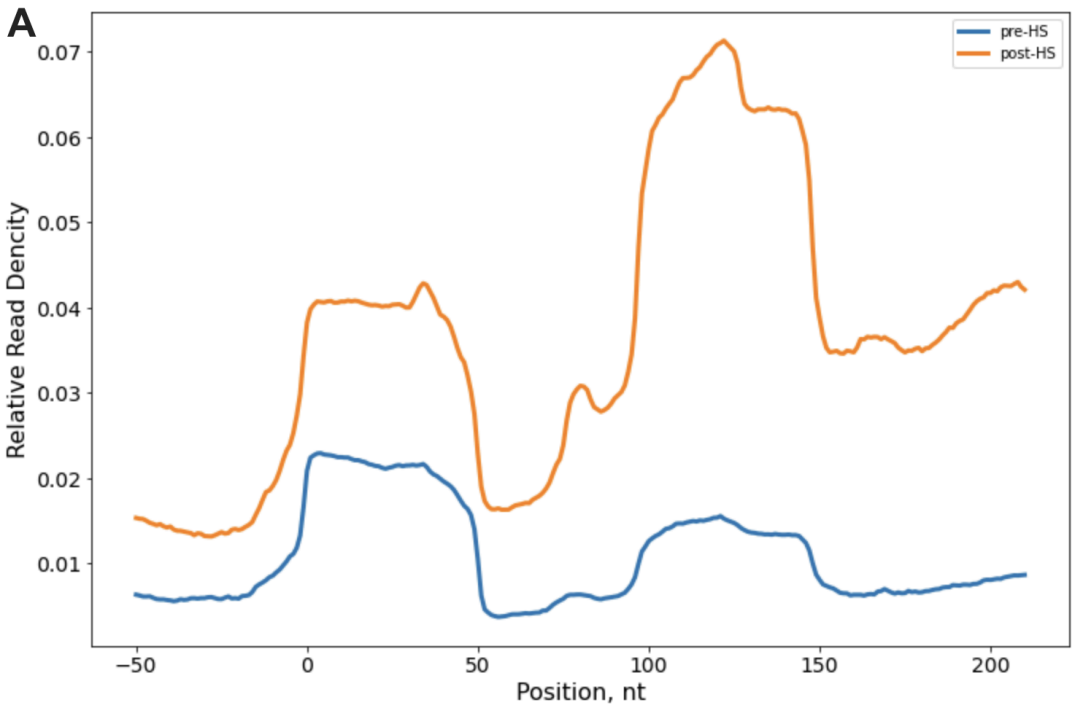

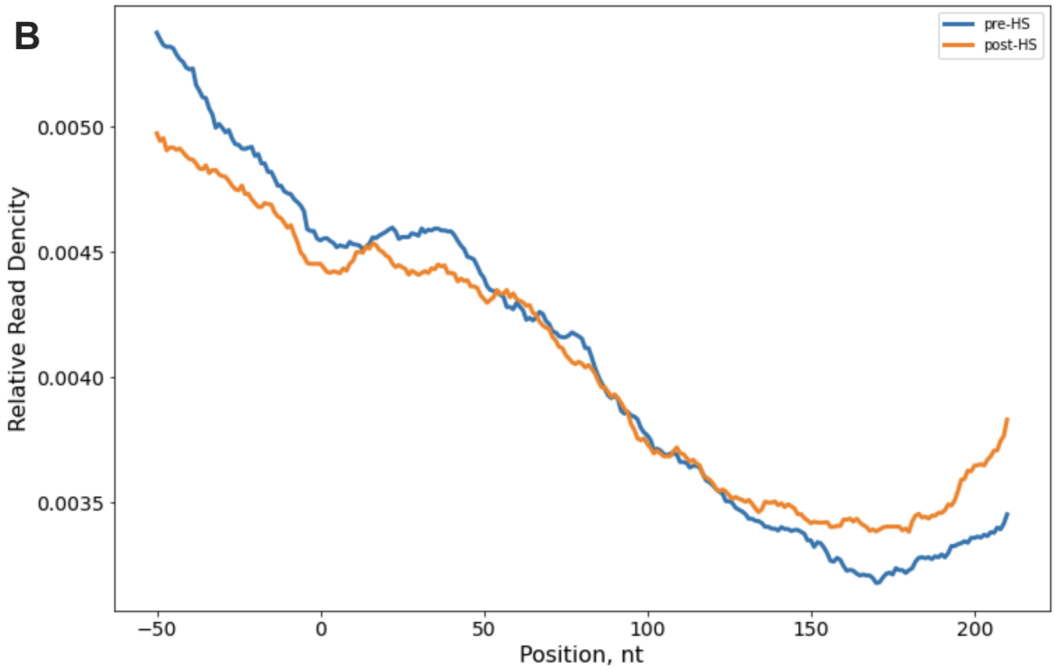

Figure 3.4.3: Short-RNA (A) and long-RNA (B) sequencing data for the LNAs transfection experiment. Sense B2 relative read density after the transfection. *The x-axis is a metagene that unites all B2 RNA loci aligned to the starting point of their consensus sequence (position +1). The y-axis shows the relative number of 5'-terminal B2 RNA fragments aligned at any position below +1. Conditions: with anti-B2 LNAs - orange, and with Scramble LNA as a control - blue. $p < 0.05$ for both A and B, KS test.*

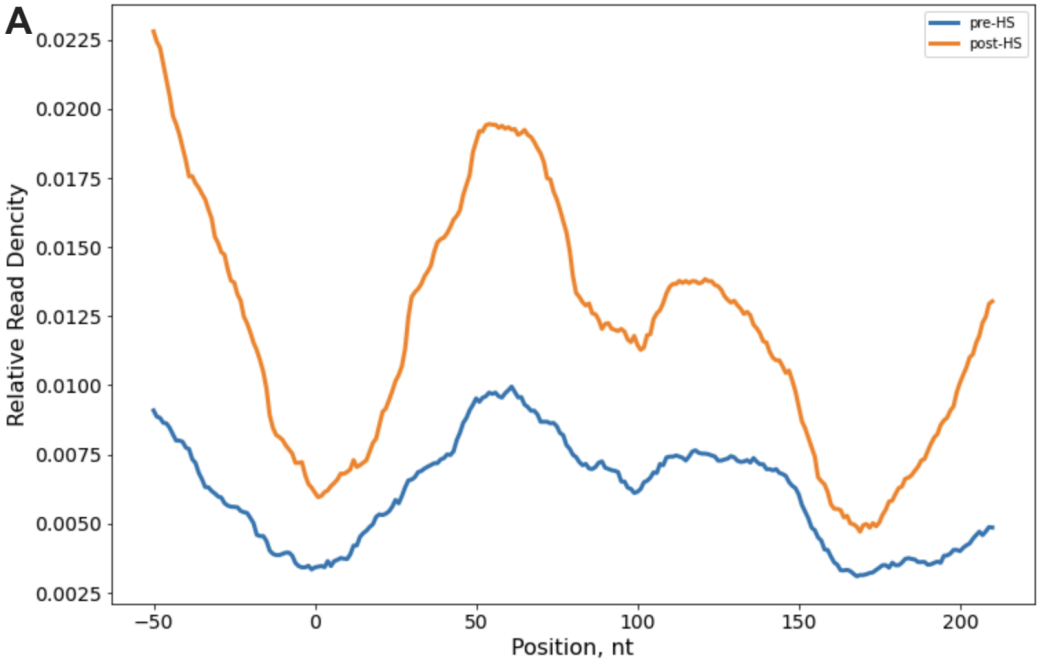

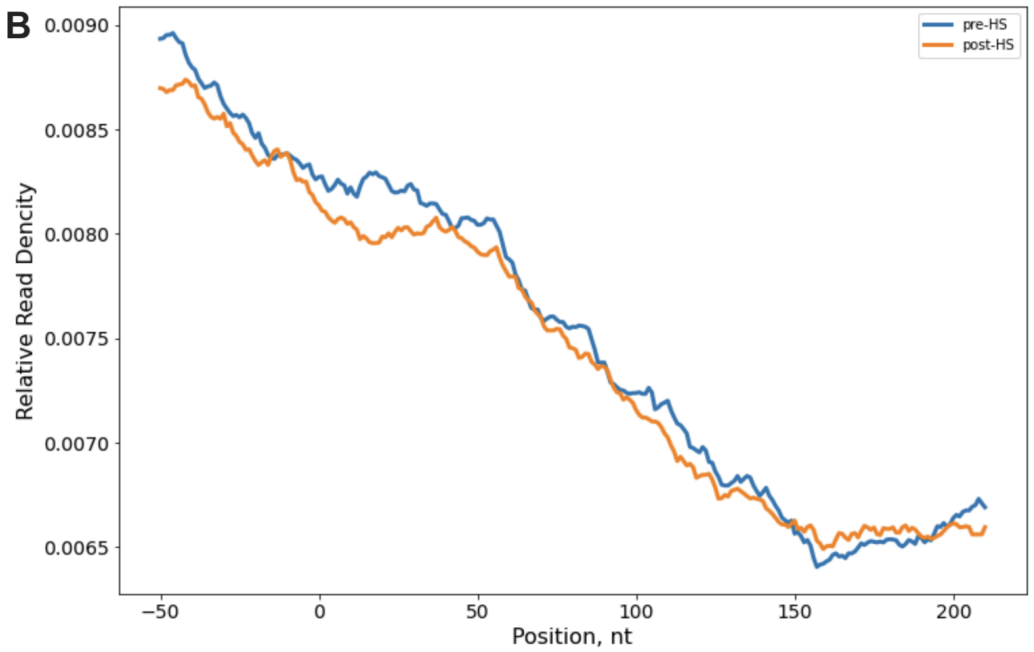

Figure 3.4.4: Short-RNA (A) and long-RNA (B) sequencing data for the LNAs transfection experiment. Antisense B2 relative read density after the transfection.

The x-axis is a metagene that unites all B2 RNA loci aligned to the starting point of their consensus sequence (position +1). The y-axis shows the relative number of 5'-terminal B2 RNA fragments aligned at any position below +1. Conditions: with anti-B2 LNAs - orange, with Scramble LNA as a control - blue. $p < 0.05$ for A, KS test.

3.4.2 Direct RNA-seq

To gain a more detailed understanding of how SE B2 SINE and AS B2 SINE levels fluctuate over time, we extended our analysis by incorporating additional time points beyond those used in the previous study (Zovoilis et al., 2016). For this purpose, we employed direct RNA sequencing using RNA samples obtained from our experiments. While this method does not allow for the separate analysis of individual B2 RNA fragments, it provides valuable insights into the overall changes in B2 expression levels throughout the study.

4.4.2.1 Heat shock data

RNA extracted from NIH-3T3 cells was used for sequencing before heat shock, immediately after 15 minutes of heating at 45°C, and 30 minutes after the completion of heating. This analysis revealed that SE B2 levels rise immediately after heating

and then decrease after 30 minutes, although they remain higher than before the heating (Figure 3.4.5, A).

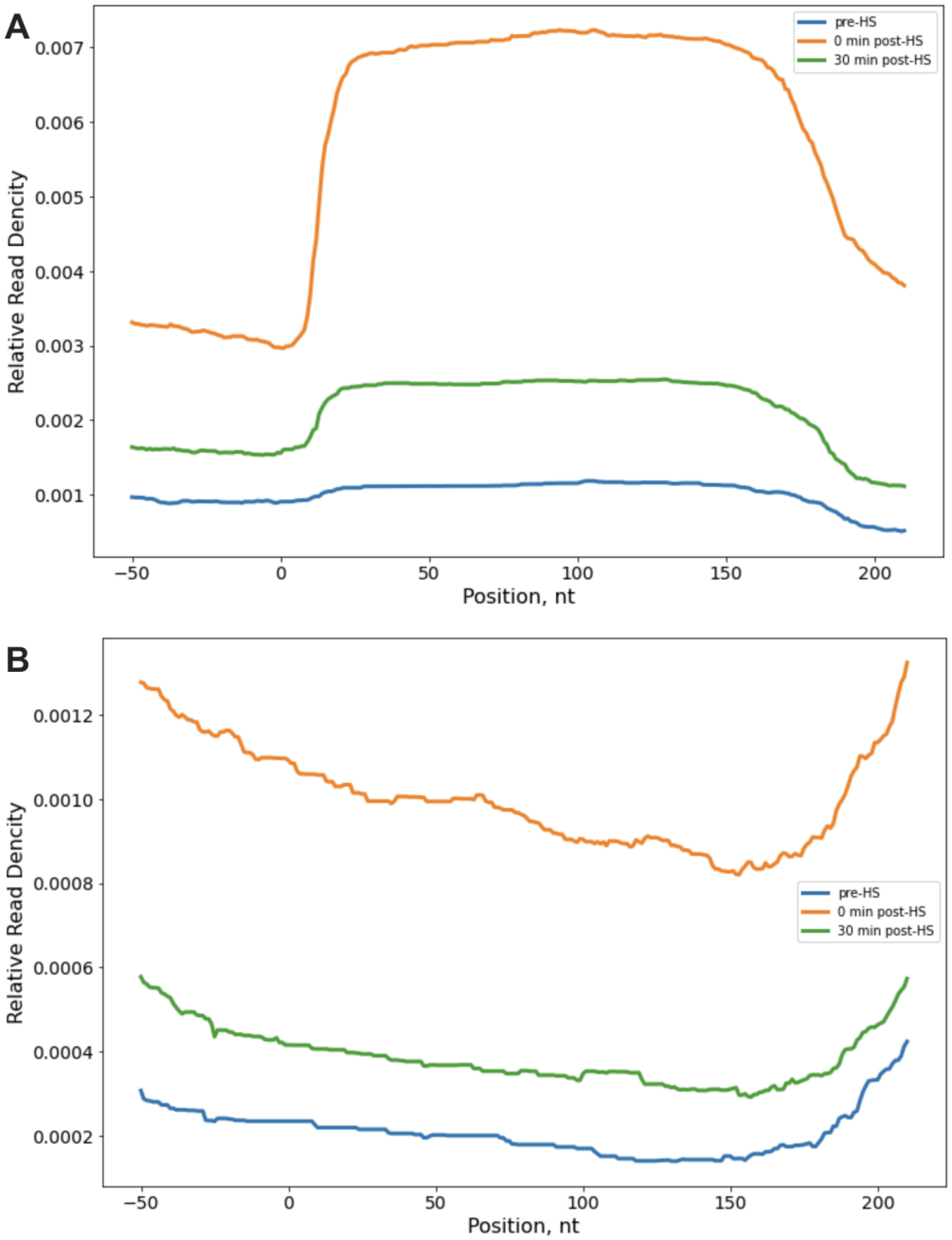

Figure 3.4.5: Direct-RNA sequencing data for the heat shock experiment. Relative read density for sense B2 (A) and antisense B2 (B).

The x-axis is a metagene that unites all B2 RNA loci aligned to the starting point of their consensus sequence (position +1). The y-axis shows the relative number of 5'-terminal B2 RNA fragments aligned at any position below +1. Conditions: before heat shock - blue, right after heat shock - orange, 30 minutes after heat shock - green. $p < 0.05$ for both A and B, KS test.

Similarly, AS B2 levels also increase immediately after heating and then decrease 30 minutes later (Figure 3.4.5, B). Overall, these findings partially align with the PCR results. Discrepancies may be attributed to the inclusion of various B2 subfamilies (B2_Mm1a, B2_Mm1t, and B2_Mm2) in the sequencing data.

3.4.2.2 Transfection of the LNAs targeting B2 SE

Furthermore, the direct RNA sequencing data revealed that following the knockdown of B2 SE, the expression of B2 AS increased compared to the control (transfection with Scramble LNA) (Figure 3.4.6). These results confirm the PCR findings, which also showed that 30 minutes after the procedure, B2 AS levels were significantly higher in samples treated with B2-specific LNAs than in those treated with Scramble LNA.

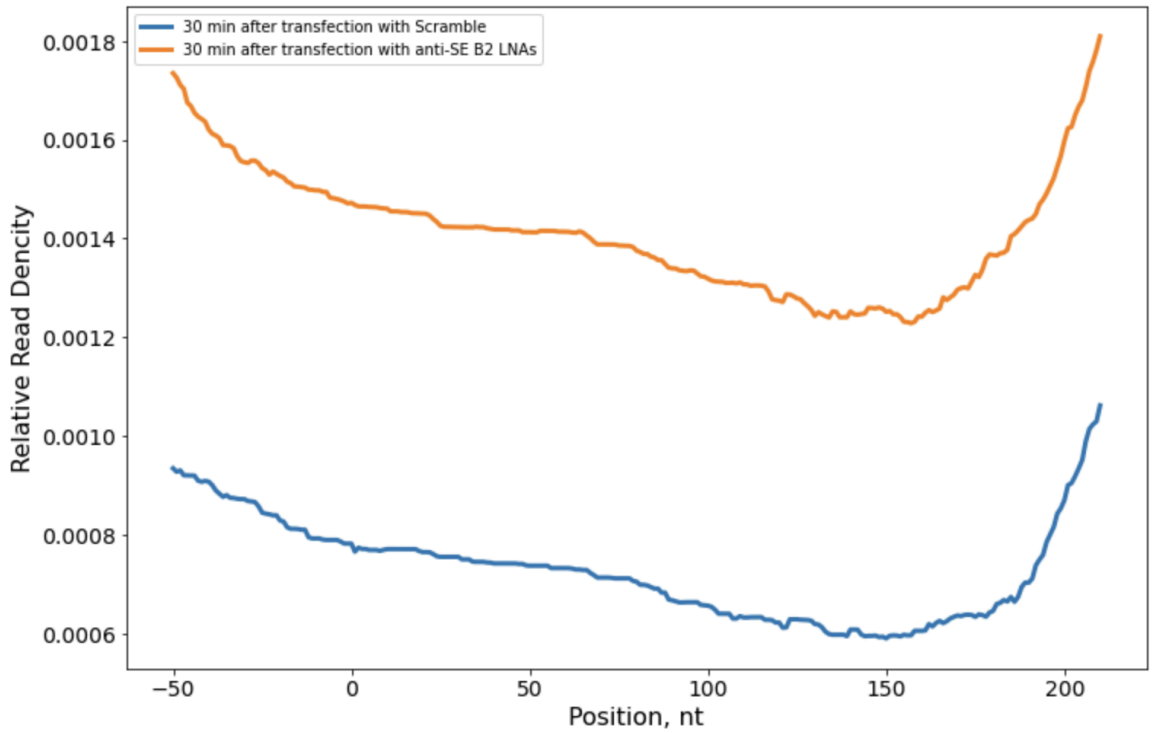

Figure 3.4.6: Direct-RNA sequencing data for the LNAs transfection experiment. Antisense B2 relative read density.

The x-axis is a metagene that unites all B2 RNA loci aligned to the starting point of their consensus sequence (position +1). The y-axis shows the relative number of 5'-terminal B2 RNA fragments aligned at any position below +1. Conditions: 30 minutes after anti-SE B2 LNAs transfection - orange, 30 minutes after Scramble LNA transfection - blue. $p < 0.05$, KS test.

Chapter 4.

Discussion

All living organisms constantly face environmental stressors in their daily lives, such as extreme temperatures, chemical toxins, radiation, and infections. To function normally and maintain homeostasis, organisms must rapidly adapt to these challenging conditions. This adaptation is crucial for survival and involves complex mechanisms at both the organismal and cellular levels. At the cellular level, adaptive changes are essential for the organism's overall survival under stress. One critical aspect of this cellular response is the activation of stress response genes (Galluzzi et al., 2018). These genes are pivotal in protecting cells from conditions that could otherwise be lethal. They help mitigate damage, repair cellular components, and maintain cellular integrity (Sheng et al., 2024). Conversely, a failure to activate or properly regulate the stress response can have detrimental consequences. An ineffective stress response leaves cells vulnerable to damage, increasing the risk of disease. Additionally, an uncontrolled stress response can lead to excessive inflammation and tissue damage, contributing to chronic illnesses (Wu et al., 2022).

Understanding stress response mechanisms could significantly improve human health outcomes. By elucidating how cells and organisms adapt to stress, researchers can develop targeted therapies and preventive strategies to mitigate the adverse effects of environmental stressors. This knowledge could lead to advancements in treating stress-related diseases and enhancing resilience against various health challenges.

Despite extensive research, many aspects of the cellular response to stress remain unclear. Non-coding RNAs, including SINEs, play critical roles in regulating the cellular stress response, yet the specific mechanisms involved are not fully understood. SINEs modulate gene expression during stress, with levels of B2 SINEs increasing under stress conditions (Espinoza et al., 2007) and their processing

becoming more pronounced (Zovoilis et al., 2016). Unprocessed B2 SINEs can bind to RNA polymerase II, inhibiting mRNA transcription (Allen et al., 2004).

Moreover, natural antisense B2 transcripts are implicated in cellular stress responses and are associated with various diseases (Pandey et al., 2011); (Vourc'h et al., 2022). However, it remains unclear whether these antisense transcripts are regulated under stress or if they influence the levels of B2 SINEs. While significant strides have been made in understanding the role of non-coding RNAs in stress responses, key questions about their regulation and function still need to be addressed.

In this MSc thesis project, the primary objective was to investigate the regulation of SINE sense and antisense SINEs during the cellular response to stress, using B2 SINE RNAs as a model system. The project focused on understanding the interplay between the expression levels of B2 SE and B2 AS RNA. Specifically, I aimed to elucidate how variations in the expression of B2 SE influence the levels of B2 AS, and conversely, how changes in B2 AS expression impact B2 SE levels (see Figure 4.1).

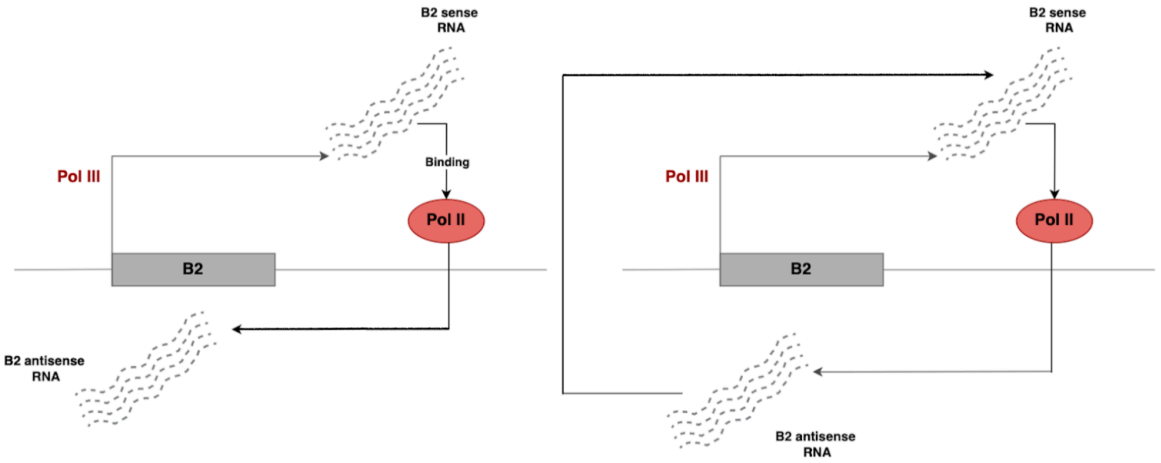

Figure 4.1: Hypothesis of sense/antisense SINE RNA regulation.

This investigation sought to provide insights into the regulatory mechanisms governing these non-coding RNAs and their roles in stress responses. By exploring

these relationships, we aimed to enhance our understanding of how B2 SINEs contribute to cellular adaptation and stress management.

The results reveal a notable relationship between the levels of B2 SINEs sense and antisense transcripts, suggesting a potential regulatory interplay where changes in the levels of one may influence the expression level of the other. This correlation indicates that B2 SE and AS may be involved in a coordinated cellular response to stress, possibly through feedback mechanisms or other forms of molecular crosstalk.

The qPCR results from the heat shock experiment show that immediately after stress, the level of B2 SE increases significantly (Figure 3.1.3), while the level of B2 AS decreases (Figure 3.1.4). These findings align with previous studies that reported increased B2 SE levels in response to stress after heating (Allen et al., 2004); (Zovoilis et al., 2016). The decrease in B2 AS levels is also understandable, as this antisense sequence carries the Pol II-associated promoter (Ferrigno et al., 2001) and can be down-regulated following cellular stress as part of a general mRNA repression.

However, after some time post-heating, the expression levels of both B2 SE and B2 AS begin to fluctuate significantly, as indicated by qPCR results. The reason for these fluctuations is currently unknown. These changes might be due to mutual regulation between B2 SE and B2 AS RNAs, with the cell attempting to restore gene expression to pre-heat shock levels.

In contrast, sequencing analysis did not confirm a similar trend for B2 AS behavior after heat shock. This discrepancy may stem from the fact that qPCR was designed using primers specific to a particular B2 subfamily (B2_Mm1a), whereas sequencing included multiple subfamilies (B2_Mm1a, B2_Mm1t, and B2_Mm2). Although sequence differences between these subfamilies are often minimal, their roles in biological processes may differ.

Long-RNA sequencing (Figure 3.4.2, B) indicates that the level of full-length B2 AS does not change after heat shock. Meanwhile, short-RNA sequencing shows that AS B2 undergoes processing (Figure 3.4.2, A), similar to B2 SE (Figure 3.4.1, A; Zovoilis et al., 2016; Espinoza et al., 2007). Direct-RNA sequencing data also showed an increase in B2 AS levels after heat shock (Figure 3.4.5, B). Further investigation into B2 AS is necessary to understand its fragmentation and potential biological significance.

On the other hand, the sequencing data confirmed the trend for B2 SE after heat shock. B2 SE levels increase (direct-RNA sequencing, Figure 3.4.5, B), with increased fragmentation and a rise in the number of fragments (short-RNA

sequencing, Figure 3.4.2, A), while the full-length B2 SE level remains unchanged (long-RNA sequencing, Figure 3.4.2, B). This behavior is consistent with previous studies showing increased B2 fragmentation during cellular stress (Espinoza et al., 2007); (Zovoilis et al., 2016); (Cheng et al., 2020). According to recent studies (Cheng et al., 2020), the fragmentation of sense B2 results in the inability of fragmented B2 RNA to block Pol II, thereby affecting gene expression.

To examine how the artificial reduction of SE B2 RNA affects its antisense transcript, an experiment with transfection of B2-specific LNAs was conducted. LNAs were chosen for their specificity and long-lasting repression of target genes compared to other reagents (Hagedorn et al., 2018); (Watts and Corey, 2012). The results indicate that suppressing B2 SE expression leads to an increase in B2 AS levels, as confirmed by both PCR (Figure 3.2.2) and sequencing data (short-/long-RNA and direct-RNA sequencing, Figure 3.4.3, A, B; Figure 3.4.6).

Conversely, after the artificial repression of B2 AS transcription, B2 SE levels increase, with qPCR results showing a significant rise 30 minutes after the procedure (Figure 3.2.3).

Additionally, when B2 SE RNA levels were artificially increased through in vitro transcription, changes in B2 AS levels were observed. Transfection with Tet150 served as a control, as it is known not to affect gene expression. Initial qPCR results showed an increase in B2 AS levels (Figure 3.3.2). This behavior of B2 AS might be due to a significant decrease in HPRT expression after B2 SE transfection. High concentrations of full-length B2 SE can influence many genes and act as a stressor itself (Espinoza et al., 2007); (Zovoilis et al., 2016); (Cheng et al., 2020), potentially leading to cell death (Zovoilis et al., 2016). When the experiment was repeated using other genes for normalization, it showed that B2 AS levels were relatively unchanged with the introduction of in vitro transcribed B2 SE compared to the control Tet150 (Figure 3.3.4). The new normalization gene was chosen from a range of Pol III transcribed genes known to maintain stable expression during heat shock (Allen et al., 2004), such as 7SK. That is because the use of Pol-II transcribed housekeeping genes has limitations of huge changes in B2 RNA expression.

Summarizing all the results, we can conclude that an increase in the expression level of B2 sense is associated with a decrease in the expression of B2 antisense. This observation suggests a possible regulatory interaction between these two types of elements, where they might modulate each other's expression levels. One potential mechanism through which B2 SE could repress B2 AS expression involves the binding of Pol II and the subsequent repression of mRNA transcription. However, the exact mechanism by which B2 AS might regulate B2 SE remains unclear.

Numerous studies have demonstrated that antisense SINEs can influence the transcription of neighboring genes, especially when they are located adjacent to and overlap with these gene sequences (Zucchelli et al., 2015); (De Brakeleer et al., 2013). Nonetheless, there is currently no direct evidence suggesting that such a mechanism is at play in this specific case. One hypothetical mechanism by which B2 AS could regulate B2 SE expression involves Argonaute2 (AGO2)-mediated translational repression. AGO2 is a crucial component of the RNA-induced silencing complex (RISC) and plays a significant role in post-transcriptional gene silencing guided by small RNAs, such as microRNAs (miRNAs) and small interfering RNAs (siRNAs). This process can lead to either mRNA degradation or translational suppression (Cho et al., 2014); (Matsui et al., 2016); (Yokota et al., 2020).

AGO2 utilizes miRNAs and siRNAs to target homologous mRNAs, which are then either degraded or translationally repressed (Lopez-Orozco et al., 2023); (Sala et al., 2023). Without the formation of the AGO2-miRNA complex, facilitated by the HSC70/Hsp90 chaperone complex, AGO2 is typically degraded (Martinez et al., 2013); (Li et al., 2020). Given the high degree of sequence homology between B2 AS and B2 SE, these elements might target each other, resulting in mutual translational suppression.

Numerous studies suggest that many mechanisms governing B2 SINE behavior in mice are mirrored by Alu elements in primates and humans (Shankar et al., 2004); (Mariner et al., 2008); (Yakovchuk et al., 2009); (Dunker et al., 2017); (Maquat et al., 2020). For instance, gene expression regulation during the stress response is conserved between Alu SINEs in humans and B2 SINEs in mice (Espinoza et al., 2007); (Zovoilis et al., 2016); (Cheng et al., 2020); (Cheng et al., 2021). This conservation extends to antisense transcripts involved in disease progression in both species (De Brakeleer et al., 2013); (Schein et al., 2016); (Takahashi et al., 2018); (Wang et al., 2019); (Espinoza et al., 2021).

Given these similarities, it is reasonable to investigate whether the Alu SINE system in humans mirrors the patterns observed in the mouse model with B2 elements. This inquiry seeks to determine whether the interplay between Alu SE and Alu AS in regulating each other’s expression levels follows a similar pattern. Understanding these analogs across species could provide deeper insights into cellular stress responses. Further research is needed to explore these parallels and clarify potential cross-species similarities in the function and regulation of SINEs.

Conclusion

In summary, this MSC project demonstrates that the expression levels of sense B2 SINEs and their corresponding antisense transcripts are interrelated. Specifically, an increase in B2 SE expression is associated with a decrease in AS levels, and vice versa - an increase in AS expression corresponds with a decrease in SE levels. This inverse relationship suggests that SE and AS mutually influence each other's expression. However, it is observed that these effects diminish over time, indicating a potential dynamic regulation between the two elements.

The underlying reasons for this behavior, as well as the specific mechanisms through which B2 SE is regulated in response to changes in AS expression levels, remain unclear. The transient nature of their interactions suggests a complex regulatory network that may involve additional factors or feedback loops. To fully understand the intricacies of this system, further research is required. Future studies should aim to elucidate the detailed mechanisms governing the interplay between B2 SE and AS, as well as the broader implications of these interactions for cellular function and stress responses.

Appendix

The PCR cycle threshold (Ct) value indicates the number of cycles required to amplify sufficient DNA for detection, crossing a set threshold.

Figure A1: Standard curves for qPCR quality assessment. *qPCR with random primers, NIH-3T3 cells after the heat shock experiment (Figure 3.1.2). B2 expression was investigated. GAPDH was used for normalization.*

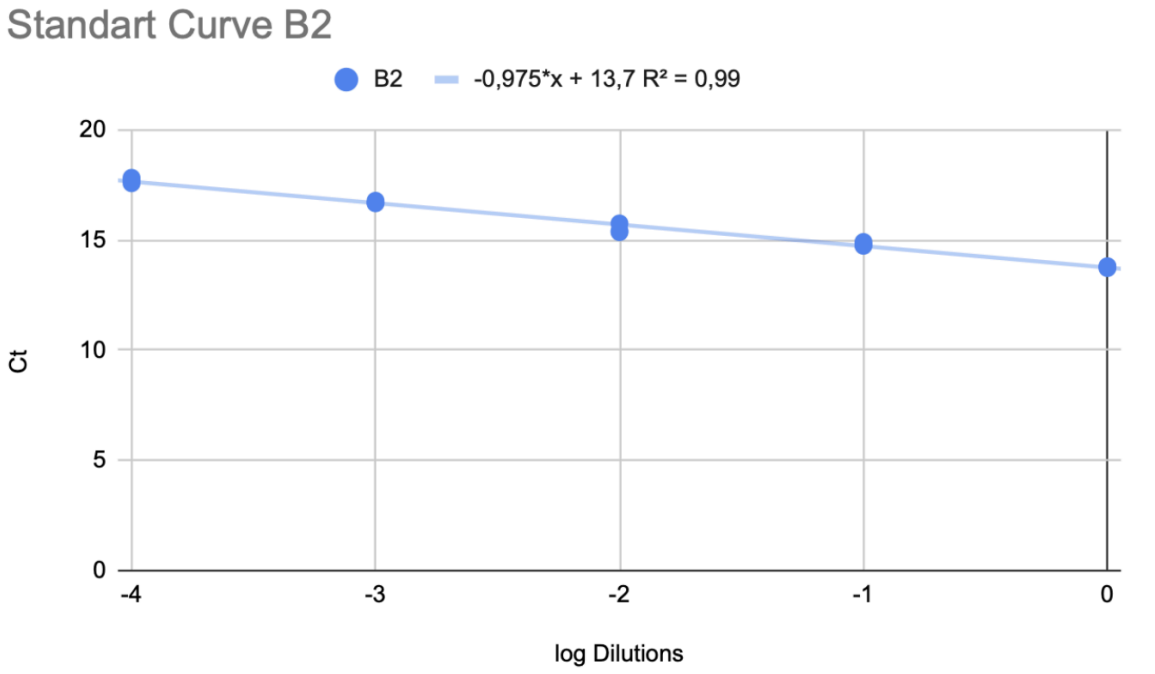

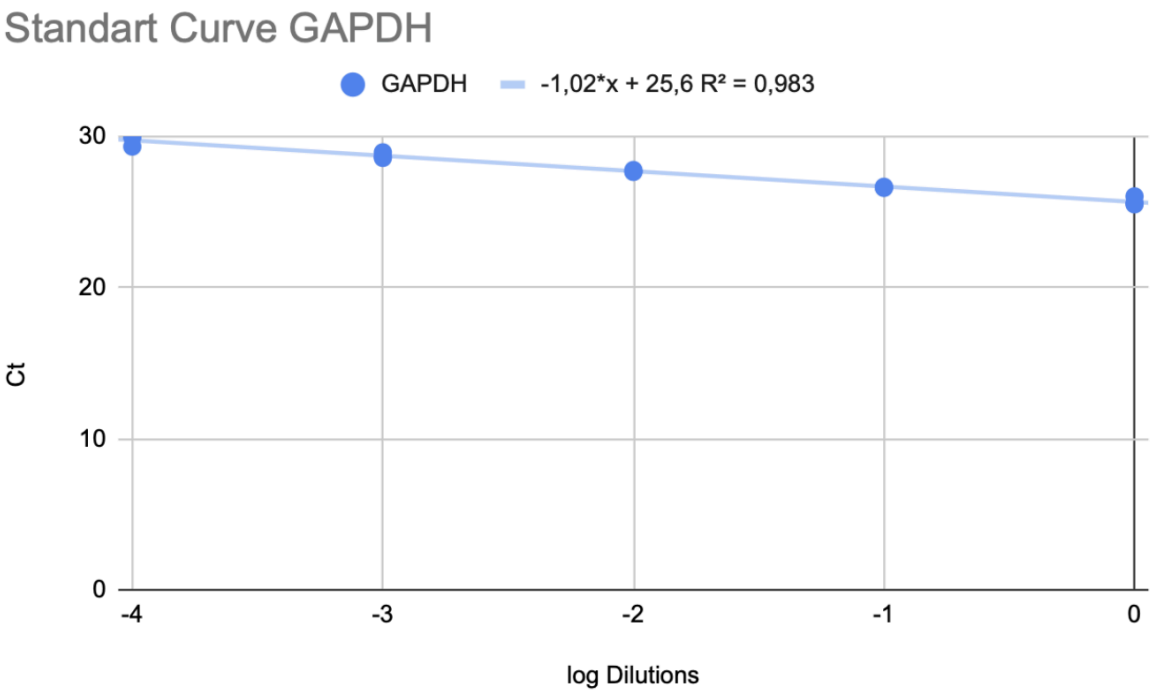

Figure A2: Standard curves for qPCR quality assessment. *qPCR with gene-specefic primers, NIH-3T3 cells after the heat shock experiment (Figure 3.1.3). B2 sense expression was investigated. GAPDH forward (F) was used for normalization.*

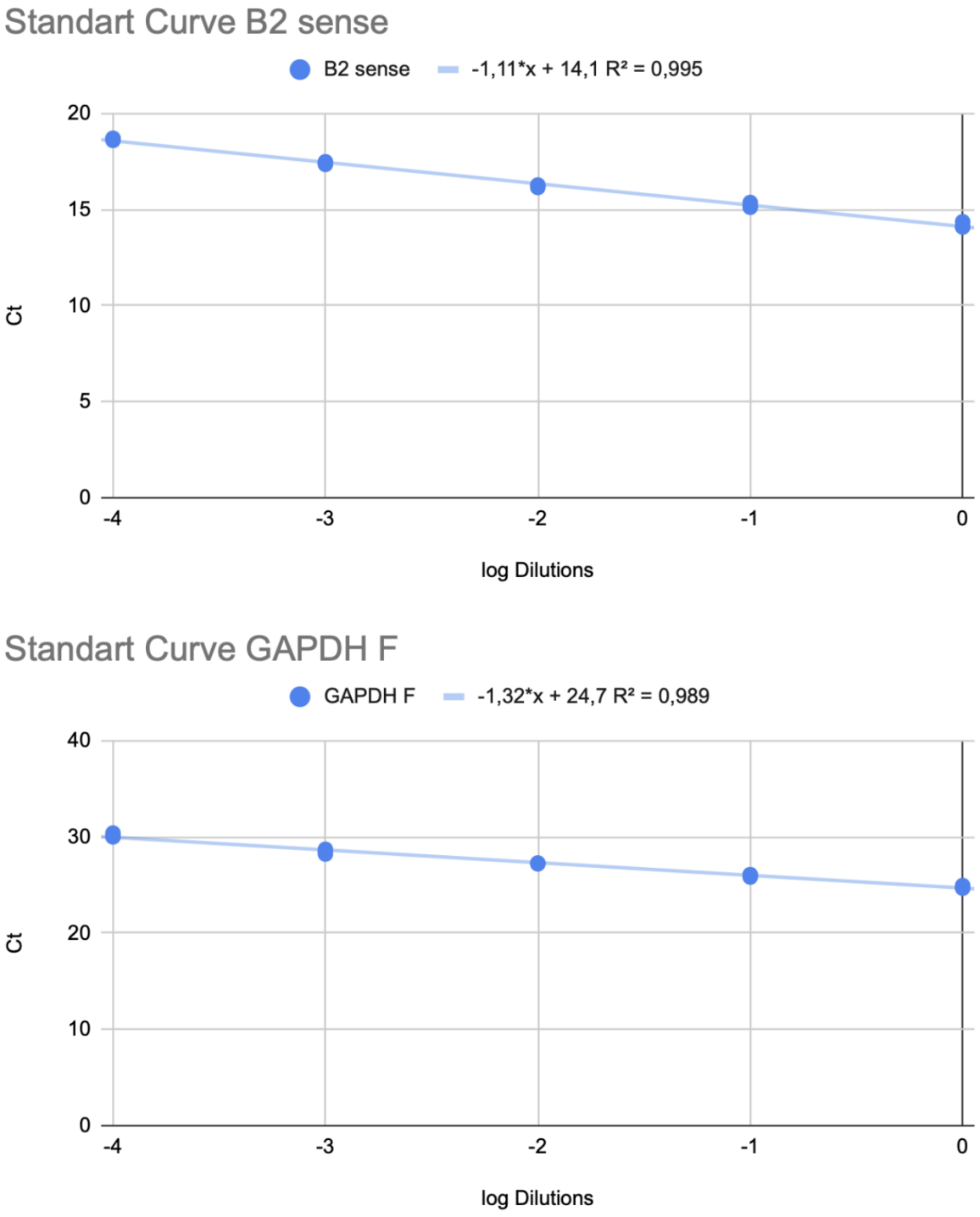

Figure A3: Standard curves for qPCR quality assessment. *qPCR with gene-specefic primers, NIH-3T3 cells after the heat shock experiment (Figure 3.1.4). B2 antisense expression was investigated. GAPDH reverse (R) was used for normalization.*

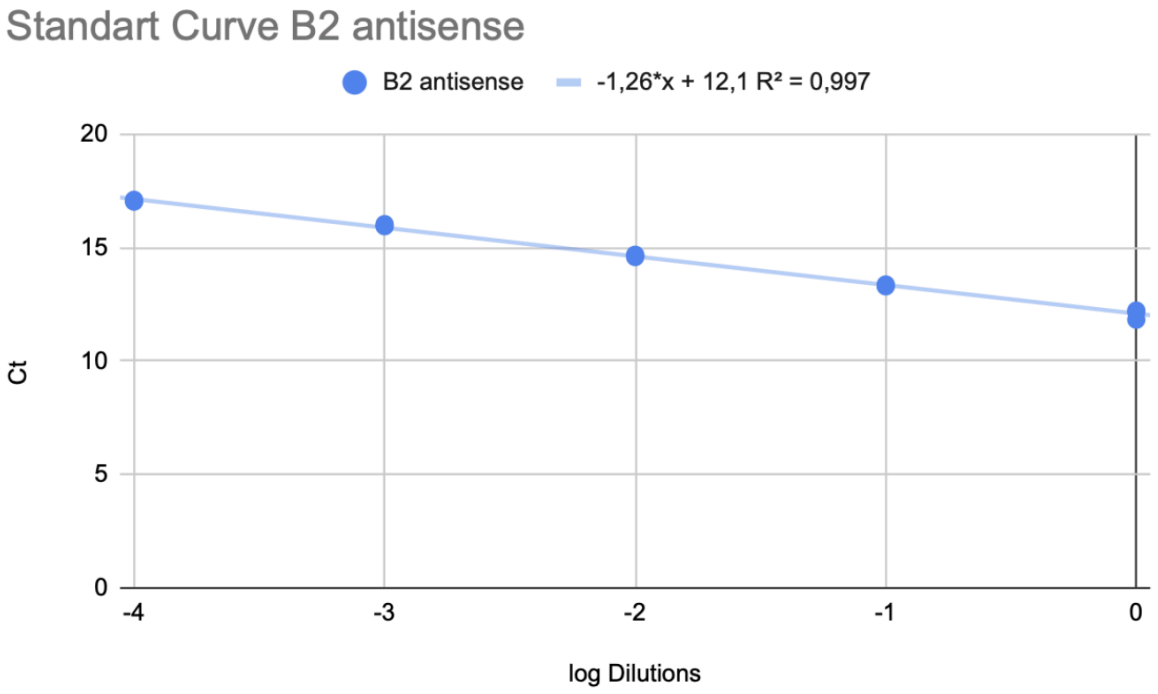
Standart Curve B2 antisense
B2 antisense
-1,26*x + 12,1 R² = 0,997
20
15
10
5
0
Ct
-4
-3
-2
-1
0
log Dilutions

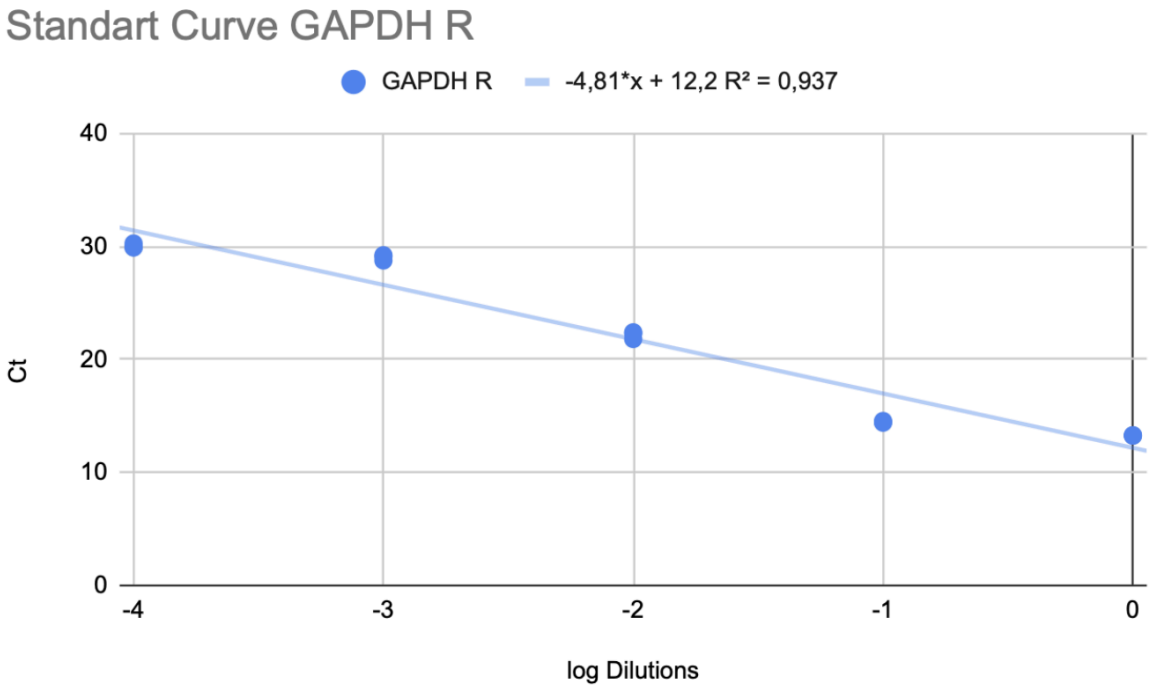
Standart Curve GAPDH R
GAPDH R
-4,81*x + 12,2 R² = 0,937
40
30
20
10
0
Ct
-4
-3
-2
-1
0
log Dilutions

Figure A4: Standard curves for qPCR quality assessment. *qPCR with gene-specefic primers, NIH-3T3 cells after transfection of LNAs against B2 sense (Figure 3.2.2). B2 antisense expression was investigated. GAPDH reverse (R) was used for normalization.*

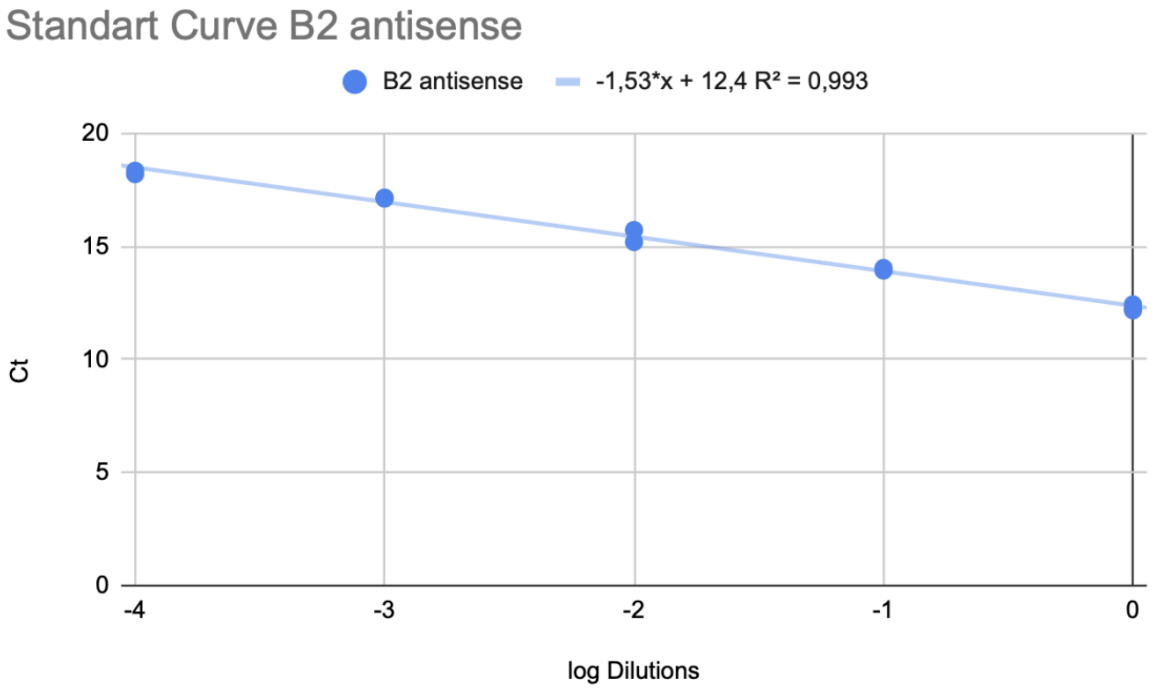

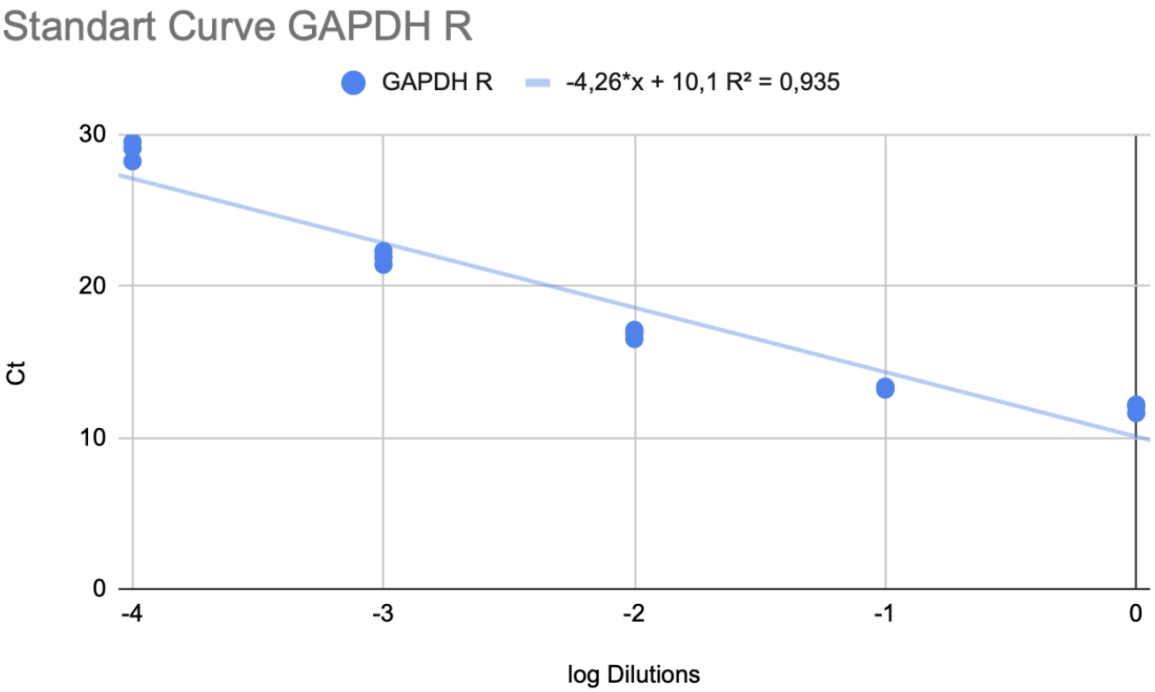

Figure A5: Standard curves for qPCR quality assessment. *qPCR with gene-specefic primers, NIH-3T3 cells after transfection of LNAs against B2 antisense (Figure 3.2.3). B2 antisense expression was investigated. GAPDH forward (F) was used for normalization.*

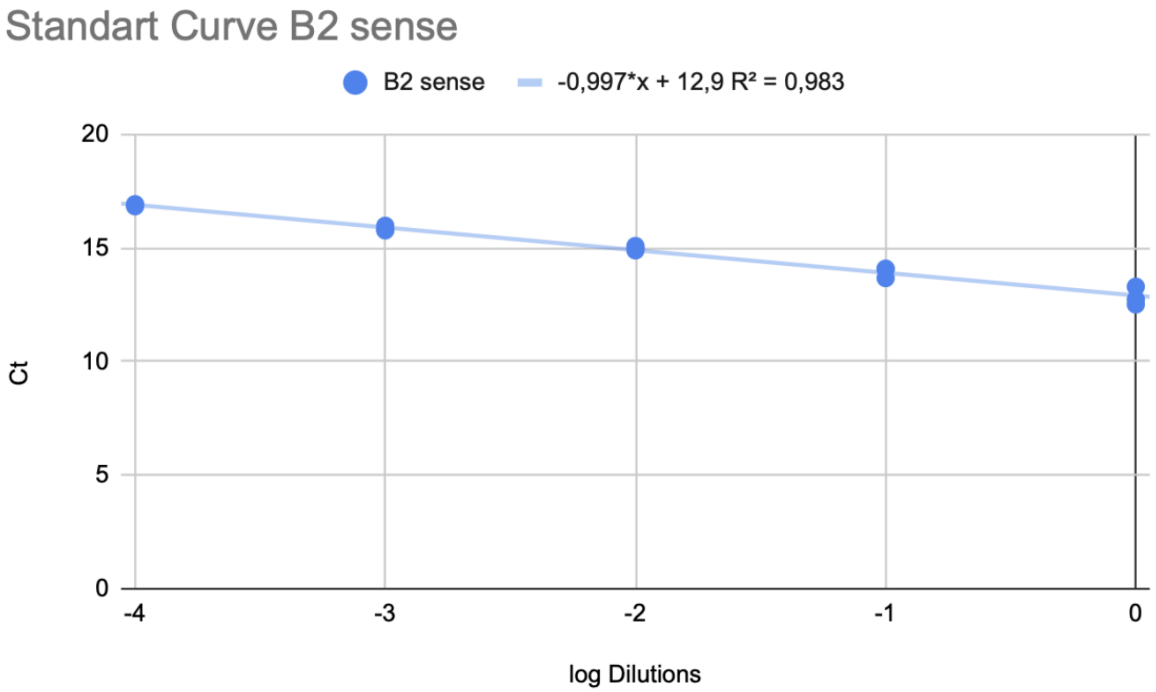

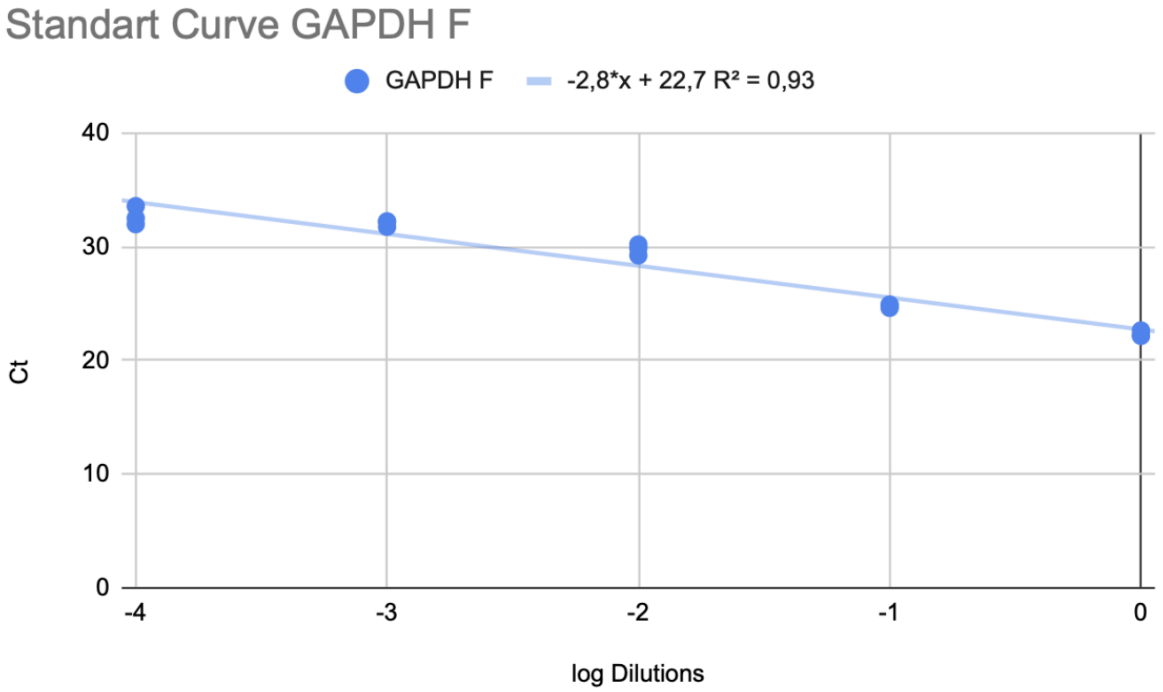

Figure A6: Standard curves for qPCR quality assessment. *qPCR with gene-specefic primers, NIH-3T3 cells after transfection of in vitro transcribed B2 sense (Figure 3.3.1). B2 sense expression was investigated. HPRT forward (F) was used for normalization.*

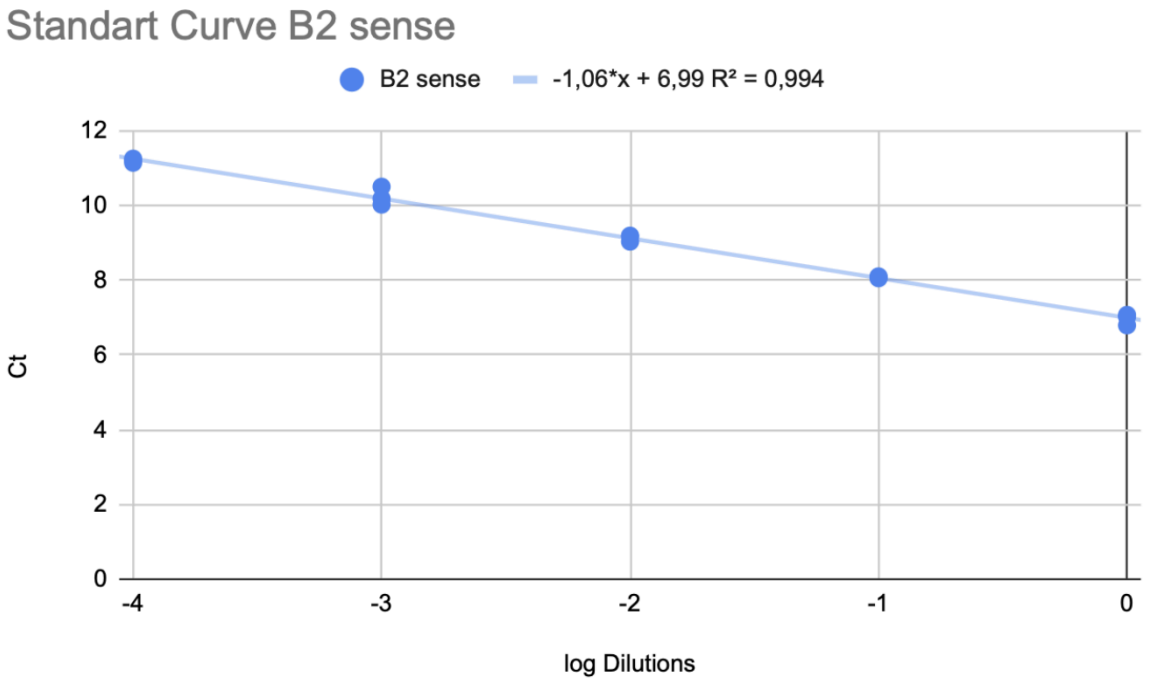

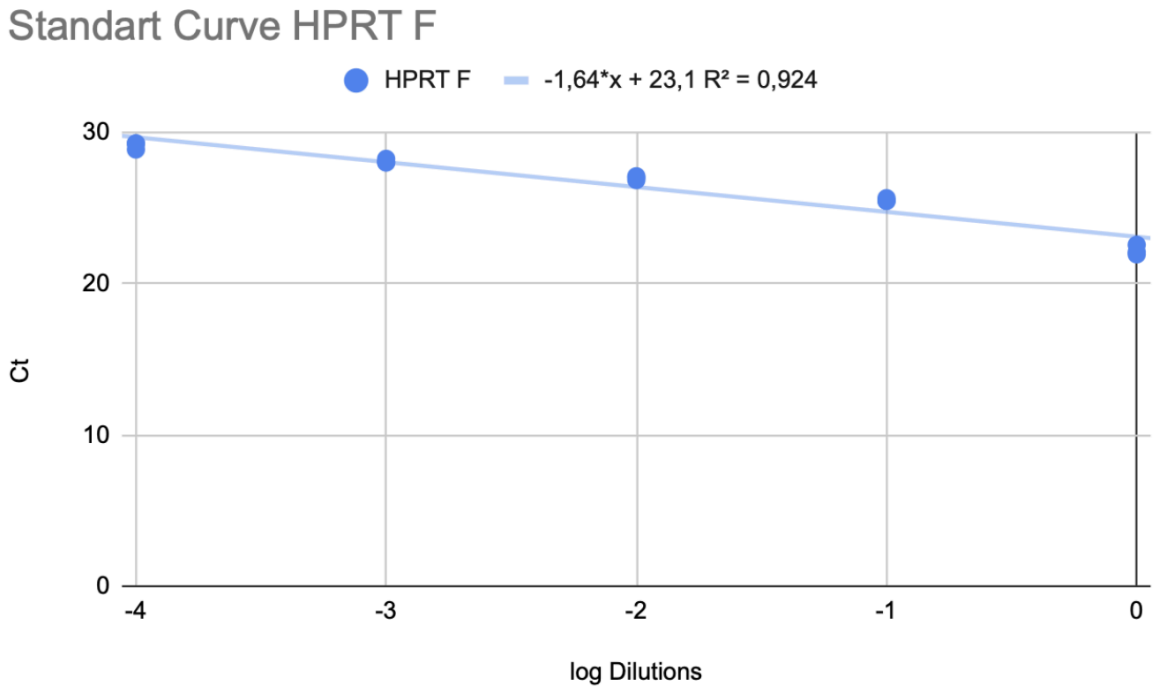

Figure A7: Standard curves for qPCR quality assessment. *qPCR with gene-specefic primers, NIH-3T3 cells after transfection of in vitro transcribed B2 sense (Figure*

3.3.2). B2 antisense expression was investigated. HPRT reverse (R) was used for normalization.

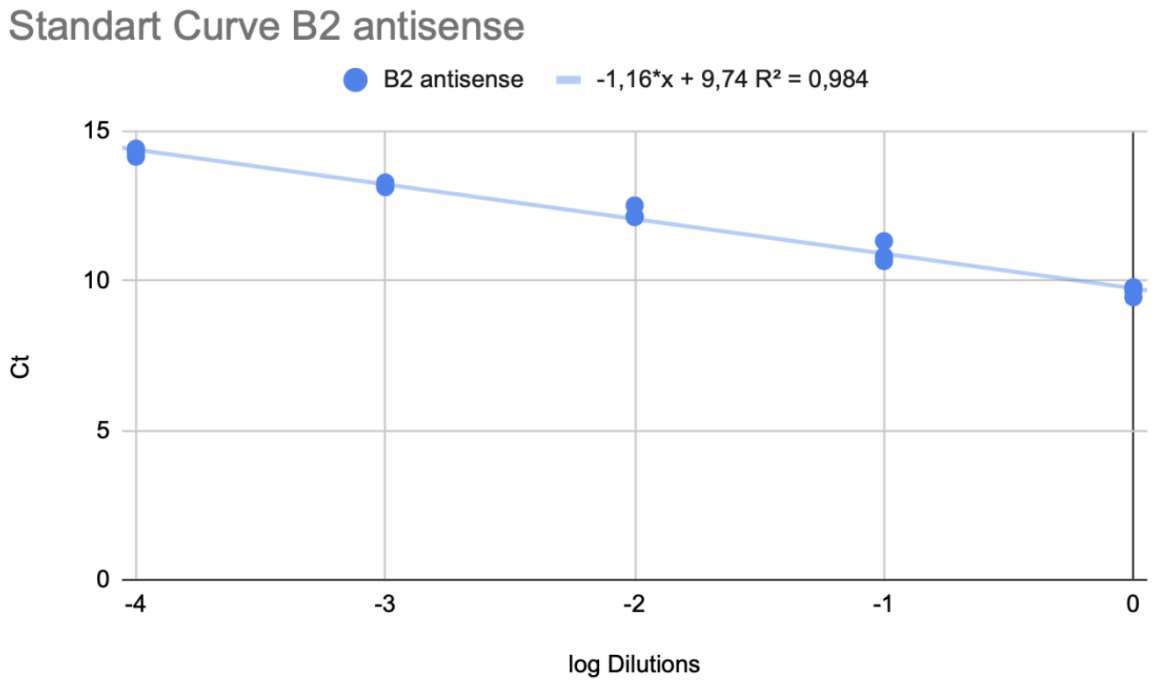

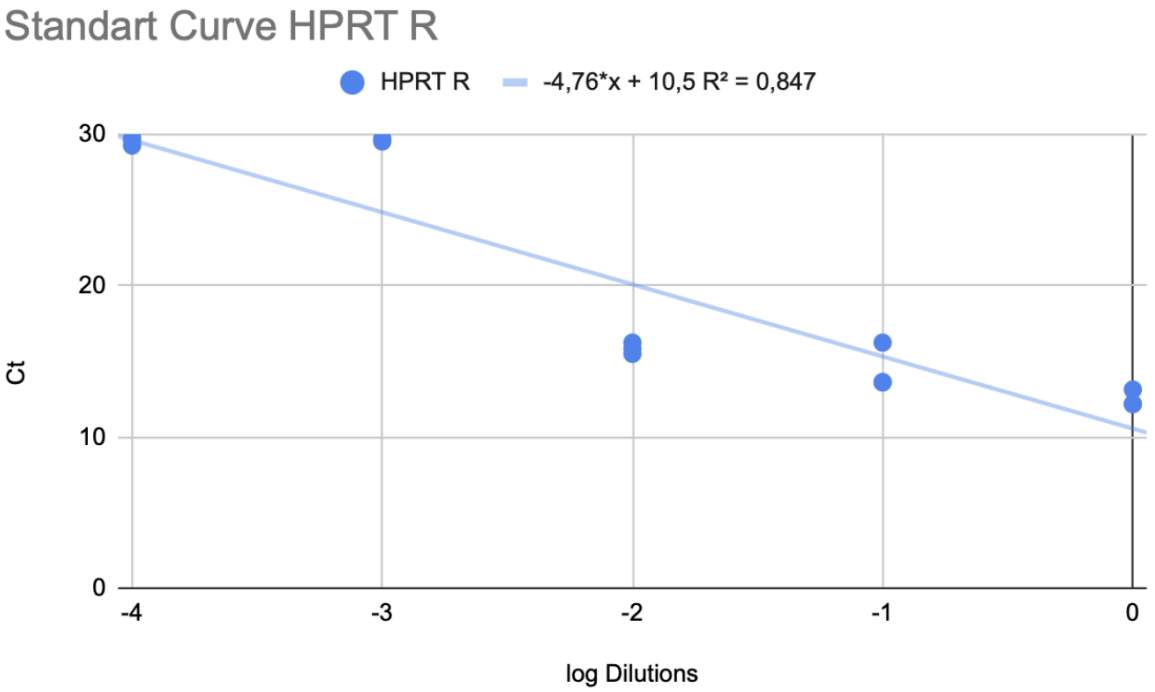

Figure A8: Standard curves for qPCR quality assessment. *qPCR with gene-specefic primers, NIH-3T3 cells after transfection of in vitro transcribed B2 sense (Figure 3.3.3). B2 sense expression was investigated. 7SK forward (F) was used for normalization.*

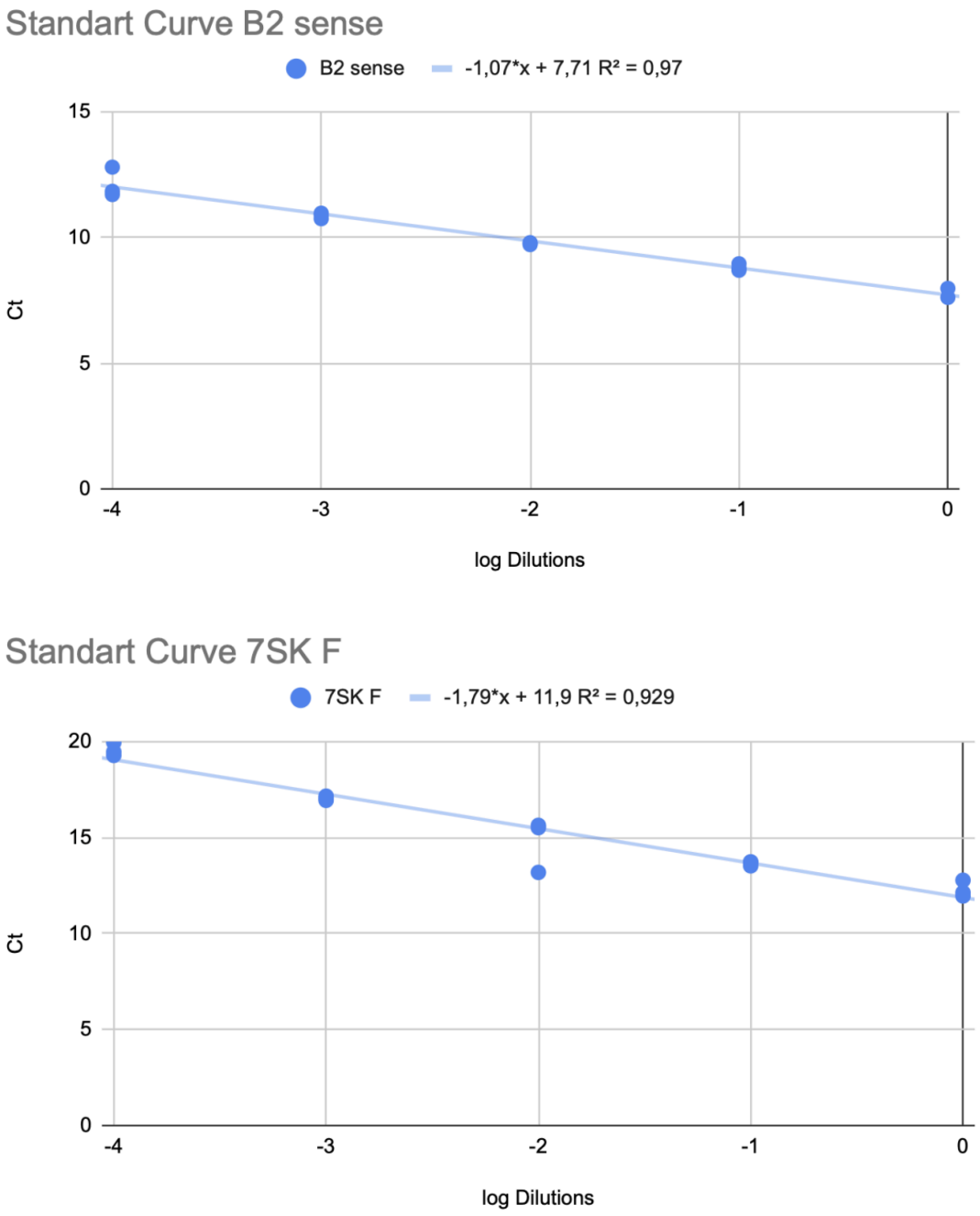

Figure A9: Standard curves for qPCR quality assessment. *qPCR with gene-specefic primers, NIH-3T3 cells after transfection of in vitro transcribed B2 sense (Figure 3.3.4). B2 antisense expression was investigated. 7SK reverse (R) was used for normalization.*

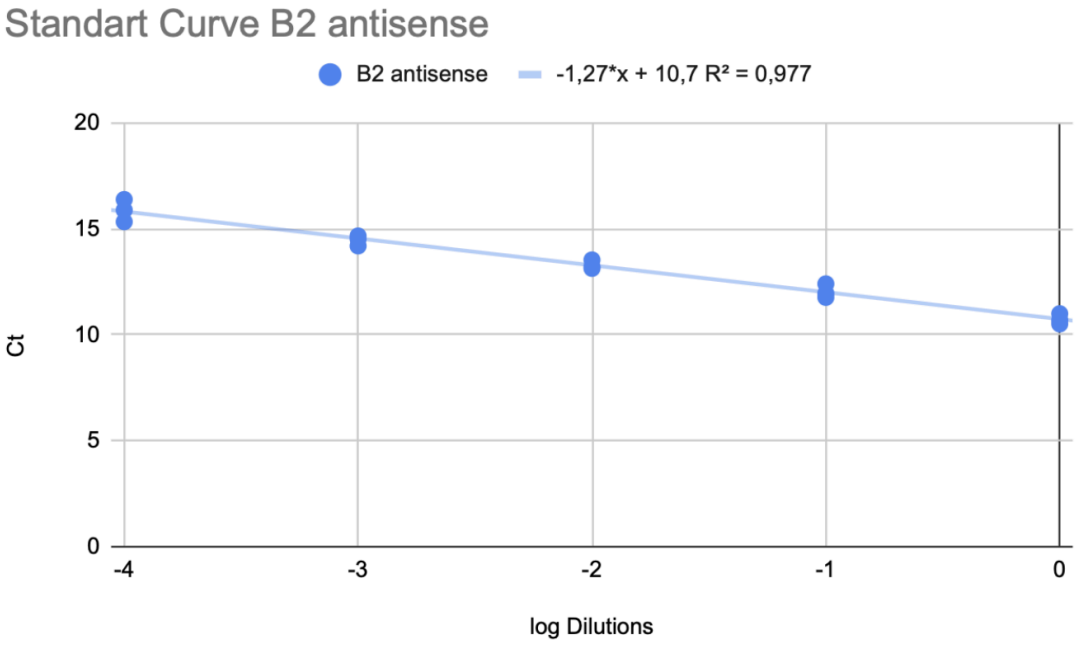

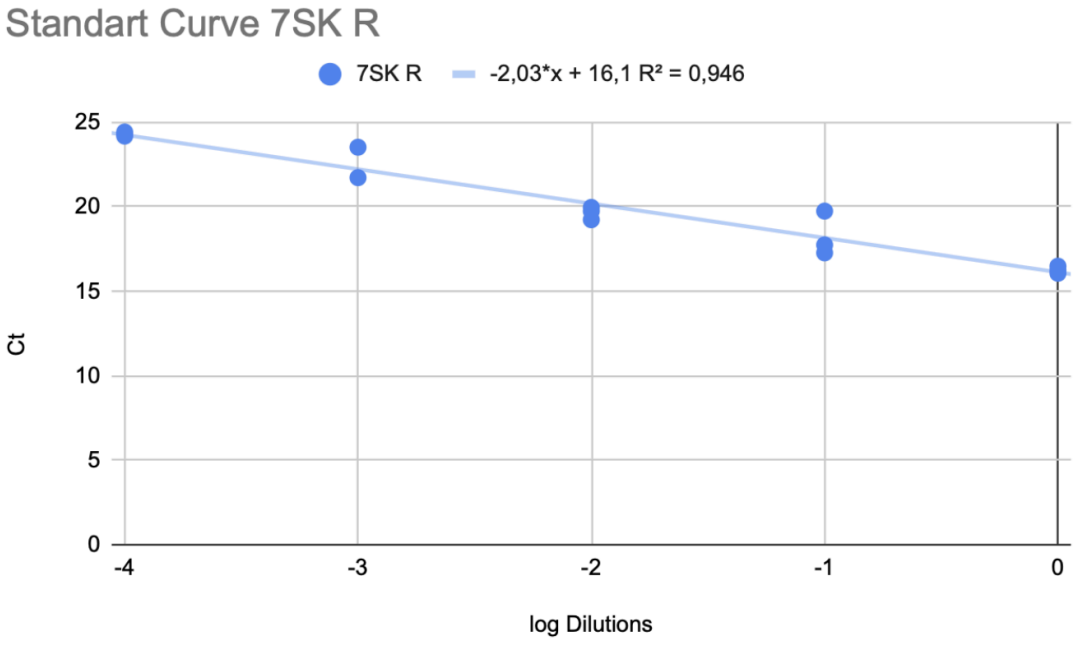

References

de Koning AP, Gu W, Castoe TA, Batzer MA, Pollock DD. Repetitive elements may comprise over two-thirds of the human genome. PLoS Genet. 2011 Dec;7(12):e1002384. doi: 10.1371/journal.pgen.1002384. Epub 2011 Dec 1. PMID: 22144907; PMCID: PMC3228813.

Palazzo AF, Gregory TR. The case for junk DNA. PLoS Genet. 2014 May 8;10(5):e1004351. doi: 10.1371/journal.pgen.1004351. PMID: 24809441; PMCID: PMC4014423.

Fernandes JCR, Acuña SM, Aoki JI, Floeter-Winter LM, Muxel SM. Long Non-Coding RNAs in the Regulation of Gene Expression: Physiology and Disease. Noncoding RNA. 2019 Feb 17;5(1):17. doi: 10.3390/ncrna5010017. PMID: 30781588; PMCID: PMC6468922.

Winkle M, El-Daly SM, Fabbri M, Calin GA. Noncoding RNA therapeutics - challenges and potential solutions. Nat Rev Drug Discov. 2021 Aug;20(8):629-651. doi: 10.1038/s41573-021-00219-z. Epub 2021 Jun 18. PMID: 34145432; PMCID: PMC8212082.

Kobayashi T. Ribosomal RNA gene repeats, their stability and cellular senescence. Proc Jpn Acad Ser B Phys Biol Sci. 2014;90(4):119-29. doi: 10.2183/pjab.90.119. PMID: 24727936; PMCID: PMC4055705.

Hori Y, Engel C, Kobayashi T. Regulation of ribosomal RNA gene copy number, transcription and nucleolus organization in eukaryotes. Nat Rev Mol Cell Biol. 2023 Jun;24(6):414-429. doi: 10.1038/s41580-022-00573-9. Epub 2023 Feb 2. PMID: 36732602.

Li P, Yu X. The role of rRNA in maintaining genome stability. DNA Repair (Amst). 2024 Jul;139:103692. doi: 10.1016/j.dnarep.2024.103692. Epub 2024 May 12. PMID: 38759435.

Fleurier S, Dapa T, Tenaillon O, Condon C, Matic I. rRNA operon multiplicity as a bacterial genome stability insurance policy. Nucleic Acids Res. 2022 Dec 9;50(22):12601-12620. doi: 10.1093/nar/gkac332. PMID: 35552441; PMCID: PMC9825170.

Fernández-Millán P, Schelcher C, Chihade J, Masquida B, Giegé P, Sauter C. Transfer RNA: From pioneering crystallographic studies to contemporary tRNA biology. Arch Biochem Biophys. 2016 Jul 15;602:95-105. doi: 10.1016/j.abb.2016.03.005. Epub 2016 Mar 8. PMID: 26968773.

Cui W, Zhao D, Jiang J, Tang F, Zhang C, Duan C. tRNA Modifications and Modifying Enzymes in Disease, the Potential Therapeutic Targets. Int J Biol Sci. 2023 Feb 13;19(4):1146-1162. doi: 10.7150/ijbs.80233. PMID: 36923941; PMCID: PMC10008702.

Wang Y, Tao EW, Tan J, Gao QY, Chen YX, Fang JY. tRNA modifications: insights into their role in human cancers. Trends Cell Biol. 2023 Dec;33(12):1035-1048. doi: 10.1016/j.tcb.2023.04.002. Epub 2023 May 12. PMID: 37179136.

Zhou Z, Sun B, Huang S, Jia W, Yu D. The tRNA-associated dysregulation in diabetes mellitus. Metabolism. 2019 May;94:9-17. doi: 10.1016/j.metabol.2019.01.017. Epub 2019 Feb 1. PMID: 30711570.

Quinn JJ, Chang HY. Unique features of long non-coding RNA biogenesis and function. Nat Rev Genet. 2016 Jan;17(1):47-62. doi: 10.1038/nrg.2015.10. PMID: 26666209.

Zong Y, Wang X, Cui B, Xiong X, Wu A, Lin C, Zhang Y. Decoding the regulatory roles of non-coding RNAs in cellular metabolism and disease. Mol Ther. 2023 Jun 7;31(6):1562-1576. doi: 10.1016/j.ymthe.2023.04.012. Epub 2023 Apr 27. PMID: 37113055; PMCID: PMC10277898.

Mercer TR, Dinger ME, Mattick JS. Long non-coding RNAs: insights into functions. Nat Rev Genet. 2009 Mar;10(3):155-9. doi: 10.1038/nrg2521. PMID: 19188922.

Bratkovič T, Božič J, Rogelj B. Functional diversity of small nucleolar RNAs. Nucleic Acids Res. 2020 Feb 28;48(4):1627-1651. doi: 10.1093/nar/gkz1140. PMID: 31828325; PMCID: PMC7038934.

Fabian MR, Sonenberg N, Filipowicz W. Regulation of mRNA translation and stability by microRNAs. Annu Rev Biochem. 2010;79:351-79. doi: 10.1146/annurev-biochem-060308-103103. PMID: 20533884.

Wang P, Zhou Y, Richards AM. Effective tools for RNA-derived therapeutics: siRNA interference or miRNA mimicry. Theranostics. 2021 Aug 11;11(18):8771-8796. doi: 10.7150/thno.62642. PMID: 34522211; PMCID: PMC8419061.

Zovoilis A, Pantazi A, Smorag L, Opitz L, Riester GS, Wolf M, Zechner U, Holubowska A, Stewart CL, Engel W. Embryonic stem cell-related miRNAs are involved in differentiation of pluripotent cells originating from the germ line. Mol Hum Reprod. 2010 Nov;16(11):793-803. doi: 10.1093/molehr/gaq053. Epub 2010 Jun 21. PMID: 20566704.

Liao B, Bao X, Liu L, Feng S, Zovoilis A, Liu W, Xue Y, Cai J, Guo X, Qin B, Zhang R, Wu J, Lai L, Teng M, Niu L, Zhang B, Esteban MA, Pei D. MicroRNA cluster 302-367 enhances somatic cell reprogramming by accelerating a mesenchymal-to-epithelial transition. J Biol Chem. 2011 May 13;286(19):17359-64. doi: 10.1074/jbc.C111.235960. Epub 2011 Mar 22. PMID: 21454525; PMCID: PMC3089577.

Zovoilis A, Mungall AJ, Moore R, Varhol R, Chu A, Wong T, Marra M, Jones SJ. The expression level of small non-coding RNAs derived from the first exon of protein-coding genes is predictive of cancer status. EMBO Rep. 2014 Apr;15(4):402-10. doi: 10.1002/embr.201337950. Epub 2014 Feb 17. PMID: 24534129; PMCID: PMC3989671.

Zovoilis A, Agbemenyah HY, Agis-Balboa RC, Stilling RM, Edbauer D, Rao P, Farinelli L, Delalle I, Schmitt A, Falkai P, Bahari-Javan S, Burkhardt S, Sananbenesi F, Fischer A. microRNA-34c is a novel target to treat dementias. EMBO J. 2011 Sep 23;30(20):4299-308. doi: 10.1038/emboj.2011.327. PMID: 21946562; PMCID: PMC3199394.

Wells JN, Feschotte C. A Field Guide to Eukaryotic Transposable Elements. Annu Rev Genet. 2020 Nov 23;54:539-561. doi: 10.1146/annurev-genet-040620-022145. Epub 2020 Sep 21. PMID: 32955944; PMCID: PMC8293684.

Wu Y, Wu X, Li S. Retrotransposons: Jump to Cancer? Trends Cancer. 2021 Jul;7(7):577-579. doi: 10.1016/j.trecan.2021.04.004. Epub 2021 May 13. PMID: 33992534.

Payer LM, Burns KH. Transposable elements in human genetic disease. Nat Rev Genet. 2019 Dec;20(12):760-772. doi: 10.1038/s41576-019-0165-8. Epub 2019 Sep 12. PMID: 31515540.

Sargurupremraj M, Wjst M. Transposable elements and their potential role in complex lung disorder. Respir Res. 2013 Oct 5;14(1):99. doi: 10.1186/1465-9921-14-99. PMID: 24093510; PMCID: PMC3851442.

Hayward A, Gilbert C. Transposable elements. Curr Biol. 2022 Sep 12;32(17):R904-R909. doi: 10.1016/j.cub.2022.07.044. PMID: 36099891.

Pace JK 2nd, Feschotte C. The evolutionary history of human DNA transposons: evidence for intense activity in the primate lineage. Genome Res. 2007 Apr;17(4):422-32. doi: 10.1101/gr.5826307. Epub 2007 Mar 5. PMID: 17339369; PMCID: PMC1832089.

Richardson SR, Doucet AJ, Kopera HC, Moldovan JB, Garcia-Perez JL, Moran JV. The Influence of LINE-1 and SINE Retrotransposons on Mammalian Genomes. Microbiol Spectr. 2015 Apr;3(2):MDNA3-0061-2014. doi: 10.1128/microbiolspec.MDNA3-0061-2014. PMID: 26104698; PMCID: PMC4498412.

Szafranski K, Dingermann T, Glöckner G, Winckler T. Template jumping by a LINE reverse transcriptase has created a SINE-like 5S rRNA retropseudogene in Dictyostelium. Mol Genet Genomics. 2004 Feb;271(1):98-102. doi: 10.1007/s00438-003-0961-9. Epub 2003 Dec 2. PMID: 14652739.

Scarfò I, Pellegrino E, Mereu E, Inghirami G, Piva R. Transposable elements: The enemies within. Exp Hematol. 2016 Oct;44(10):913-6. doi: 10.1016/j.exphem.2016.06.251. Epub 2016 Jul 1. PMID: 27377925.

Crow MK. Long interspersed nuclear elements (LINE-1): potential triggers of systemic autoimmune disease. Autoimmunity. 2010 Feb;43(1):7-16. doi: 10.3109/08916930903374865. PMID: 19961365.

Takahashi T, Stoiljkovic M, Song E, Gao XB, Yasumoto Y, Kudo E, Carvalho F, Kong Y, Park A, Shanabrough M, Szigeti-Buck K, Liu ZW, Kristant A, Zhang Y, Sulkowski P, Glazer PM, Kaczmarek LK, Horvath TL, Iwasaki A. LINE-1 activation in the cerebellum drives ataxia. Neuron. 2022 Oct 19;110(20):3278-3287.e8. doi: 10.1016/j.neuron.2022.08.011. Epub 2022 Sep 6. PMID: 36070749; PMCID: PMC9588660.

Toda T, Bedrosian TA, Schafer ST, Cuoco MS, Linker SB, Ghassemzadeh S, Mitchell L, Whiteley JT, Novaresi N, McDonald AH, Gallina IS, Yoon H, Hester ME, Pena M, Lim C, Suljic E, AlFatah Mansour A, Boulard M, Parylak SL, Gage FH. Long interspersed nuclear elements safeguard neural progenitors from precocious differentiation. Cell Rep. 2024 Feb 27;43(2):113774. doi: 10.1016/j.celrep.2024.113774. Epub 2024 Feb 13. PMID: 38349791; PMCID: PMC10948021.

Terry DM, Devine SE. Aberrantly High Levels of Somatic LINE-1 Expression and Retrotransposition in Human Neurological Disorders. Front Genet. 2020 Jan 8;10:1244. doi: 10.3389/fgene.2019.01244. PMID: 31969897; PMCID: PMC6960195.

Zhang XO, Pratt H, Weng Z. Investigating the Potential Roles of SINEs in the Human Genome. Annu Rev Genomics Hum Genet. 2021 Aug 31;22:199-218. doi: 10.1146/annurev-genom-111620-100736. Epub 2021 Apr 1. PMID: 33792357.

Tshilenge KT, Bons J, Aguirre CG, Geronimo-Olvera C, Shah S, Rose J, Gerencser AA, Mak SK, Ehrlich ME, Bragg DC, Schilling B, Ellerby LM. Proteomic analysis of X-linked dystonia parkinsonism disease striatal neurons reveals altered RNA metabolism and splicing. Neurobiol Dis. 2024 Jan;190:106367. doi: 10.1016/j.nbd.2023.106367. Epub 2023 Nov 30. PMID: 38042508; PMCID: PMC11103251.

Mustafin RN, Khusnutdinova EK. Involvement of transposable elements in Alzheimer's disease pathogenesis. Vavilovskii Zhurnal Genet Selektsii. 2024 Apr;28(2):228-238. doi: 10.18699/vjgb-24-27. PMID: 38680184; PMCID: PMC11043511.

Kaneko H, Dridi S, Tarallo V, Gelfand BD, Fowler BJ, Cho WG, Kleinman ME, Ponicsan SL, Hauswirth WW, Chiodo VA, Karikó K, Yoo JW, Lee DK, Hadziahmetovic M, Song Y, Misra S, Chaudhuri G, Buaas FW, Braun RE, Hinton DR, Zhang Q, Grossniklaus HE, Provis JM, Madigan MC, Milam AH, Justice NL, Albuquerque RJ, Blandford AD, Bogdanovich S, Hirano Y, Witta J, Fuchs E, Littman DR, Ambati BK, Rudin CM, Chong MM, Provost P, Kugel JF, Goodrich JA, Dunaief JL, Baffi JZ, Ambati J. DICER1 deficit induces Alu RNA toxicity in age-related macular degeneration. Nature. 2011 Mar 17;471(7338):325-30. doi: 10.1038/nature09830. Epub 2011 Feb 6. PMID: 21297615; PMCID: PMC3077055.

Tarallo V, Hirano Y, Gelfand BD, Dridi S, Kerur N, Kim Y, Cho WG, Kaneko H, Fowler BJ, Bogdanovich S, Albuquerque RJ, Hauswirth WW, Chiodo VA, Kugel JF, Goodrich JA, Ponicsan SL, Chaudhuri G, Murphy MP, Dunaief JL, Ambati BK, Ogura Y, Yoo JW, Lee DK, Provost P, Hinton DR, Núñez G, Baffi JZ, Kleinman ME, Ambati J. DICER1 loss and Alu RNA induce age-related macular degeneration via the NLRP3 inflammasome and MyD88. Cell. 2012 May 11;149(4):847-59. doi: 10.1016/j.cell.2012.03.036. Epub 2012 Apr 26. PMID: 22541070; PMCID: PMC3351582.

Vergani-Junior CA, Tonon-da-Silva G, Inan MD, Mori MA. DICER: structure, function, and regulation. Biophys Rev. 2021 Nov 16;13(6):1081-1090. doi: 10.1007/s12551-021-00902-w. PMID: 35059029; PMCID: PMC8724510.

Sundermeier TR, Sakami S, Sahu B, Howell SJ, Gao S, Dong Z, Golczak M, Maeda A, Palczewski K. MicroRNA-processing Enzymes Are Essential for Survival and Function of Mature Retinal Pigmented Epithelial Cells in Mice. J Biol Chem. 2017

Feb 24;292(8):3366-3378. doi: 10.1074/jbc.M116.770024. Epub 2017 Jan 19. PMID: 28104803; PMCID: PMC5336169.

Magliacane Trotta S, Adinolfi A, D'Orsi L, Panico S, Mercadante G, Mehlen P, Ambati J, De Falco S, Tarallo V. Cancer-derived exosomal Alu RNA promotes colorectal cancer progression. Exp Mol Med. 2024 Mar;56(3):700-710. doi: 10.1038/s12276-024-01166-6. Epub 2024 Mar 14. PMID: 38486106; PMCID: PMC10984964.

Stenz L. The L1-dependant and Pol III transcribed Alu retrotransposon, from its discovery to innate immunity. Mol Biol Rep. 2021 Mar;48(3):2775-2789. doi: 10.1007/s11033-021-06258-4. Epub 2021 Mar 16. PMID: 33725281; PMCID: PMC7960883.

Schmitz J, Brosius J. Exonization of transposed elements: A challenge and opportunity for evolution. Biochimie. 2011 Nov;93(11):1928-34. doi: 10.1016/j.biochi.2011.07.014. Epub 2011 Jul 26. PMID: 21787833.

Dunker W, Zhao Y, Song Y, Karijolich J. Recognizing the SINEs of Infection: Regulation of Retrotransposon Expression and Modulation of Host Cell Processes. Viruses. 2017 Dec 18;9(12):386. doi: 10.3390/v9120386. PMID: 29258254; PMCID: PMC5744160.

Sharma H, Valentine MNZ, Toki N, Sueki HN, Gustincich S, Takahashi H, Carninci P. Decryption of sequence, structure, and functional features of SINE repeat elements in SINEUP non-coding RNA-mediated post-transcriptional gene regulation. Nat Commun. 2024 Feb 21;15(1):1400. doi: 10.1038/s41467-024-45517-3. PMID: 38383605; PMCID: PMC10881587.

Pélissier T, Bousquet-Antonelli C, Lavie L, Deragon JM. Synthesis and processing of tRNA-related SINE transcripts in Arabidopsis thaliana. Nucleic Acids Res. 2004 Jul 28;32(13):3957-66. doi: 10.1093/nar/gkh738. PMID: 15282328; PMCID: PMC506818.

Nikaido M, Nishihara H, Okada N. SINEs as Credible Signs to Prove Common Ancestry in the Tree of Life: A Brief Review of Pioneering Case Studies in Retroposon Systematics. Genes (Basel). 2022 May 31;13(6):989. doi: 10.3390/genes13060989. PMID: 35741751; PMCID: PMC9223172.

Kriegs JO, Churakov G, Jurka J, Brosius J, Schmitz J. Evolutionary history of 7SL RNA-derived SINEs in Supraprimates. Trends Genet. 2007 Apr;23(4):158-61. doi: 10.1016/j.tig.2007.02.002. Epub 2007 Feb 20. PMID: 17307271.

Walters RD, Kugel JF, Goodrich JA. InvAluable junk: the cellular impact and function of Alu and B2 RNAs. IUBMB Life. 2009 Aug;61(8):831-7. doi: 10.1002/iub.227. PMID: 19621349; PMCID: PMC4049031.

Maquat LE. Short interspersed nuclear element (SINE)-mediated post-transcriptional effects on human and mouse gene expression: SINE-UP for active duty. Philos Trans R Soc Lond B Biol Sci. 2020 Mar 30;375(1795):20190344. doi: 10.1098/rstb.2019.0344. Epub 2020 Feb 10. PMID: 32075563; PMCID: PMC7061979.

Nossent AY. The epitranscriptome: RNA modifications in vascular remodelling. Atherosclerosis. 2023 Jun;374:24-33. doi: 10.1016/j.atherosclerosis.2022.11.004. Epub 2022 Nov 9. PMID: 36400603.

Witman NM, Behm M, Ohman M, Morrison JI. ADAR-related activation of adenosine-to-inosine RNA editing during regeneration. Stem Cells Dev. 2013 Aug 15;22(16):2254-67. doi: 10.1089/scd.2013.0104. Epub 2013 May 3. PMID: 23534823.

Chen LL, Carmichael GG. Gene regulation by SINES and inosines: biological consequences of A-to-I editing of Alu element inverted repeats. Cell Cycle. 2008 Nov 1;7(21):3294-301. doi: 10.4161/cc.7.21.6927. Epub 2008 Nov 5. PMID: 18948735.

Rottman FM, Bokar JA, Narayan P, Shambaugh ME, Ludwiczak R. N6-adenosine methylation in mRNA: substrate specificity and enzyme complexity. Biochimie. 1994;76(12):1109-14. doi: 10.1016/0300-9084(94)90038-8. PMID: 7748945.

Liu J, Yue Y, Han D, Wang X, Fu Y, Zhang L, Jia G, Yu M, Lu Z, Deng X, Dai Q, Chen W, He C. A METTL3-METTL14 complex mediates mammalian nuclear RNA N6-adenosine methylation. Nat Chem Biol. 2014 Feb;10(2):93-5. doi: 10.1038/nchembio.1432. Epub 2013 Dec 6. PMID: 24316715; PMCID: PMC3911877.

Schwartz S, Bernstein DA, Mumbach MR, Jovanovic M, Herbst RH, León-Ricardo BX, Engreitz JM, Guttman M, Satija R, Lander ES, Fink G, Regev A. Transcriptome-wide mapping reveals widespread dynamic-regulated pseudouridylation of ncRNA and mRNA. Cell. 2014 Sep 25;159(1):148-162. doi: 10.1016/j.cell.2014.08.028. Epub 2014 Sep 11. PMID: 25219674; PMCID: PMC4180118.

Ketele A, Kiss T, Jády BE. Human intron-encoded AluACA RNAs and telomerase RNA share a common element promoting RNA accumulation. RNA Biol. 2016

Dec;13(12):1274-1285. doi: 10.1080/15476286.2016.1239689. Epub 2016 Oct 11. PMID: 27726486; PMCID: PMC5207380.

Crooke PS 3rd, Tossberg JT, Porter KP, Aune TM. Reduced A-to-I editing of endogenous Alu RNAs in lung after SARS-CoV-2 infection. Curr Res Immunol. 2021;2:52-59. doi: 10.1016/j.crimmu.2021.04.001. Epub 2021 Apr 30. PMID: 33969287; PMCID: PMC8084883.

Tossberg JT, Heinrich RM, Farley VM, Crooke PS 3rd, Aune TM. Adenosine-to-Inosine RNA Editing of Alu Double-Stranded (ds)RNAs Is Markedly Decreased in Multiple Sclerosis and Unedited Alu dsRNAs Are Potent Activators of Proinflammatory Transcriptional Responses. J Immunol. 2020 Nov 15;205(10):2606-2617. doi: 10.4049/jimmunol.2000384. Epub 2020 Oct 12. PMID: 33046502; PMCID: PMC7872017.

Vlachogiannis NI, Gatsiou A, Silvestris DA, Stamatelopoulos K, Tektonidou MG, Gallo A, Sfikakis PP, Stellos K. Increased adenosine-to-inosine RNA editing in rheumatoid arthritis. J Autoimmun. 2020 Jan;106:102329. doi: 10.1016/j.jaut.2019.102329. Epub 2019 Sep 5. PMID: 31493964; PMCID: PMC7479519.

Aune TM, Tossberg JT, Heinrich RM, Porter KP, Crooke PS 3rd. Alu RNA Structural Features Modulate Immune Cell Activation and A-to-I Editing of Alu RNAs Is Diminished in Human Inflammatory Bowel Disease. Front Immunol. 2022 Jan 20;13:818023. doi: 10.3389/fimmu.2022.818023. PMID: 35126398; PMCID: PMC8813004.

Datta R, Adamska JZ, Bhate A, Li JB. A-to-I RNA editing by ADAR and its therapeutic applications: From viral infections to cancer immunotherapy. Wiley Interdiscip Rev RNA. 2023 Sep 17:e1817. doi: 10.1002/wrna.1817. Epub ahead of print. PMID: 37718249; PMCID: PMC10947335.

Liao Y, Jung SH, Kim T. A-to-I RNA editing as a tuner of noncoding RNAs in cancer. Cancer Lett. 2020 Dec 1;494:88-93. doi: 10.1016/j.canlet.2020.08.004. Epub 2020 Aug 19. PMID: 32822814.

Rodriguez Morales D, Ilieva M, Rennie S, Uchida S. Potential usages of A-to-I RNA editing patterns as diagnostic biomarkers. Am J Physiol Cell Physiol. 2023 Apr 1;324(4):C837-C842. doi: 10.1152/ajpcell.00024.2023. Epub 2023 Feb 27. PMID: 36847441.

Hancks DC, Kazazian HH Jr. Active human retrotransposons: variation and disease. Curr Opin Genet Dev. 2012 Jun;22(3):191-203. doi: 10.1016/j.gde.2012.02.006. Epub 2012 Mar 8. PMID: 22406018; PMCID: PMC3376660.

Jiang Y, Zong W, Ju S, Jing R, Cui M. Promising member of the short interspersed nuclear elements (*Alu* elements): mechanisms and clinical applications in human cancers. J Med Genet. 2019 Oct;56(10):639-645. doi: 10.1136/jmedgenet-2018-105761. Epub 2019 Mar 9. PMID: 30852527.

Clayton EA, Rishishwar L, Huang TC, Gulati S, Ban D, McDonald JF, Jordan IK. An atlas of transposable element-derived alternative splicing in cancer. Philos Trans R Soc Lond B Biol Sci. 2020 Mar 30;375(1795):20190342. doi: 10.1098/rstb.2019.0342. Epub 2020 Feb 10. PMID: 32075558; PMCID: PMC7061986.

Pfaff AL, Singleton LM, Kõks S. Mechanisms of disease-associated SINE-VNTR-Alus. Exp Biol Med (Maywood). 2022 May;247(9):756-764. doi: 10.1177/15353702221082612. Epub 2022 Apr 6. PMID: 35387528; PMCID: PMC9134764.

Di Ruocco F, Basso V, Rivoire M, Mehlen P, Ambati J, De Falco S, Tarallo V. Alu RNA accumulation induces epithelial-to-mesenchymal transition by modulating miR-566 and is associated with cancer progression. Oncogene. 2018 Feb 1;37(5):627-637. doi: 10.1038/onc.2017.369. Epub 2017 Oct 9. PMID: 28991230; PMCID: PMC5799714.

Roos D, de Boer M. Retrotransposable genetic elements causing neutrophil defects. Eur J Clin Invest. 2018 Nov;48 Suppl 2:e12953. doi: 10.1111/eci.12953. Epub 2018 Jun 14. PMID: 29774526.

Leong DW, Komen JC, Hewitt CA, Arnaud E, McKenzie M, Phipson B, Bahlo M, Laskowski A, Kinkel SA, Davey GM, Heath WR, Voss AK, Zahedi RP, Pitt JJ, Chrast R, Sickmann A, Ryan MT, Smyth GK, Thorburn DR, Scott HS. Proteomic and metabolomic analyses of mitochondrial complex I-deficient mouse model generated by spontaneous B2 short interspersed nuclear element (SINE) insertion into NADH dehydrogenase (ubiquinone) Fe-S protein 4 (Ndufs4) gene. J Biol Chem. 2012 Jun 8;287(24):20652-63. doi: 10.1074/jbc.M111.327601. Epub 2012 Apr 25. PMID: 22535952; PMCID: PMC3370248.

Schulze M, Sommer A, Plötz S, Farrell M, Winner B, Grosch J, Winkler J, Riemenschneider MJ. Sporadic Parkinson's disease-derived neuronal cells show disease-specific mRNA and small RNA signatures with abundant deregulation of

piRNAs. Acta Neuropathol Commun. 2018 Jul 10;6(1):58. doi: 10.1186/s40478-018-0561-x. PMID: 29986767; PMCID: PMC6038190.

Zhang D, Zhang J, Wang Y, Wang G, Tang P, Liu Y, Zhang Y, Ouyang L. Targeting epigenetic modifications in Parkinson's disease therapy. Med Res Rev. 2023 Sep;43(5):1748-1777. doi: 10.1002/med.21962. Epub 2023 Apr 29. PMID: 37119043.

Richter TA, Aiken AA, Puracchio MJ, Maganga-Bakita I, Hunter RG. Maternal Immune Activation and Enriched Environments Impact B2 SINE Expression in Stress Sensitive Brain Regions of Rodent Offspring. Genes (Basel). 2023 Apr 1;14(4):858. doi: 10.3390/genes14040858. PMID: 37107616; PMCID: PMC10137338.

Karijolich J, Zhao Y, Alla R, Glaunsinger B. Genome-wide mapping of infection-induced SINE RNAs reveals a role in selective mRNA export. Nucleic Acids Res. 2017 Jun 2;45(10):6194-6208. doi: 10.1093/nar/gkx180. PMID: 28334904; PMCID: PMC5449642.

Khan M, Hou S, Chen M, Lei H. Mechanisms of RNA export and nuclear retention. Wiley Interdiscip Rev RNA. 2023 May-Jun;14(3):e1755. doi: 10.1002/wrna.1755. Epub 2022 Aug 17. PMID: 35978483.

Ichiyanagi T, Katoh H, Mori Y, Hirafuku K, Boyboy BA, Kawase M, Ichiyanagi K. B2 SINE Copies Serve as a Transposable Boundary of DNA Methylation and Histone Modifications in the Mouse. Mol Biol Evol. 2021 May 19;38(6):2380-2395. doi: 10.1093/molbev/msab033. PMID: 33592095; PMCID: PMC8136502.

Vassetzky NS, Borodulina OR, Ustyantsev IG, Kosushkin SA, Kramerov DA. Analysis of SINE Families B2, Dip, and Ves with Special Reference to Polyadenylation Signals and Transcription Terminators. Int J Mol Sci. 2021 Sep 13;22(18):9897. doi: 10.3390/ijms22189897. PMID: 34576060; PMCID: PMC8466645.

Tatosyan KA, Kramerov DA. Heat shock increases lifetime of a small RNA and induces its accumulation in cells. Gene. 2016 Aug 1;587(1):33-41. doi: 10.1016/j.gene.2016.04.025. Epub 2016 Apr 13. PMID: 27085482.

Espinoza CA, Goodrich JA, Kugel JF. Characterization of the structure, function, and mechanism of B2 RNA, an ncRNA repressor of RNA polymerase II transcription. RNA. 2007 Apr;13(4):583-96. doi: 10.1261/rna.310307. Epub 2007 Feb 16. PMID: 17307818; PMCID: PMC1831867.

Allen TA, Von Kaenel S, Goodrich JA, Kugel JF. The SINE-encoded mouse B2 RNA represses mRNA transcription in response to heat shock. Nat Struct Mol Biol. 2004 Sep;11(9):816-21. doi: 10.1038/nsmb813. Epub 2004 Aug 8. PMID: 15300240.

Joshi CJ, Ke W, Drangowska-Way A, O'Rourke EJ, Lewis NE. What are housekeeping genes? PLoS Comput Biol. 2022 Jul 13;18(7):e1010295. doi: 10.1371/journal.pcbi.1010295. PMID: 35830477; PMCID: PMC9312424.

Zovoilis A, Cifuentes-Rojas C, Chu HP, Hernandez AJ, Lee JT. Destabilization of B2 RNA by EZH2 Activates the Stress Response. Cell. 2016 Dec 15;167(7):1788-1802.e13. doi: 10.1016/j.cell.2016.11.041. PMID: 27984727; PMCID: PMC5552366.

Hernandez AJ, Zovoilis A, Cifuentes-Rojas C, Han L, Bujisic B, Lee JT. B2 and ALU retrotransposons are self-cleaving ribozymes whose activity is enhanced by EZH2. Proc Natl Acad Sci U S A. 2020 Jan 7;117(1):415-425. doi: 10.1073/pnas.1917190117. Epub 2019 Dec 23. PMID: 31871160; PMCID: PMC6955291.

Ponicsan SL, Kugel JF, Goodrich JA. Repression of RNA Polymerase II Transcription by B2 RNA Depends on a Specific Pattern of Structural Regions in the RNA. Noncoding RNA. 2015 Jun;1(1):4-16. doi: 10.3390/ncrna1010004. PMID: 26405685; PMCID: PMC4578731.

Cheng Y, Saville L, Gollen B, Isaac C, Belay A, Mehla J, Patel K, Thakor N, Mohajerani MH, Zovoilis A. Increased processing of SINE B2 ncRNAs unveils a novel type of transcriptome deregulation in amyloid beta neuropathology. Elife. 2020 Nov 16;9:e61265. doi: 10.7554/eLife.61265. PMID: 33191914; PMCID: PMC7717908.

Ivanova E, Berger A, Scherrer A, Alkalaeva E, Strub K. Alu RNA regulates the cellular pool of active ribosomes by targeted delivery of SRP9/14 to 40S subunits. Nucleic Acids Res. 2015 Mar 11;43(5):2874-87. doi: 10.1093/nar/gkv048. Epub 2015 Feb 19. PMID: 25697503; PMCID: PMC4357698.

Deininger P. Alu elements: know the SINEs. Genome Biol. 2011 Dec 28;12(12):236. doi: 10.1186/gb-2011-12-12-236. PMID: 22204421; PMCID: PMC3334610.

Konkel MK, Walker JA, Hotard AB, Ranck MC, Fontenot CC, Storer J, Stewart C, Marth GT; 1000 Genomes Consortium; Batzer MA. Sequence Analysis and Characterization of Active Human Alu Subfamilies Based on the 1000 Genomes Pilot Project. Genome Biol Evol. 2015 Aug 29;7(9):2608-22. doi: 10.1093/gbe/evv167. PMID: 26319576; PMCID: PMC4607524.

Hadjiargyrou M, Delihas N. The intertwining of transposable elements and non-coding RNAs. Int J Mol Sci. 2013 Jun 26;14(7):13307-28. doi: 10.3390/ijms140713307. PMID: 23803660; PMCID: PMC3742188.

Shankar R, Grover D, Brahmachari SK, Mukerji M. Evolution and distribution of RNA polymerase II regulatory sites from RNA polymerase III dependant mobile Alu elements. BMC Evol Biol. 2004 Oct 4;4:37. doi: 10.1186/1471-2148-4-37. PMID: 15461819; PMCID: PMC524483.

Mariner PD, Walters RD, Espinoza CA, Drullinger LF, Wagner SD, Kugel JF, Goodrich JA. Human Alu RNA is a modular transacting repressor of mRNA transcription during heat shock. Mol Cell. 2008 Feb 29;29(4):499-509. doi: 10.1016/j.molcel.2007.12.013. PMID: 18313387.

Yakovchuk P, Goodrich JA, Kugel JF. B2 RNA and Alu RNA repress transcription by disrupting contacts between RNA polymerase II and promoter DNA within assembled complexes. Proc Natl Acad Sci U S A. 2009 Apr 7;106(14):5569-74. doi: 10.1073/pnas.0810738106. Epub 2009 Mar 23. PMID: 19307572; PMCID: PMC2667051.

Pandey R, Mandal AK, Jha V, Mukerji M. Heat shock factor binding in Alu repeats expands its involvement in stress through an antisense mechanism. Genome Biol. 2011 Nov 23;12(11):R117. doi: 10.1186/gb-2011-12-11-r117. PMID: 22112862; PMCID: PMC3334603.

Vourc'h C, Dufour S, Timcheva K, Seigneurin-Berny D, Verdel A. HSF1-Activated Non-Coding Stress Response: Satellite lncRNAs and Beyond, an Emerging Story with a Complex Scenario. Genes (Basel). 2022 Mar 27;13(4):597. doi: 10.3390/genes13040597. PMID: 35456403; PMCID: PMC9032817.

Zucchelli S, Cotella D, Takahashi H, Carrieri C, Cimatti L, Fasolo F, Jones MH, Sblattero D, Sanges R, Santoro C, Persichetti F, Carninci P, Gustincich S. SINEUPs: A new class of natural and synthetic antisense long non-coding RNAs that activate translation. RNA Biol. 2015;12(8):771-9. doi: 10.1080/15476286.2015.1060395. PMID: 26259533; PMCID: PMC4615742.

Zucchelli S, Fasolo F, Russo R, Cimatti L, Patrucco L, Takahashi H, Jones MH, Santoro C, Sblattero D, Cotella D, Persichetti F, Carninci P, Gustincich S. SINEUPs are modular antisense long non-coding RNAs that increase synthesis of target proteins in cells. Front Cell Neurosci. 2015 May 13;9:174. doi: 10.3389/fncel.2015.00174. PMID: 26029048; PMCID: PMC4429562.

Fan J, Papadopoulos V. Transcriptional regulation of translocator protein (Tspo) via a SINE B2-mediated natural antisense transcript in MA-10 Leydig cells. Biol Reprod. 2012 May 10;86(5):147, 1-15. doi: 10.1095/biolreprod.111.097535. PMID: 22378763; PMCID: PMC3364927.

De Brakeleer S, De Grève J, Lissens W, Teugels E. Systematic detection of pathogenic alu element insertions in NGS-based diagnostic screens: the BRCA1/BRCA2 example. Hum Mutat. 2013 May;34(5):785-91. doi: 10.1002/humu.22297. Epub 2013 Mar 11. PMID: 23420552.

Wang Y, Bernhardy AJ, Nacson J, Krais JJ, Tan YF, Nicolas E, Radke MR, Handorf E, Llop-Guevara A, Balmaña J, Swisher EM, Serra V, Peri S, Johnson N. BRCA1 intronic Alu elements drive gene rearrangements and PARP inhibitor resistance. Nat Commun. 2019 Dec 11;10(1):5661. doi: 10.1038/s41467-019-13530-6. PMID: 31827092; PMCID: PMC6906494.

Arnoldi M, Zarantonello G, Espinoza S, Gustincich S, Di Leva F, Biagioli M. Design and Delivery of SINEUP: A New Modular Tool to Increase Protein Translation. Methods Mol Biol. 2022;2434:63-87. doi: 10.1007/978-1-0716-2010-6_4. PMID: 35213010; PMCID: PMC9703201.

Podbevšek P, Fasolo F, Bon C, Cimatti L, Reißer S, Carninci P, Bussi G, Zucchelli S, Plavec J, Gustincich S. Structural determinants of the SINE B2 element embedded in the long non-coding RNA activator of translation AS Uchl1. Sci Rep. 2018 Feb 16;8(1):3189. doi: 10.1038/s41598-017-14908-6. PMID: 29453387; PMCID: PMC5816658.

Espinoza S, Bon C, Valentini P, Pierattini B, Matey AT, Damiani D, Pulcrano S, Sanges R, Persichetti F, Takahashi H, Carninci P, Santoro C, Cotella D, Gustincich S. SINEUPs: a novel toolbox for RNA therapeutics. Essays Biochem. 2021 Oct 27;65(4):775-789. doi: 10.1042/EBC20200114. PMID: 34623427; PMCID: PMC8564737.

Schein A, Zucchelli S, Kauppinen S, Gustincich S, Carninci P. Identification of antisense long noncoding RNAs that function as SINEUPs in human cells. Sci Rep.

2016 Sep 20;6:33605. doi: 10.1038/srep33605. PMID: 27646849; PMCID: PMC5028707.

Takahashi H, Kozhuharova A, Sharma H, Hirose M, Ohyama T, Fasolo F, Yamazaki T, Cotella D, Santoro C, Zucchelli S, Gustincich S, Carninci P. Identification of functional features of synthetic SINEUPs, antisense lncRNAs that specifically enhance protein translation. PLoS One. 2018 Feb 7;13(2):e0183229. doi: 10.1371/journal.pone.0183229. PMID: 29414979; PMCID: PMC5802440.

Park E, Maquat LE. Staufen-mediated mRNA decay. Wiley Interdiscip Rev RNA. 2013 Jul-Aug;4(4):423-35. doi: 10.1002/wrna.1168. Epub 2013 May 16. PMID: 23681777; PMCID: PMC3711692.

LeGendre JB, Campbell ZT, Kroll-Conner P, Anderson P, Kimble J, Wickens M. RNA targets and specificity of Staufen, a double-stranded RNA-binding protein in Caenorhabditis elegans. J Biol Chem. 2013 Jan 25;288(4):2532-45. doi: 10.1074/jbc.M112.397349. Epub 2012 Nov 29. PMID: 23195953; PMCID: PMC3554921.

Heber S, Gáspár I, Tants JN, Günther J, Moya SMF, Janowski R, Ephrussi A, Sattler M, Niessing D. Staufen2-mediated RNA recognition and localization requires combinatorial action of multiple domains. Nat Commun. 2019 Apr 10;10(1):1659. doi: 10.1038/s41467-019-09655-3. PMID: 30971701; PMCID: PMC6477676.

Li H, Handsaker B, Wysoker A, Fennell T, Ruan J, Homer N, Marth G, Abecasis G, Durbin R; 1000 Genome Project Data Processing Subgroup. The Sequence Alignment/Map format and SAMtools. Bioinformatics. 2009 Aug 15;25(16):2078-9. doi: 10.1093/bioinformatics/btp352. Epub 2009 Jun 8. PMID: 19505943; PMCID: PMC2723002.

Li H, Durbin R. Fast and accurate short read alignment with Burrows-Wheeler transform. Bioinformatics. 2009 Jul 15;25(14):1754-60. doi: 10.1093/bioinformatics/btp324. Epub 2009 May 18. PMID: 19451168; PMCID: PMC2705234.

Li H, Durbin R. Fast and accurate long-read alignment with Burrows-Wheeler transform. Bioinformatics. 2010 Mar 1;26(5):589-95. doi: 10.1093/bioinformatics/btp698. Epub 2010 Jan 15. PMID: 20080505; PMCID: PMC2828108.

Li H. Minimap2: pairwise alignment for nucleotide sequences. Bioinformatics. 2018 Sep 15;34(18):3094-3100. doi: 10.1093/bioinformatics/bty191. PMID: 29750242; PMCID: PMC6137996.

Cheng Y, Saville L, Gollen B, Veronesi AA, Mohajerani M, Joseph JT, Zovoilis A. Increased Alu RNA processing in Alzheimer brains is linked to gene expression changes. EMBO Rep. 2021 May 5;22(5):e52255. doi: 10.15252/embr.202052255. Epub 2021 Mar 1. PMID: 33645898; PMCID: PMC8097388.

Murray JI, Whitfield ML, Trinklein ND, Myers RM, Brown PO, Botstein D. Diverse and specific gene expression responses to stresses in cultured human cells. Mol Biol Cell. 2004 May;15(5):2361-74. doi: 10.1091/mbc.e03-11-0799. Epub 2004 Mar 5. PMID: 15004229; PMCID: PMC404029.

Ferrigno O, Virolle T, Djabari Z, Ortonne JP, White RJ, Aberdam D. Transposable B2 SINE elements can provide mobile RNA polymerase II promoters. Nat Genet. 2001 May;28(1):77-81. doi: 10.1038/ng0501-77. PMID: 11326281.

Beane RL, Ram R, Gabillet S, Arar K, Monia BP, Corey DR. Inhibiting gene expression with locked nucleic acids (LNAs) that target chromosomal DNA. Biochemistry. 2007 Jun 26;46(25):7572-80. doi: 10.1021/bi700227g. Epub 2007 May 31. PMID: 17536839; PMCID: PMC2527755.

Veedu RN, Wengel J. Locked nucleic acids: promising nucleic acid analogs for therapeutic applications. Chem Biodivers. 2010 Mar;7(3):536-42. doi: 10.1002/cbdv.200900343. PMID: 20232325.

Galluzzi L, Yamazaki T, Kroemer G. Linking cellular stress responses to systemic homeostasis. Nat Rev Mol Cell Biol. 2018 Nov;19(11):731-745. doi: 10.1038/s41580-018-0068-0. PMID: 30305710.

Sheng X, Xia Z, Yang H, Hu R. The ubiquitin codes in cellular stress responses. Protein Cell. 2024 Feb 29;15(3):157-190. doi: 10.1093/procel/pwad045. PMID: 37470788; PMCID: PMC10903993.

Wu YZ, Su YH, Kuo CY. Stressing the Regulatory Role of Long Non-Coding RNA in the Cellular Stress Response during Cancer Progression and Therapy. Biomedicines. 2022 May 23;10(5):1212. doi: 10.3390/biomedicines10051212. PMID: 35625948; PMCID: PMC9138696.

Hagedorn PH, Persson R, Funder ED, Albæk N, Diemer SL, Hansen DJ, Møller MR, Papargyri N, Christiansen H, Hansen BR, Hansen HF, Jensen MA, Koch T. Locked nucleic acid: modality, diversity, and drug discovery. Drug Discov Today. 2018 Jan;23(1):101-114. doi: 10.1016/j.drudis.2017.09.018. Epub 2017 Oct 6. PMID: 28988994.

Cho S, Park JS, Kang YK. AGO2 and SETDB1 cooperate in promoter-targeted transcriptional silencing of the androgen receptor gene. Nucleic Acids Res. 2014 Dec 16;42(22):13545-56. doi: 10.1093/nar/gku788. Epub 2014 Sep 2. PMID: 25183519; PMCID: PMC4267665.

Matsui M, Prakash TP, Corey DR. Argonaute 2-dependent Regulation of Gene Expression by Single-stranded miRNA Mimics. Mol Ther. 2016 May;24(5):946-55. doi: 10.1038/mt.2016.39. Epub 2016 Feb 23. PMID: 26903376; PMCID: PMC4881773.

Yokota A, Hiramoto M, Hino H, Tokuhisa M, Miyazaki M, Kazama H, Takano N, Miyazawa K. Sequestosome 1 (p62) accumulation in breast cancer cells suppresses progesterone receptor expression via argonaute 2. Biochem Biophys Res Commun. 2020 Oct 15;531(2):256-263. doi: 10.1016/j.bbrc.2020.07.058. Epub 2020 Aug 13. PMID: 32800344.

Lopez-Orozco J, Fayad N, Khan JQ, Felix-Lopez A, Elaish M, Rohamare M, Sharma M, Falzarano D, Pelletier J, Wilson J, Hobman TC, Kumar A. The RNA Interference Effector Protein Argonaute 2 Functions as a Restriction Factor Against SARS-CoV-2. J Mol Biol. 2023 Aug 15;435(16):168170. doi: 10.1016/j.jmb.2023.168170. Epub 2023 Jun 3. PMID: 37271493; PMCID: PMC10238125.